Characterizing and Designing Engine Manifolds for Single-Cylinder Engine Turbocharging

by

Michael Buchman

Submitted to the Department of Mechanical Engineering
in partial fulfillment of the requirements for the degree of

PhD in Mechanical Engineering

at the

MASSACHUSETTS INSTITUTE OF TECHNOLOGY

September 2018

© Massachusetts Institute of Technology 2018. All rights reserved.

Signature redacted

Author .....
Department of Mechanical Engineering
July 20, 2018

Certified by..... Signature redacted
Amos Winter
Associate Professor
Thesis Supervisor

Accepted by ..... Signature redacted
Rohan Abeyaratne
Chairman, Department Committee on Graduate Theses

MASSACHUSETTS INSTITUTE OF TECHNOLOGY
OCT 02 2018
LIBRARIES
ARCHIVES

Characterizing and Designing Engine Manifolds for Single-Cylinder Engine Turbocharging

by

Michael Buchman

Submitted to the Department of Mechanical Engineering
on July 20, 2018, in partial fulfillment of the
requirements for the degree of
PhD in Mechanical Engineering

Abstract

Turbocharging can provide a cost-effective means for increasing the power output and fuel economy of an internal combustion engine. It is commonly used on multi-cylinder engines, but not on commercial single-cylinder engines due to the phase mismatch between the exhaust stroke (when the turbocharger is powered) and the intake stroke (when the engine requires the compressed air). This work explores overcoming the phase mismatch problem by adding an air capacitor: a volume added in series with the intake manifold between the turbocharger compressor and the engine intake. The function of the air capacitor is to buffer the output from the turbocharger compressor and deliver pressurized air during the intake stroke.

This research focuses on demonstrating the feasibility of using an air capacitor to enable turbocharging single cylinder internal combustion engines. An analytical model of the system was created from first principles, which showed that the air capacitor turbocharging method could increase power output by up to 40% without heat transfer and up to 70% with heat transfer elements included in the intake manifold (such as an intercooler). An initial, proof-of-concept experiment was created using a generator as a dynamometer. With an air capacitor volume seven times the engine capacity, this setup was able to produce 29% more power compared to the same engine naturally aspirated.

A numerical model was developed in Ricardo Wave to predict the performance of turbocharged single cylinder engines with air capacitors under different conditions. An experimental engine with accompanying dynamometer was constructed to demonstrate the effects of manifold sizing on engine performance and to experimentally validate the model. The experiment showed that the model was able to predict power output with an accuracy of 8% of peak power, fuel consumption within 7% error, air mass flow rates with 10% error, and manifold pressures within 7% error. The model was then combined with a simulated annealing optimization scheme in Matlab in order to conceptualize designs for the geometry and timings of single-cylinder turbocharged engines intended for different commercial applications. The optimization showed that adding an air capacitor and turbocharger to a 0.44L engine, with slight

modifications to the valve and injector timings, could increase power by 88% compared to natural aspiration. By also modifying the bore and stroke, the turbocharged engine with an air capacitor could reduce fuel consumption by 8% compared to a naturally aspirated engine with equivalent peak power output.

Thesis Supervisor: Amos Winter
Title: Associate Professor

Acknowledgments

The last five years I have been lucky enough to have an amazing support network to advise and help me with both research and life. The person most critical to my success was my advisor, Professor Amos Winter. He offered me the opportunity to work on this project. Over the course of my research he was there to guide me when anything went wrong and encourage me to make the most of my successes. The process of obtaining a PhD would have been significantly more difficult without his support and guidance throughout the process. It is reassuring to know that when I need guidance in the future Amos will be there to give me advice.

I am grateful to have had the support of my fellow members of the of Global Engineering and Research lab (GEAR Lab) for the last five years. As far as I can tell, there is no lab on campus that is as supportive and social as GEAR. When I started, the lab was one year old and there were seven of us. Whenever I had any problems I could count on Dan Dorsch to help me debug them. I could also count on Dan to help me design parts, move my experiment, machine items, be a shop buddy, and find free food around campus. If I needed help with heat transfer, fluids, or general guidance Natasha Wright was there to help. Murthy has always been a great resource for design advice. I could always count on Jaya and Guillermo to be there to assist me and to be available for bar trivia. Our administrator Cakky was key to me being able to get anything done. Without her my experiment would still be a series of purchase orders waiting to be filed and nothing would get done. My work would be significantly worse if I did not have Brett and Dev to help me edit my papers and thesis. The whole of GEAR Lab should be able to take partial credit for my success at MIT. Without them this project would have taken longer and my time in graduate school would have been considerably less joyful.

I would not be here without the many MIT faculty members who were always around to provide guidance, support, and help with any issues I was having. I am grateful to my committee members, Professor Ahmed Ghoniem, Professor Wai Cheng, and Dr. Luca Marmorini who helped me refine my research and gave me guidance

when I ran into problems.

My family has always been there for me and supported me even from three thousand miles away. They went beyond the traditional family support of being there for personal issues. I always had difficulty writing and when I was diagnosed with dyslexia in high school my difficulties started to make sense. My mom, dad, sister, and brother in law went out of their way to help me with my writing difficulties. They would help look over and edit drafts of papers (including this thesis) to catch any errors I made. Without them I would have struggled to learn how to effectively communicate my ideas in writing.

Without my amazing group of friends I would have been miserable. My girlfriend, Kaitlyn, has provided support, kept me amused, and fed me during the most stressful periods of graduate school. Adin, Max, and my other friends from undergraduate school have been available at a moment's notice to help me move or to play board games. All the friends I have made in graduate school have made me appreciate how great this department is. They were there to help me study for Quals, move my experimental setups, and organize fun events.

The MIT community is special to me. I have been here for nine years, or one third of my life so far. There is a reason I chose to keep coming back, first after undergraduate studies, and then after completing my Master's degree. MIT is a unique place in that the most intelligent people in the world make amazing things happen, yet everyone is always supportive and eager to help those around them learn. In addition to learning through classrooms I have had the opportunity to learn by building a solar car, founding a maker space, trying different research projects, and interacting with those around me.

There are a couple of friends who are not in GEAR Lab or associated with my research in any way who still gave of their time to help me with problems I could not solve on my own. Ari Frankel helped me with some math to describe the flows during my master thesis, work which saved me a significant amount of time. Kevin Cedrone helped me debug both my initial experiment and my current dynamometer and found bugs that no one else could find in both setups. Sebastian Ahling saved

me when my research engine failed. He helped me find the parts I need and fix the system.

When I was a first-year graduate student Dan Dorsch got me and a couple of other friends to go to a couple of meetings about maker spaces on campus. Within two years we built Maker Workshop, an MIT community maker space. This space has provided me with a place to work on both personal projects and research as well as an amazing group of friends.

This work would not be possible without financial sponsorship. For the first year of research Professor Winter believed in me enough to fund this research out of his startup package. Afterwards, I was sponsored by the Tata Center for Technology and Design at MIT and by the National Science Foundation. This material is based upon work supported by the National Science Foundation Graduate Research Fellowship under Grant No. 1122374. Any opinions, findings, conclusions or recommendations expressed in this material are those of the authors(s) and do not necessarily reflect the views of the National Science Foundation.

Contents

List of Figures

List of Tables

Chapter 1

Introduction

Turbocharging is a cost effective way to increase the performance of multi-cylinder diesel engines: it can boost power output, increase fuel efficiency, improve emissions quality [34, 67, 19], lower cost per unit power, and reduce weight per unit power [67, 26, 62]. A turbocharged engine can be smaller size than a naturally aspirated engine, which reduces frictional area between the piston and the cylinder and, thus, will have fewer frictional losses. Due to larger rates of air flow with turbocharging, there is also better heat transfer in the engine, which can reduce thermal losses [67]. According to Makartchouk [44], turbocharging a diesel engine increases the mechanical efficiency between 2%-10%. In practice, most stationary applications for turbocharged engines will result in a 5% efficiency gain compared to naturally aspirated engines of the same power [44].

Turbocharging single-cylinder engines is not currently implemented commercially due to the mismatch between the intake and exhaust strokes, despite the advantages mentioned earlier [11]. When the engine is exhausting (and the turbocharger is being powered), the intake valve is closed and the compressed air from the turbocharger has nowhere to flow.

Previous work has demonstrated that turbocharging single-cylinder engines can be achieved by buffering the intake air between the exhaust and intake strokes using an air capacitor: an additional volume added in series to the intake manifold (Fig. 1-1) [14]. The capacitor stores air compressed by the turbocharger during the exhaust

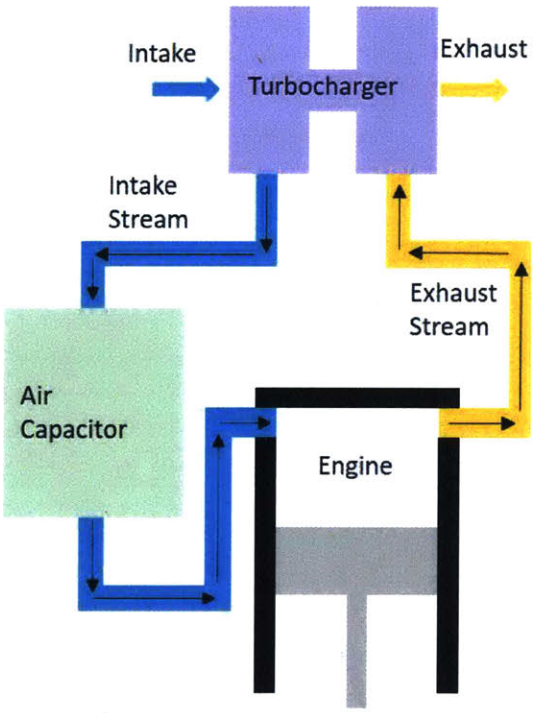

Figure 1-1: Block diagram that shows the layout of the air capacitor system.

stroke and then uses the pressure in the vessel to force air into the cylinder during the intake stroke.

The goal of this research is to analyze the commercial viability of single-cylinder turbocharging technology by understanding how adding a turbocharger and an air capacitor affects emissions, fuel economy, and power density. By understanding these effects it will be possible to design an engine and optimize its timing for turbocharging.

This thesis builds on an analytical model and an initial experiment that demonstrate the feasibility of turbocharging a single-cylinder engine using an air capacitor. In order to achieve this, a computational engine model is presented that is used to predict the emissions, efficiency, and power output of a single-cylinder turbocharged engine with an air capacitor. An experiment was built in order to demonstrate the effect of air capacitor volume on power output, emissions, manifold pressure, transient response, and fuel consumption on a physical engine. This experiment was also used to validate the computational model. Finally the computational model was integrated with a simulated annealing optimization scheme in order to recommend engine

designs and modifications for different applications.

1.1 Motivation

The primary value proposition of this technology for engine users is to improve the specific power for low-cost, engine-powered equipment, such as small vehicles, tractors, and generators, while maintaining or improving fuel economy. Turbocharging increases power by increasing the amount of oxygen in the engine available for combustion [67]. Turbocharging single-cylinder engines can improve fuel economy by increasing power density. This allows smaller engines to produce the same power output as a larger engine, but with fewer frictional losses due to the smaller frictional area between the piston and the cylinder [34, 67]. However, care should be taken as turbocharging can also increase fuel consumption by increasing pumping losses [34, 67].

The value of this technology is especially apparent in the agricultural sector. In many developing countries the agricultural sector is inefficient, while a significant portion of the population is involved in the agricultural sector, which only makes up a relatively small portion of GDP (Fig. 1-2) [9, 3]. This results in population migration, a shortage of agricultural workers, and a large population of subsistence farmers. This problem is compounded by poor yield due to a lack of proper agricultural tools, fertilizer, and available farm power [50]. Countries with a lower GDP tend to have worse yield than wealthier countries (Fig. 1-3) [9, 4].

Farm mechanization is closely correlated to farm output (Fig. 1-4, 1-5). Multiple studies have been commissioned by the Indian government to generate ideas on how to address agricultural issues in India. Two of the key studies were done by the Bhopal Indian Counsel of Agricultural Research and by the Indian Department of Agriculture [45, 50]. It was found that while there was large growth in farm manpower in the 1980's and 1990's, over the last decade the growth in available farm manpower has slowed to a little over 2% per year. The other key finding was that increasing farm mechanization could save seed and fertilizer utilization by 15-20%, increase crop yield

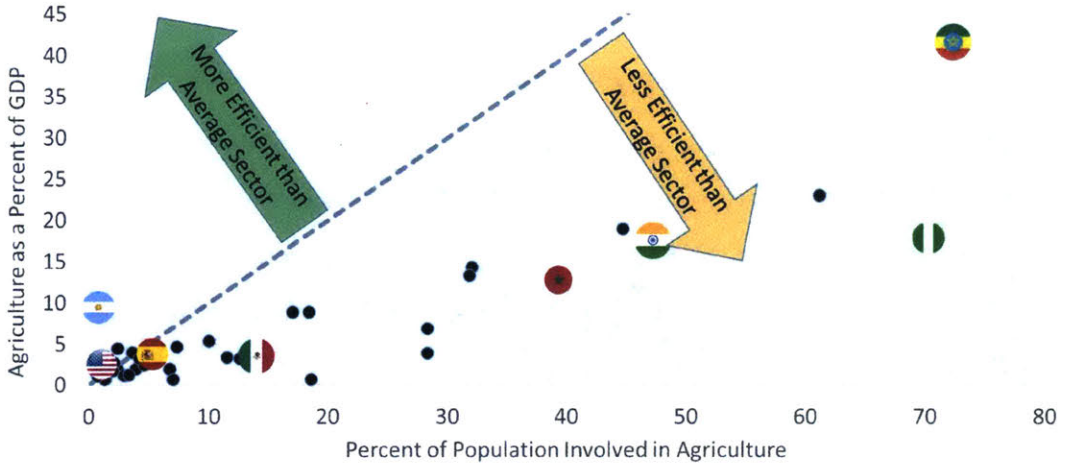

Figure 1-2: Plot that compares the percent of population involved in agriculture to the percent of a country's GDP due to agriculture with select countries highlighted. The dashed line represents an efficient agricultural sector where percent employment matches percent of GDP due to agriculture. [9, 4]

Figure 1-3: Map that compares per capita GDP with yield. Selected countries are highlighted with their flag. [4, 22]

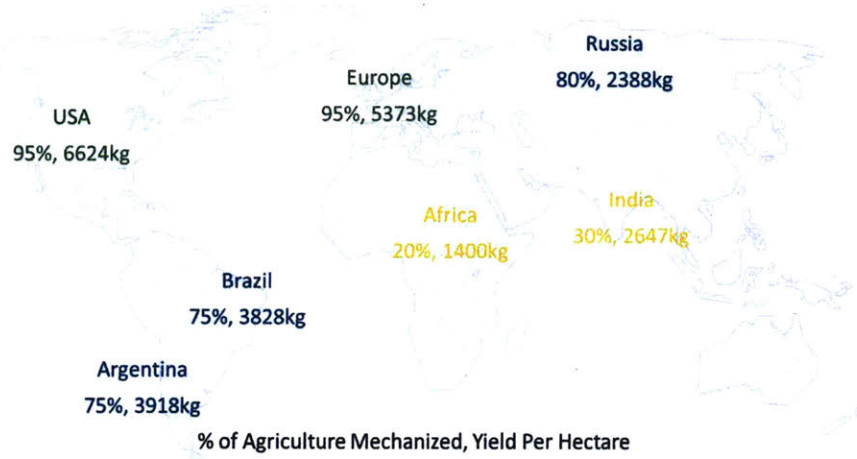

Figure 1-4: Map that compares the level of mechanization to farm yield in selected regions.[4, 22]

by 5-20%, reduce manual labor by 20-30%, and increase farm productivity by 10-15% [59, 10]. Mechanization is made more urgent since crop yield has to increase by a third over the next couple of decades, in order to feed the growing population of India. Figures 1-4 & 1-5 show how farm yield is correlated with available power. Turbocharging single-cylinder engines is an effective way to increase the available power for farmers since over a million single-cylinder engines are sold every year in India.

Turbochargers increase the power density of engines, which is crucial for weight sensitive applications such as aircraft, and portable equipment such as irrigation pumps on small farms [13, 22]. Increased power density results in a lighter device, which improves fuel economy in commercial vehicles [19]. Studies on turbocharging two-cylinder engines in India showed increased power density (12-25%), reduced emissions, and reduced fuel consumption relative to a naturally aspirated engine [51, 64].

In commercial vehicles, turbocharging has been shown to reduce engine size by an average of 30% [11]. Adding a turbocharger to an engine costs between 10-20% of what it would cost to add another cylinder [11]. A study of passenger cars found

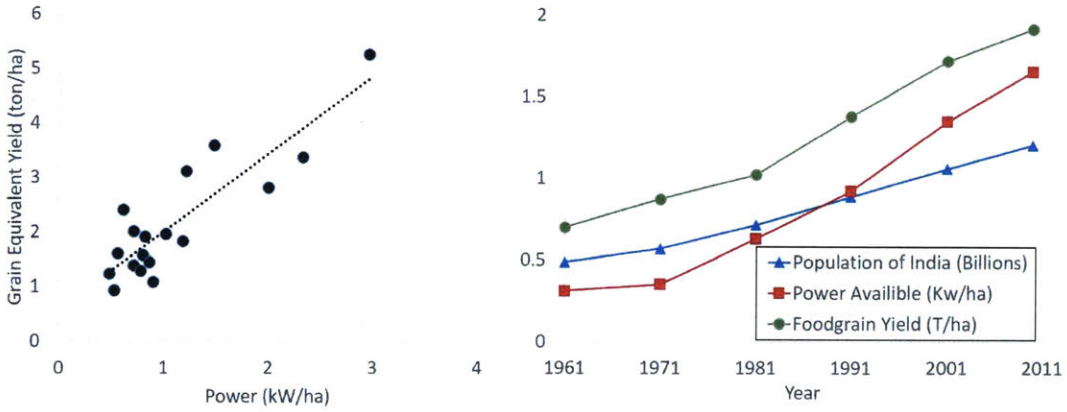

Figure 1-5: Left: Plot that compares available power to farm yield in different provinces in India. Right: Plot that compares available power to farm yield in India over time. This plot also shows the growing population that needs to be fed.[3, 22, 32, 50]

that there was a $300 advantage in cost of ownership to turbocharging compared to a naturally aspirated engine, despite the added cost of the turbocharger [24].

Turbochargers could improve multiple aspects of single-cylinder engines and provide value to manufacturers [11, 22]. The first was is to help meet new emissions standards. Diesel emissions can cause environmental damage and impact health both chronically and acutely, and with the large volume of single-cylinder engines sold each year, even incremental improvements in emissions can result in significant improvements in air quality. Therefore, regulatory bodies have set emissions restrictions on these engines that are constantly tightening. For example, manufacturers in India must bring their single-cylinder engines up to BS 6 (equivalent to stage 5 European standards) emissions standards by 2020 [39]. This will be the first time that engines under 19 kW will have to meet emission standards. The exhaust treatments required to do this will reduce the mechanical power of the engine due to back pressure [55, 12]. Turbocharging can be used to mitigate some of the performance losses caused by the emissions after treatment that is required to meet new emissions standards.

Furthermore, turbocharging single-cylinder engines will reduce particulate emissions in high altitude operations by supplying more air to the engine for more complete combustion. Areas such as the Altiplano Plateau in Bolivia would benefit from this

technology, as 60% of the farms there are at an altitude above 4,000 meters. In addition, local small-scale farmers would also benefit from the power increases provided by turbocharging. Air density, and consequentially engine power output, decreases by over 30% at these high altitudes and turbocharging would help counteract these losses [1, 5].

The target market for this technology is developing world agricultural equipment such as tractors, water pumps, and generators. To ensure that our technology is commercializable, an active dialog was created with equipment manufacturers that could use turbocharged single-cylinder engines with air capacitors. Along with Mahindra and Kohler/Lombardini, additional companies include USHA (one of the largest water pump manufacturers in India), Peugeot (the largest small scooter manufacturer in Europe), and Tata Motors (manufacturer of small delivery vehicles). These companies agree that creating a method for turbocharging single-cylinder engines presents an attractive solution to their challenges. USHA did a 'willingness to pay' study for different features in the single-cylinder water pump market in India (1.2 million units a year). They found that farmers would be willing to pay 967 Indian rupees ($15) for better fuel efficiency, and 608 rupees ($9) for each additional 10% power increase. These increases are significant, as they are based on engines that cost approximately 16,500 rupees (~$250) [22]. If the technology increases power by 50%, it would provide a total value to farmers of ~3,040 rupees ($48). At scaled production, adding a turbocharger to a small engine costs only 2,500 rupees ($38); the air capacitor, which is only a small canister, would cost negligibly more than a standard intake manifold [11].

Furthermore, Table 1.1 shows the potential cost advantages of turbocharging based on commercial prices in the United States. Additionally, engines with the turbocharged air capacitor technology could fill the gap between the largest air-cooled diesel single-cylinder engine Kohler makes (rated at 7.35 kW) and their smallest air-cooled two-cylinder diesel engine (rated at 14.1 kW). Table 1.2 shows that these trends also exist in India; based on commercial prices and conversations with our partners [21, 22, 11]. These analyses demonstrate how our technology can be more economical

Table 1.1: Cost breakdown for turbocharging a high-end diesel engine based on off-the-shelf prices in the United States and an analogous price breakdown for a low cost system based on conversations with partners in India and engines made by USHA.

	Naturally Aspirated Single-Cylinder[1]	**Turbocharged Single-Cylinder Engine Experiment**[2]	**Turbocharged Single-Cylinder Engine Optimized Model**[3]	**NA Two Cylinder Engine** [4]
Power (kW) at an air to fuel ratio of 30	6.8(rated) 7.3(modeled) 7.13(measured)	8.62(measured) 8.58(model)	10 kW(modeled)	14.1(rated)
Engine Cost (US retail)	$2624	$2624	$2624	$4,665
US Retail Estimated Cost of Additional Components	-	$525	$525	-
Cost Density based on US Retail (W/$)	2.6 (W/$)	2.7 (W/$)	3.2 (W/$)	3.0 (W/$)

1. Data from the Kohler KD440 engine manual and experiments run on our dynamometer. In the experiment this power was achieved at an air to fuel ratio of 30. As a result, all of the engine comparisons were done for an air to fuel ratio of 30 [41].
2. Based on experiments on a Kohler engine with a Garrett turbocharger and an intercooler that has yet to be optimized. Engine runs at an air to fuel ratio of 30. Note that at lower air to fuel ratios the turbocharged engine outperforms the naturally aspirated engine by a larger margin. Estimated cost of turbocharger and other components comes from conversations with Mahindra. Their conservative estimate is that turbocharging adds 20% to the engine cost. [11]
3. Based on our multivariable optimized Kohler engine, designed to maximize power density and fuel economy at an air to fuel ratio of 30. Estimated cost of turbocharger and other components comes from conversations with Mahindra. Their conservative estimate is that turbocharging adds 20% to the engine cost.[11]
4. Based on a two-cylinder Kohler KD425-2 engine. This engine is the two-cylinder version of the KD440 used in our experiments. All data are taken from the engine manual [41].

Table 1.2: Cost breakdown for turbocharging a standard Indian diesel engine based on off-the-shelf prices in India and on conversations with our partners in India.

	Naturally Aspirated USHA Air Cooled Single-Cylinder Engine[1]	**Turbocharged USHA Air Cooled Cylinder Engine**[2]	**NA USHA Air Cooled Two Cylinder Engine** [4]
Peak Power (kW)	4.5 kW (rated)	6 kW (estimated)	9.75 kW(rated)
Engine Cost (India retail)	44430 rupees	44430 rupees	88110 rupees
Estimated Cost of Additional components	-	8886 rupees	-
Cost Density (W/rupee)	0.10 (W/rupee)	0.11 (W/rupee)	0.11 (W/rupee)

1. Based on data from USHA's standard Air Cooled Engines [21].
2. Based on a 33% power gain which we have shown to be feasible computationally and experimentally [15].
3.Based on the USHA Twin Cylinder Vertical Diesel Engine [21].

than comparable technologies with a lower power per unit of cost.

1.2 Turbocharging Background

An internal combustion engine is limited by the amount of air it can intake: the more air the engine can intake the more fuel the engine can burn and the more power the engine can output [34]. As a result, the power generated by a naturally aspirated engine (an engine which intakes directly from the environment around it) is limited by the density of air around it. In order to significantly increase engine power, the intake air density has to be increased through compression [34]. This is called charging an engine.

There are two primary technologies to charge an internal combustion engine; supercharging and turbocharging. Supercharging uses mechanical power from the engine in order to power a compressor that compresses the intake air (Fig. 1-6). This

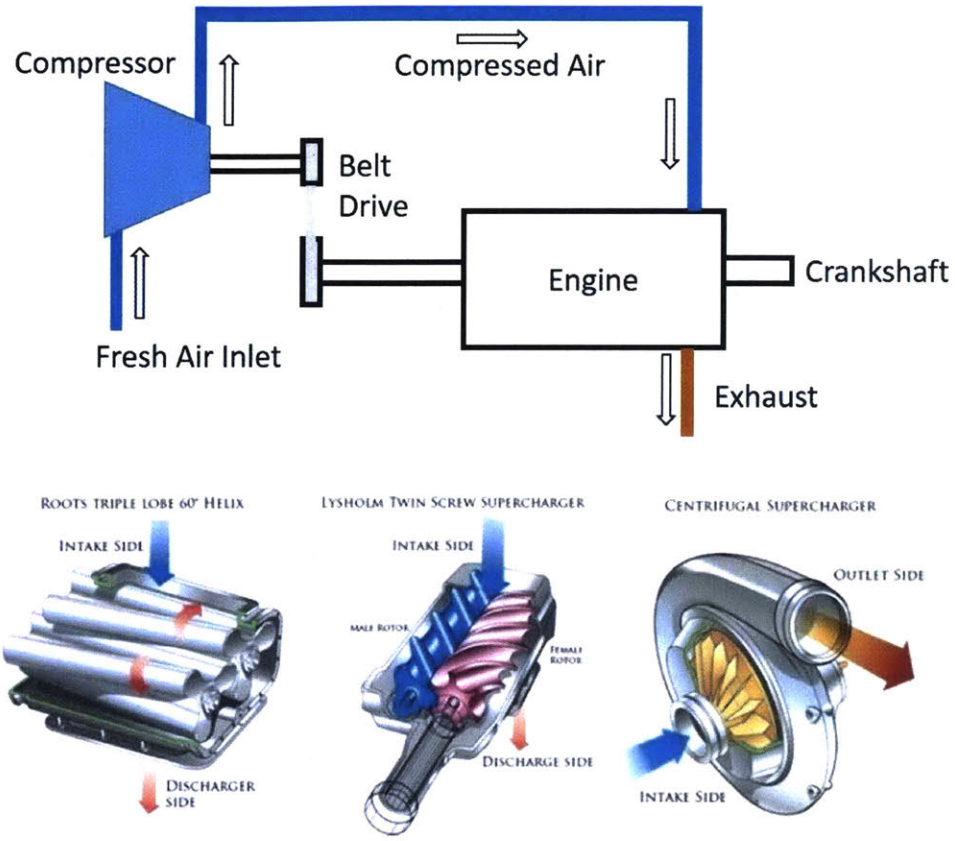

Figure 1-6: Top: Diagram of how a supercharger is integrated into an engine system. Bottom: figures of how three common types of superchargers work [7]

is an effective technology that can increase the power output of any engine and is resistant to the pulsating nature of the intake air. However, supercharging is inefficient since it draws power from the engine's mechanical output [67, 61]. A turbocharger uses an axially connected compressor and turbine. The turbine is powered by the energy from the exhaust gas (Fig. 1-7). The turbine then spins the compressor which pressurizes the intake air. This technology was chosen because it can be used to make the engine more efficient in addition to increasing power density [67].

The idea of charging an engine in order to increase the amount of air in the engine and thus its power output dates back to the late nineteenth century when internal combustion engines were first being introduced [35]. The original schemes involved supercharging. In 1905 the first turbocharging scheme was proposed in a patent

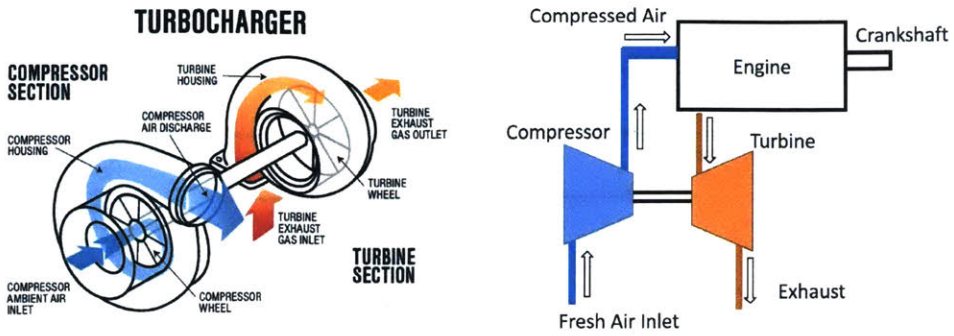

Figure 1-7: Left: Diagram of a turbocharger [8] Right: Diagram of how a turbocharger is integrated into an engine system.

by Alfred Buechi [35]. However, not until 1925 were the first turbocharged engines manufactured for a pair of passenger ships [35]. In 1938 the first turbocharged truck engine was produced by Swiss Machine Works [6]. During the Second World War supercharging schemes became commonly used in order to increase the power density of planes operating at high altitude.

The first attempt at turbocharging automobile engines was by Chevrolet and Oldsmobile in the early sixties [6]. This attempt was considered a failure due to reliability issues. It took until the OPEC oil embargo, a decade after the failed first attempt, for turbochargers to become popular due to the fuel efficiency advantages that they provide [6]. Today turbocharging is common in almost all truck engines and diesel vehicles as a means to reduce fuel consumption and emissions. Turbocharging has been shown to reduce both fuel consumption and CO_2 emissions by 2-6% [2].

Due to the pulsating nature of the manifold flows, turbocharging is not currently used in four-stroke single-cylinder engines [11]. It has been shown that when the engine is exhausting the turbocharger is energized and provides the power that is needed to make the compressor effective [33, 56]. In a multi-cylinder engine the system can be tuned such that when one cylinder is intaking a different cylinder exhausting; as a result the turbocharger is always powered when air is needed. In a direct application to a single-cylinder engine, a turbocharger would be powered during the exhaust stroke; however, it would not pump air to the engine during the intake stroke. As a result single-cylinder engines are not currently commercially

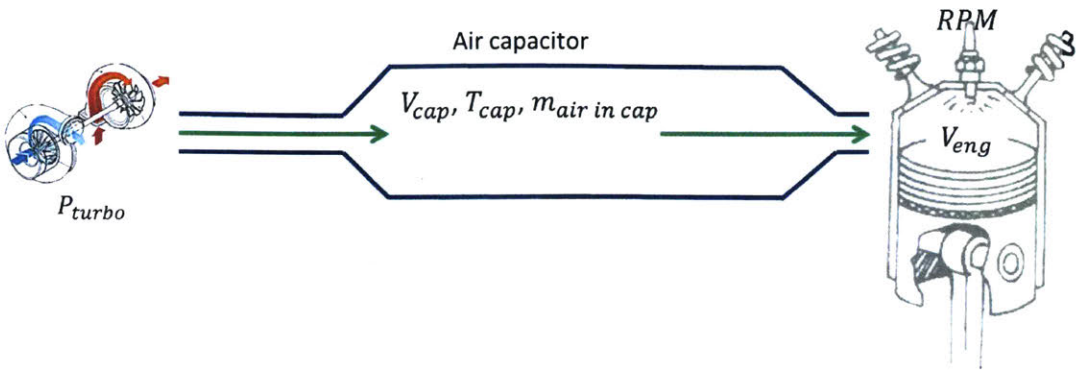

Figure 1-8: Diagram of the simple mass flow model used to describe flow in the intake manifold

turbocharged.

There are examples of single-cylinder engines that have been turbocharged by hobbyists and motor-sports enthusiasts [58]. In all these cases an oversized inter-cooler was used, which acted as an air capacitor. This supports the idea that the air capacitor method for turbocharging single-cylinder engines is feasible and that a better understanding of this effect can result in a commercially viable engine technology.

1.3 Previous Work

This work is based on a patent and an initial feasibility study on air capacitor turbocharging that demonstrated how this method could be used to increase the power output of a single-cylinder engine by up to 30% [15]. The initial work was based on an analytical model that predicted how an air capacitor affects a turbocharged single-cylinder engine [68].

A simple mass flow model can be used to describe the flow in the intake manifold during steady state operations and explain how the air capacitor works. Figure 1-8 shows how this model is laid out. The turbocharger is assumed to operate at a constant pressure P_{turbo}. The capacitor has a volume V_{cap}, a temperature T_{cap}, and contains a mass of air that fluctuates throughout the engine cycle. The engine is operating at a set speed and has a volume V_{eng}. For each cycle, the mass of air

flowing from the turbocharger into the air capacitor equals the mass of air flowing out of the air capacitor and into the engine (Eqn. 1.1).

$$\dot{m}_{in} = \dot{m}_{out} \tag{1.1}$$

For this simple model the assumption is that during the intake stroke the pressures in the air capacitor and in the engine equalize. From this assumption the mass flow out per cycle can be approximated as: (Eqns. 1.2 - 1.4). [42]

$$mass\ flow\ per\ cycle = \dot{m}_{out} * Cycle\ Duration = \frac{V_{eng}}{V_{eng} + V_{cap}} * m_{air\ in\ manifold} \tag{1.2}$$

$$Cycle\ Duration = \frac{120}{RPM} \tag{1.3}$$

$$\dot{m}_{out} = \frac{V_{eng}}{V_{eng} + V_{cap}} * m_{air\ in\ manifold} * \frac{RPM}{120} \tag{1.4}$$

The mass of air inside the manifold can be approximated using the ideal gas law and as a result the mass flow out of the air capacitor and into the engine can be calculated from known variables: (Eqns. 1.5- 1.6). [42]

$$m_{air\ in\ manifold} = \frac{P_{turbo} * V_{cap}}{R * T_{cap}} \tag{1.5}$$

$$\dot{m}_{out} = \frac{V_{eng}}{V_{eng} + V_{cap}} * \frac{P_{turbo} * V_{cap}}{R * T_{cap}} * \frac{RPM}{120} \tag{1.6}$$

Using the ideal gas law, the airflow through a naturally aspirated engine can be approximated as: (Eqns. 1.7-1.9).

$$\dot{m}_{Naturally\ Aspirated} = \frac{P_{ATM} * \dot{V}}{R * T_{ATM}} \tag{1.7}$$

$$\dot{V} = V_{eng} * \frac{RPM}{120} \tag{1.8}$$

$$\dot{m}_{Naturally\ Aspirated} = \frac{P_{ATM} * V_{eng}}{R * T_{ATM} * 120} \tag{1.9}$$

By knowing the mass flow in the turbocharged case and the naturally aspirated case, we calculate the density gain due to turbocharging (Eqn. 1.10). Note that the density gain will be equivalent to the change in mass flow rate since the engine volume remains constant in both cases. Density gain is proportional to power gain. This result shows the influence of air capacitor size on power output. The influence of cooling in the air capacitor can also be modeled by assuming the air undergoes isotropic compression inside the turbocharger (Eqn. 1.11). From this simple analysis it can be shown that increasing the volume of an air capacitor increases the effectiveness of a turbocharged single-cylinder engine with diminishing marginal return and that adding heat transfer elements to the air capacitor can significantly improve the performance (Fig. 1-9). [42]

$$Density\ Gain = \frac{m_{turbo}}{\dot{m}_{Naturally\ Aspirated}} = \frac{P_{cap} * V_{cap} * T_{atm}}{P_{atm} * T_{Cap} * (V_{eng} + V_{cap})} \tag{1.10}$$

$$T_{cap\ no\ heat\ transfer} = T_{atm} * (\frac{P_{turbo}}{P_{atm}})^{(\gamma-1)/\gamma} \tag{1.11}$$

An initial experiment was built to validate the turbocharging concept (Fig. 1-10). A single-cylinder diesel generator was retrofitted into a simple dynamometer. The generator engine was fitted with a turbocharger and an array of sensors. The load on the engine was provided by a series of space heaters [15]. This experiment showed that peak power output was directly affected by air capacitor size in a trend that closely matched the analytical model (Fig 1-11). In addition to the power output increase, it was shown that as the air capacitor size increased so did the intake pressure and

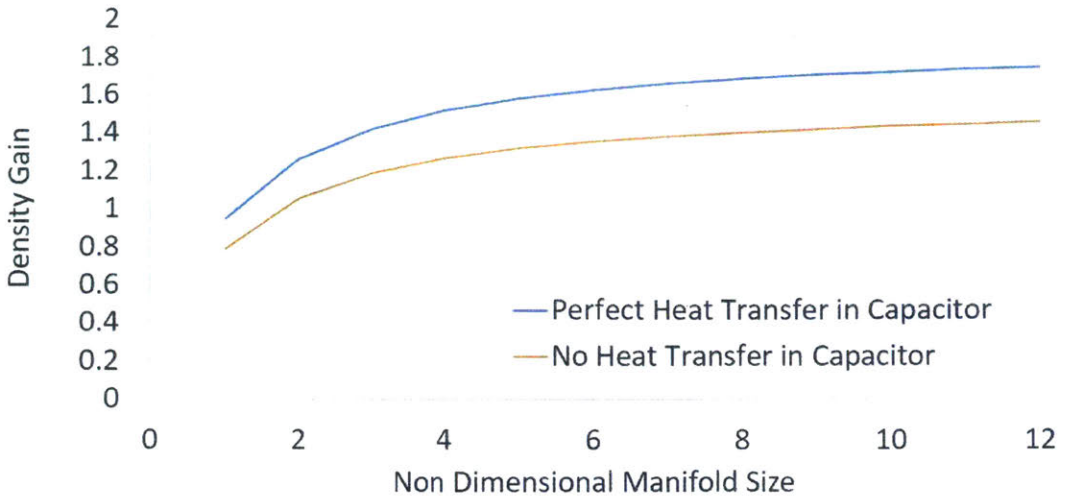

Figure 1-9: Plot showing the results for the simple mass flow model with and without heat transfer. In this scenario the turbocharger is operating at pressure of one bar.

the intake air density. This simple experimental setup was able to show that air capacitor turbocharging could increase the power output of a single-cylinder engine by 33% without cooling [15].

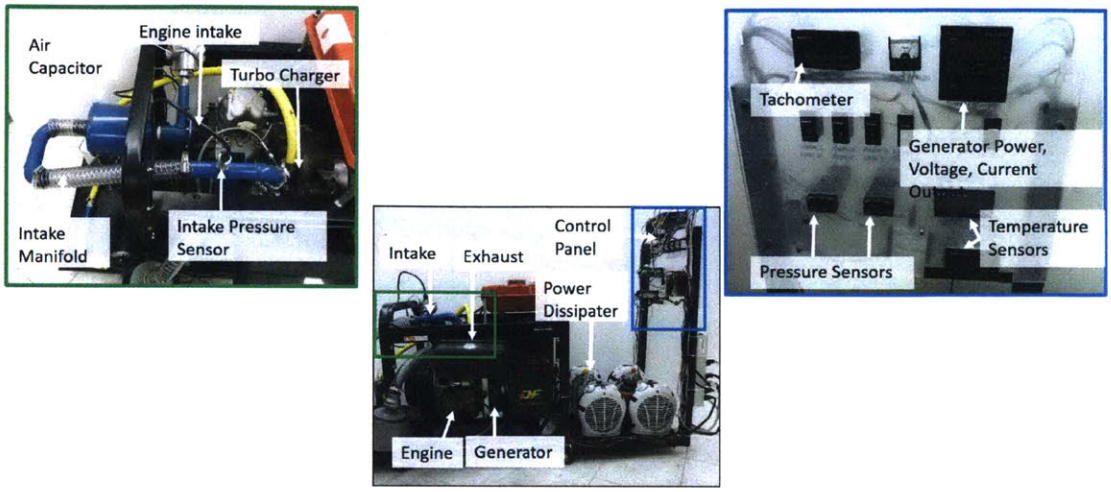

Figure 1-10: The initial experiment used to validate the air capacitor theory.

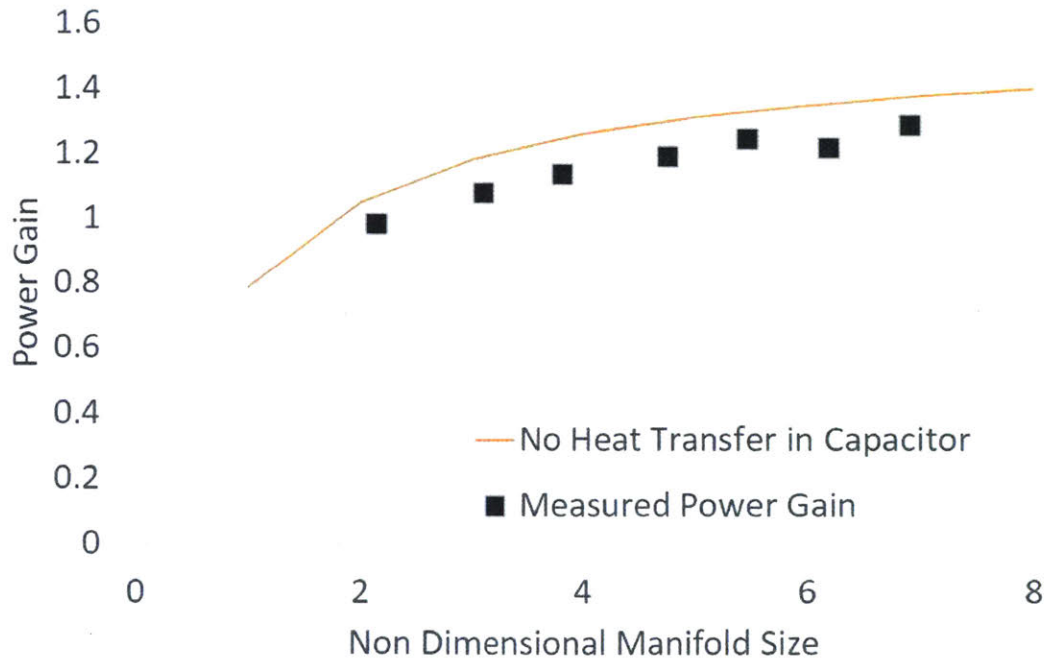

Figure 1-11: Results of the initial experiment compared to the simple mass flow model with no heat transfer and a turbocharger pressure of 13 psi (waste-gate pressure).

Chapter 2

Computational Model

An initial computational model was built in Ricardo Wave. The goal of this model was to predict the impact of air capacitor sizing and engine parameters on overall engine performance. Since this initial model was unvalidated, it was not designed to accurately predict engine performance. Instead, the model was used to predict trends on how the engine with an air capacitor would perform relative to its naturally aspirated state and to gain insights on trends and relative impact of engine parameters on performance. Initially, a naturally aspirated model of the engine was created and then it was augmented with a turbocharger to generate a turbocharged model.

These models were initially run directly in Ricardo Wave. However, it was found that the results of the models were more accurate and the post-processing of results was simpler when the models were run through Matlab and Simulink. The improvement in accuracy was due to the custom convergence detection that was built into the Simulink model.

2.1 Goals of Model

There were two key goals for this initial model. The first was to be able to predict trends and magnitudes. The model could be used to understand the impact of manifold characteristics and engine parameters on the overall performance of the system. This was used to predict how to size the air capacitor as well as how to adjust engine

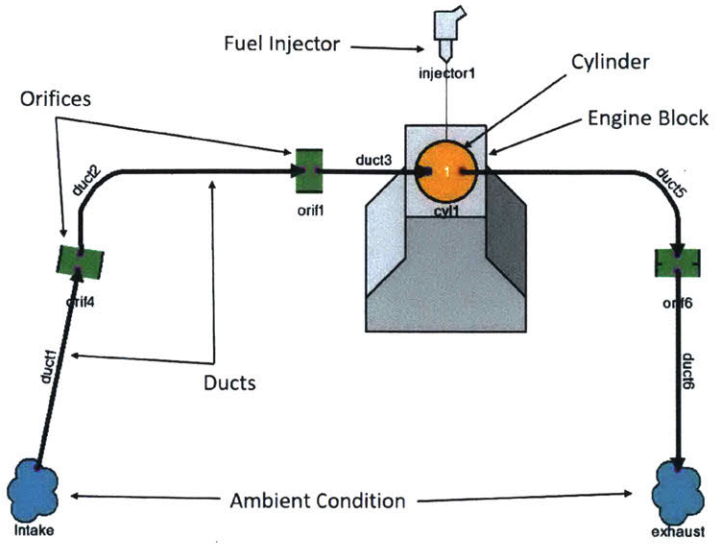

Figure 2-1: Block diagram that shows the layout of the naturally aspirated model, each subsystem is defined by a series of parameters.

timings to best utilize the boost coming from the capacitor.

The second key goal was to create a framework that could be calibrated to the data generated by the engine experiment. Using the experimental data it was possible to validate the model and to further optimize the system. The model validation is shown in Chapter 4 and how it was used to optimize the engine is discussed in Chapter 6.

2.2 Model Overview

The model was built in Ricardo Wave, a one dimensional engine modeling software. The parameters of the initial model were based on the engine used in the experiment (Kohler KD440), values recommended by Ricardo Wave, and literature. The naturally aspirated model is pictured in Figure 2-1. The model consists of a series of blocks that define the engine, the manifolds, the fuel injector, and the valves.

The turbocharged model builds on the naturally aspirated model by adding a compressor, a turbine, and a turbine shaft to the system. The turbocharger was

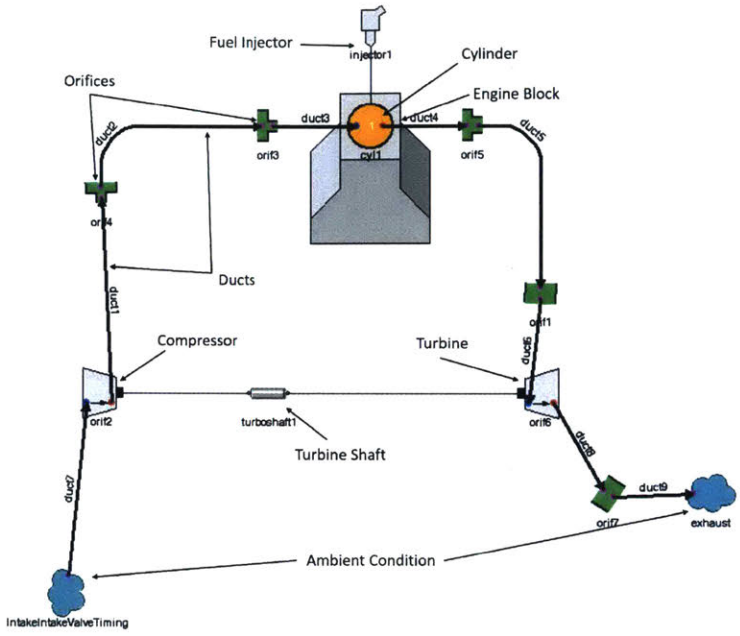

Figure 2-2: Block diagram that shows the layout of the turbocharged engine model, each subsystem is defined by a series of parameters.

modeled after the Garrett GT0632SZ, a small turbocharger manufactured by Honeywell Garrett. Its comprehensive set of operating specifications was used to create a virtual model of the turbocharger in Ricardo Wave.

2.2.1 Valves

In order to accurately model the engine air flow, the valves were defined. The valve geometry and lift were taken from the engine's operation manual and verified by measurements taken on the engine used in the experiment (Kohler KD440). The valve lift profile was defined by the Ricardo Wave fast lift polynomial equation based on the distance from valve max lift (Fig. 2-3 & Eqn. 2.1). x is the distance from valve max lift. $x = -1$ at valve open and $x = 1$ at valve close. The valve flow coefficient was defined by the Ricardo Wave high performance valve flow sub-model 2-4.

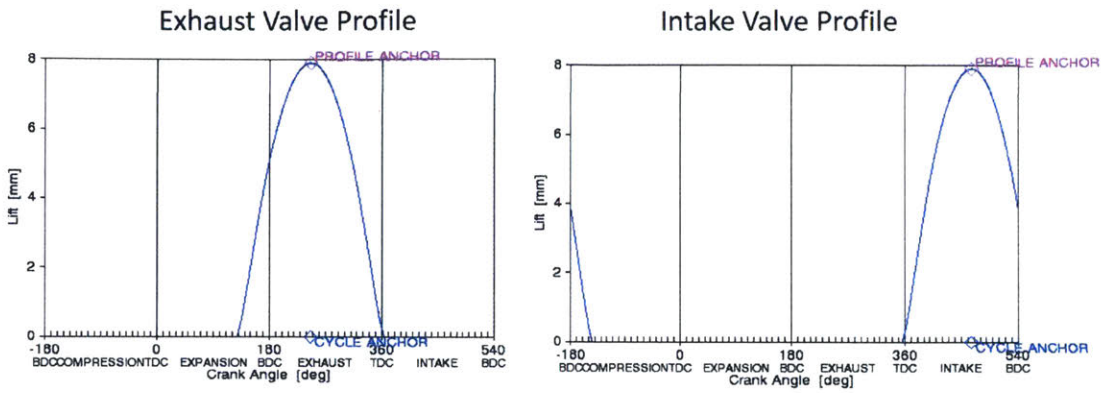

Figure 2-3: Plot showing the valve lift profile used in the Ricardo Wave mode.

$$ValveLift = MaxLift * (1 + -1.242x^2 + 0.255 * x^{12} + 0.102 * x^{68}) \quad (2.1)$$

2.2.2 Engine Sub-models

The engine friction, combustion, heat transfer, and emissions are defined by a series of models built into the Ricardo Wave software. Engine friction was modeled with the Chen-Flynn friction model (Eqn. 2.2) [18]. The friction constants were based on literature (Tab. 2.1) [46]. A Diesel Wiebe model with a centane number of 50 [30, 36] was used to calculate engine combustion. Heat transfer is modeled using the Woschni model with the heat transfer multipliers both set to 1 [70]. Emissions were calculated using an arrhenius equation to predict rate of formation of NOx [38].

$$FMEP = A + B * PeakPressure + C * n + D * n^2 \quad (2.2)$$

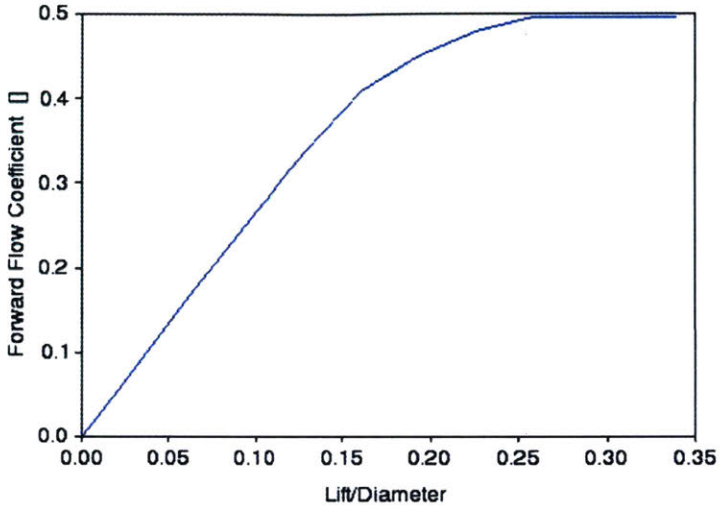

Figure 2-4: Ricardo Wave high performance valve flow model. This model was used to estimate the flow through both the intake and exhaust valve.

Table 2.1: Friction constants that were obtained from literature [46].

Calibration Constant	**Units**	**Range**	**Mean Value**
Chen-Flynn Friction A	bar	0-0.5	0.3
Chen-Flynn Friction B	1	0.004-0.006	0.005
Chen-Flynn Friction C	$\frac{pa*min}{m}$	130-170	150
Chen-Flynn Friction D	$\frac{pa*min^2}{m^2}$	0.016-0.032	0.024

2.2.3 Cylinder Geometry

The cylinder geometry was based on the Kohler KD440 engine specifications. The engine was modeled as having the properties in Table 2.2. These values were verified on the real engine through measurement.

Table 2.2: Kholer engine geometry based on data from manufacturer [41]

Bore	86 mm
Stroke	86 mm
Connecting Rod Length	125 mm
Compression Ratio	20.3 mm
Bore	86 mm
Piston Bowl Depth	5 mm
Piston Bowl Diameter	50 mm

2.2.4 Ducts & Orifices

Heat transfer, pressure losses, and the air capacitor effect in the manifolds are modeled using duct and orifice elements. These elements are modeled in the software as one dimensional flow elements that are broken down into a series of small cells. In addition to modeling the air flow in the engine manifolds, the model also uses the pressures inside these cells to check for model convergence.

2.2.5 Ambient Conditions

The ambient condition controlled the way the model treated the intake air properties, the conditions at the exhaust port, and the conditions on the outside surfaces of the modeled engine (engine block & ducts). The ambient temperature was defined as 298k and the ambient pressure was defined as 1 bar.

2.2.6 Fuel Injection

The fuel and the injector properties were based on the Kohler KD440 engine specifications and the model defaults for a diesel engine. The injection pressure was defined

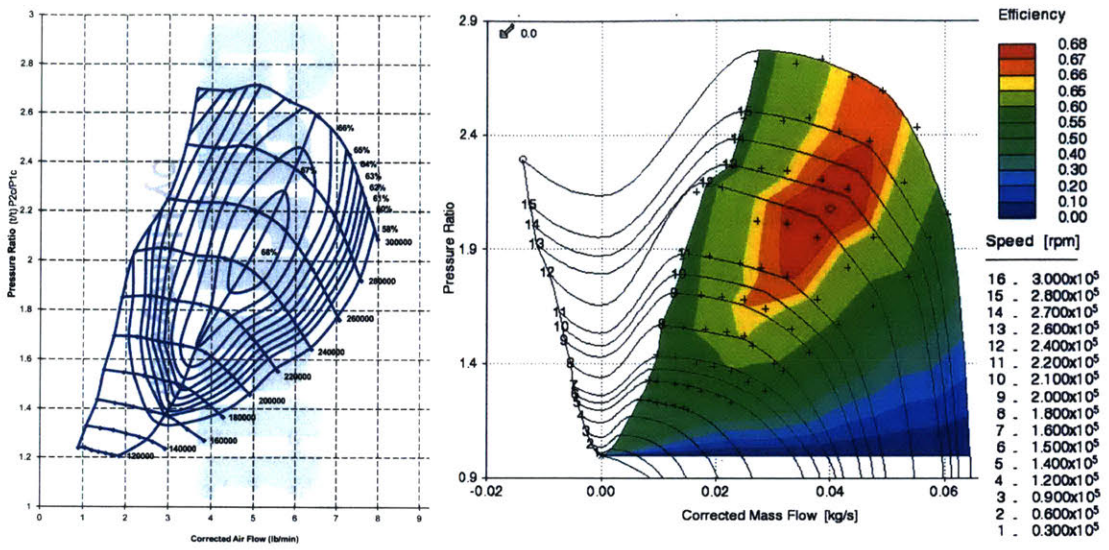

Figure 2-5: Left: Real compressor map for the Garrett GT0632SZ. Right: Garrett GT0632SZ compressor map that was recreated in Ricardo Wave.

as 500 bar. The injection was timed to start six degrees before top dead center and to last twenty degrees. The model defines a set air-to-fuel ratio in the injector element and solves for power output. In the cases where the power was defined and air-to-fuel ratio needed to be solved for, the Matlab/Simulink simulation controller iteratively adjusted the fuel-to-air ratio until the power output converged at the target power output.

2.2.7 Turbocharger

The turbocharger used in the model is the Garrett GT0632SZ. Using manufacturer data the Garrett compressor map was recreated in the Ricardo Wave software (Fig. 2-5). The turbine map was similarly recreated in the Wave model. The turbocharger shaft element was used to model the inertia of the system ($2.4 * 10^{-6} kg \cdot m^2$) and to couple the turbine speed and compressor speed in the model [29].

2.2.8 Integration with Matlab & Simulink

In order to better control the convergence and to better process data output, the model was integrated with Matlab and Simulink. Simulink acted as an interface between Matlab and Ricardo Wave. The Matlab code fed model parameters into Simulink, such as equivalence ratio, engine speed, and any other relevant running parameters. These parameters were then fed into Ricardo Wave. The Ricardo Wave model was then run while the Simulink model checked for convergence. Convergence was defined as the point where every cell pressure and temperature was within 0.1% of its value from the previous iteration. The Simulink model then fed the results back into the Matlab control code and the results were stored in a CSV file.

2.3 Model Results

This initial model was used to predict the effects of turbocharging and air capacitor sizing on the engine's performance. The model was run for a sweep of air to fuel equivalence ratios (Eqm. 2.3) at low, mid, and high speed. The model was also run at fixed equivalence ratios to explore the effects of air capacitor sizing, injection timing and heat transfer in the air capacitor on power output, fuel consumption, and NOx emissions.

$$\lambda = \frac{Air\ to\ fuel\ Ratio}{Stoichiometric\ Air\ to\ fuel\ Ratio} \tag{2.3}$$

2.3.1 Initial Model

Initially, the model was used to evaluate the effect of turbocharging on power density, fuel economy, and emissions performance on the engine. The turbocharged engine configuration modeled was the same as the experiment presented in Chapter 3 (Fig. 2-6). Figure 2-7 shows the results of this model. At high equivalence ratios, the turbocharger acts as a constriction and reduces the power density. However, at low

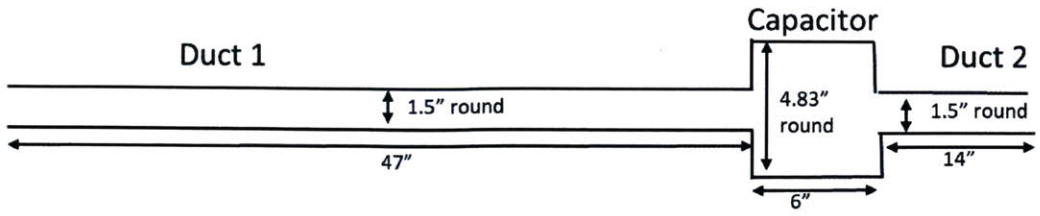

Figure 2-6: Intake manifold used in the model. The ducts are modeled as rubber while the capacitor is modeled as steel. This is identical to the manifold dimensions used in the experiment.

equivalence ratios the turbocharger can improve engine power density by over 30%.

The model predicts that turbocharging will increase nitrous oxide emissions. This is most likely due to two factors

- The increase in air density in the engine results in more oxygen for the nitrogen to react with.
- The increase in the amount of energy released in the turbocharged combustion raises the temperature in the cylinder.

The engine is predicted to be less efficient then the naturally aspirated engine and as a result have an increase in fuel consumption. In order to determine where the inefficiency is coming from, the modeled engine losses are plotted in Figure 2-8. The three main losses are pumping, frictional, and heat transfer losses.

The plot of heat transfer losses shows that the turbocharged engine will have an increase in losses of over a kilowatt at higher power. This accounts for a significant portion of the total losses. The friction losses plot shows that the turbocharger increases frictional losses slightly (up to 0.4 kW). This is due to the increase in peak cylinder pressure that happens during turbocharging. This effect on friction is directly accounted for in the Chen-Flynn friction model (EQN. 2.2) [18]. Finally, pumping losses, which is the energy used to pump the air into and out of the engine, accounts for up to 2 kW of additional losses.

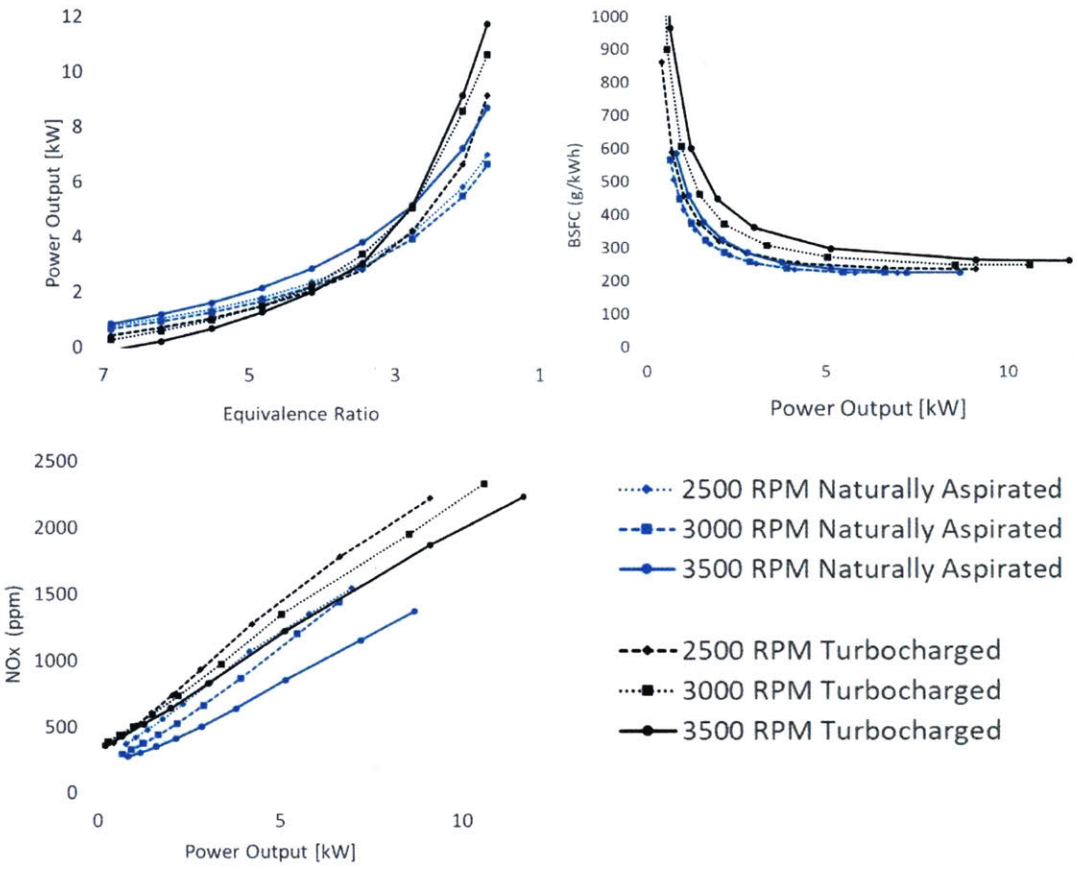

Figure 2-7: Model comparison of the naturally aspirated case to the turbocharged case (in the configuration that matches the experiment). Top left: Power output as a function of equivalence ratio. Top right: Brake-specific fuel consumption as a function of power output. Bottom left: Nitrous oxide emissions as a function of power output.

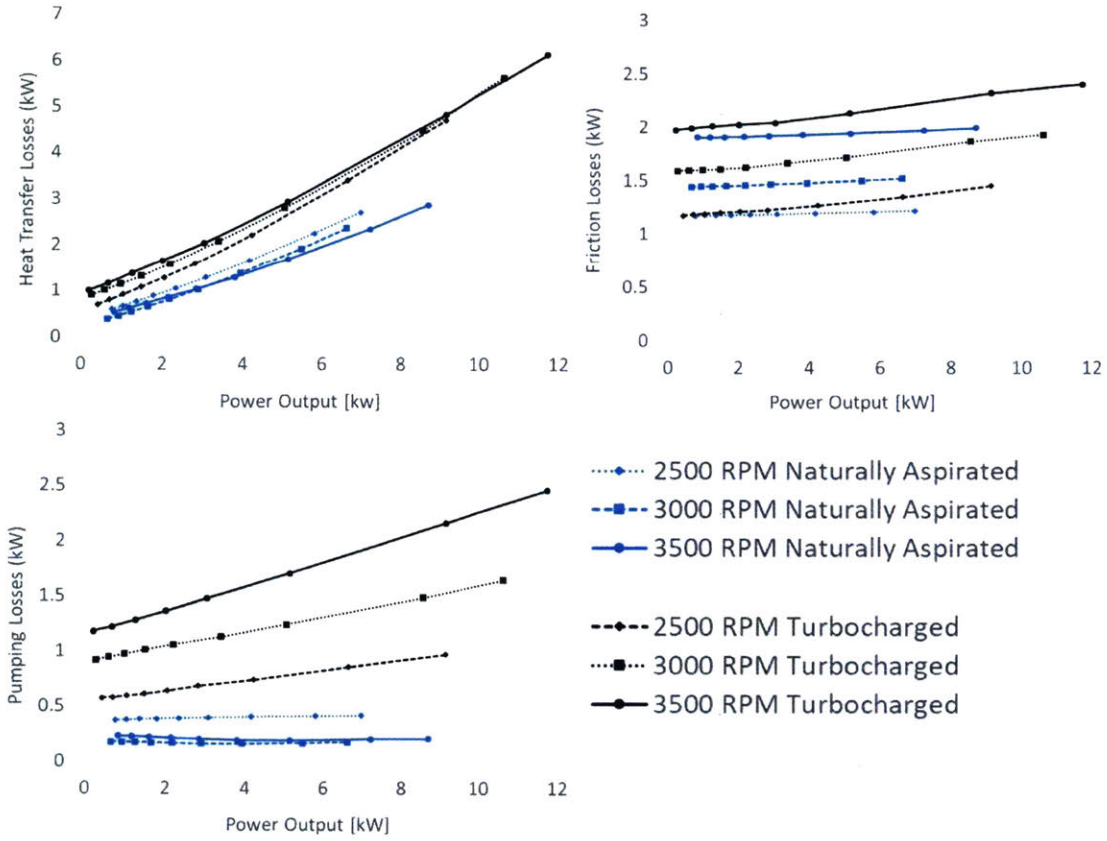

Figure 2-8: Model comparison of the losses in the naturally aspirated case to the losses in the turbocharged case (in the configuration that matches the experiment). Top left: Heat transfer losses as a function of power. Top right: Engine friction losses as a function of power. Bottom Left: Pumping losses as a function of power.

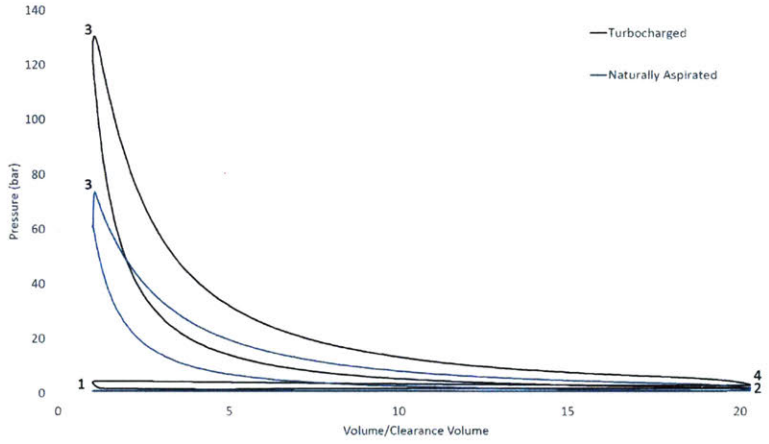

Figure 2-9: Comparison of pressure vs. volume plot for the turbocharged case to the naturally aspirated case at 3500 RPM with an equivalence ratio of 2. 1→2: Intake stroke. 2→3 Compression Stroke. 3 → 4: Power Stroke. 4→1: Exhaust stroke. The loop made by 4→1→2 is the pumping loop. The loop made by 1→3→4 is the power loop.

The effect of turbocharging on a thermodynamic level cn be observed through the pressure vs. volume (PV) and temperature vs. entropy curves (TS) which are plotted for the 3500 RPM case with an equivalence ratio of 2 (Figs. 2-9 & 2-10). The PV curve shows that the turbocharged case operates at higher pressures and as a result produces more power per cycle (demonstrated by the larger power loop) than the naturally aspirated case. However, the turbocharged case has a significantly larger pumping loop which results in significantly higher pumping losses.

The TS curve shows that the turbocharged case operates at a higher temperature than the naturally aspirated case and as a result operates at a larger temperature difference. This also results in less heat added per unit of working fluid during the heat addition stage and less heat rejected during the heat rejection stage of the cycle per unit of working fluid.

2.3.2 Capacitor Size Effects

One of the key effects that was analyzed was the impact of manifold volume on the performance of the engine. The engine was modeled with the air capacitor layout

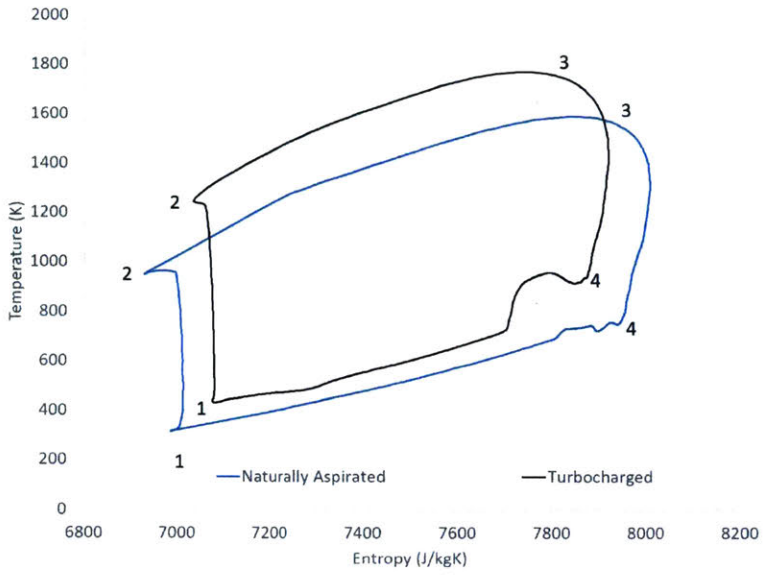

Figure 2-10: Comparison of temperature vs. entropy for the turbocharged case to the naturally aspirated case at 3500 RPM with an equivalence ratio of 2. 1→2: Compression. 2→3 Heat Addition. 3 → 4: Expansion. 4→1: Heat Rejection.

shown in Figure 2-11. The model consisted of two rubber ducts and a fixed diameter metal air capacitor. Rubber ducting was used to allow for the experiment to be run with multiple manifolds sizes. The length of the capacitor was varied in order to model different capacitor volumes.

The engine was modeled with a fixed equivalence ratio of 2 and at 2500, 3000, and 3500 RPM with capacitor sizes ranging from 3 to 10 times the engine volume. The results of the model are shown in Figure 2-12. The model showed that as the capacitor size increased, the engine power output increased by 16% between the largest and smallest capacitor size modeled. This effect of air capacitor volume was more pronounced at higher speeds. The gains come from two sources:

- The increase in efficiency shown by the reduction in the brake specific fuel consumption as manifold size increase (by 2.1% between the largest and smallest capacitor size modeled).

- The improvement in the air mass flow rate due to the air capacitors buffering effect (by 13.9% between the largest and smallest capacitor size modeled).

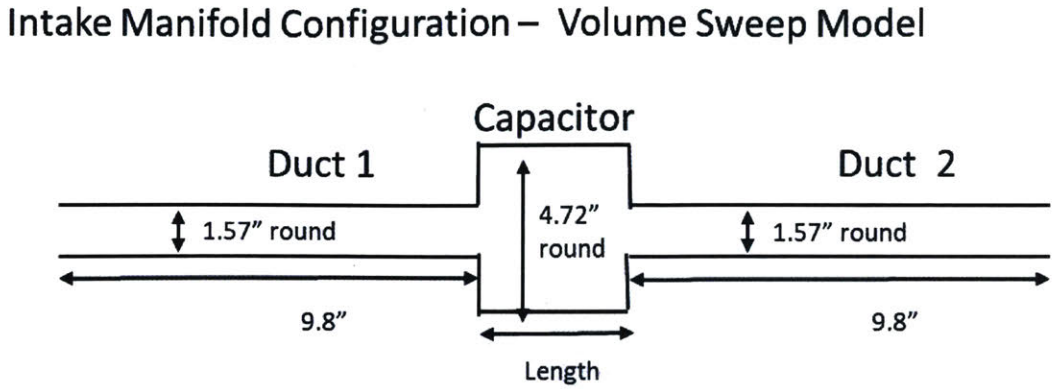

Figure 2-11: Intake manifold used in variable volume model where the ducts are modeled as rubber while the capacitor is modeled as steel. The volume is varied by changing the length of the manifold.

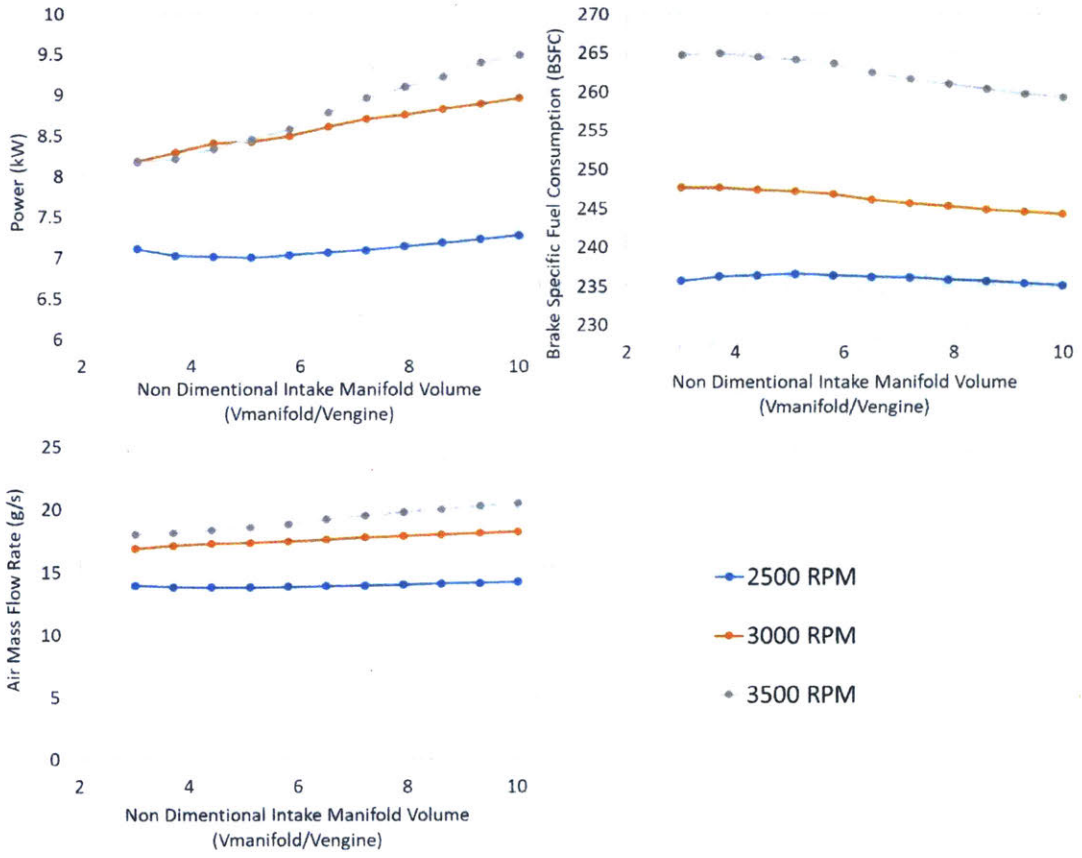

Figure 2-12: The results of the variable volume model for an engine running at an air to fuel equivalence ratio of 2. The effect of manifold volume on power, brake specific fuel consumption, and air mass flow rate are shown.

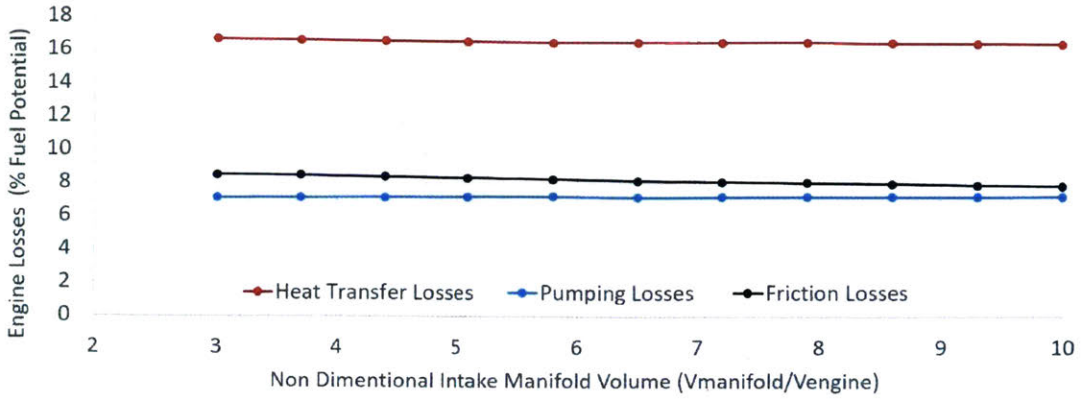

Figure 2-13: The effect of manifold volume on engine losses for an engine running at an air to fuel equivalence ratio of 2. The losses are shown as a percent of the fuel energy that they consume.

The modeled engine losses for the 3500 RPM case are plotted in to determine the effect of capacitor size on engine losses (Fig. 2-13). The larger air capacitor has a negligible effect on pumping losses. However, it reduces friction losses by 8% between the largest and smallest capacitor size modeled. This is most likely due to the increase in power density of the engine, which results in more power being produced with the same frictional area. Increasing air capacitor size also reduces heat transfer losses by 2% between the largest and smallest capacitor size modeled. This is most likely due to the better heat transfer in the larger capacitor.

In order to see the effect of the air capacitor volume on the engine's performance, the air flow through the intake manifold of the engine over a cycle was modeled in Ricardo Wave since air flow is directly related to the amount of power the engine can produce. The model was run for the two extreme cases: the ten times engine volume air capacitor and the two times engine volume air capacitor.

The effect of the air capacitor on air flow into the engine is shown in Figure 2-14. This shows the mass flow of air 10 cm before the intake valve. It is clear from the plot that the mass flow of air into the engine is larger with the larger air capacitor. There is a negative spike in air mass flow rate just after the intake valve opens and just after the exhaust valve closes. This back flow is most likely due to the cylinder pressure being higher than the intake pressure. The average mass flow is approximately zero

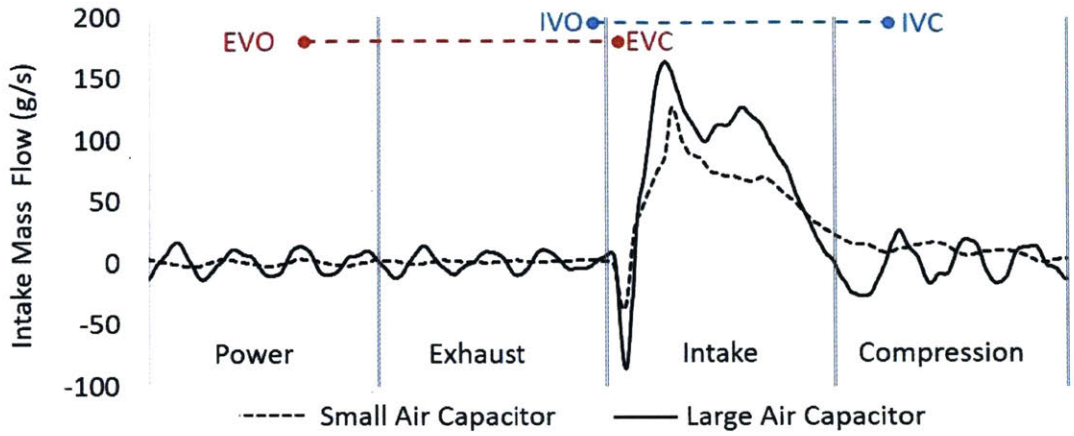

Figure 2-14: Comparison of the inlet mass flow of air in the capacitor throughout the cycle for the large air capacitor (10 times engine volume) and the small air capacitor (2 times engine volume) sfor an engine running at 3500 rpm with an equivalence ratio of 2. The unsteadiness in the air mass flow during the compression, power and wxhaust strokes are due to pressure waves in the air capacitor.

when the intake valve is closed since the air has nowhere to go. The slight variation in mass flow numbers while the intake valve is closed are most likely due to pressure waves in the manifold.

The effect of the air capacitor on the air flow through the engine can be better understood by modeling the pressure and density of air in the capacitor over an engine cycle (Figs. 2-15 & 2-16). The intake air pressure and density of air is higher with the large air capacitor than with the small air capacitor. Both capacitors experience a drop in air pressure and density during the intake followed by a gradual recharge during the other three strokes. Both engine configurations reach approximately the same pressure and density during recharge. However, during intake, the smaller air capacitor experiences a drop in air pressure and density more than three times that of the large capacitor. The smaller air capacitor results in the engine intaking less air than the large air capacitor configuration and, therefore, produces less power. The pressure and density in the air capacitor spiked right after the intake valve opens. This is most likely due to back flow of air from the exhaust and could be mitigated by adjusting valve timings.

The analysis of air flow in the capacitor throughout a cycle showed the effect of

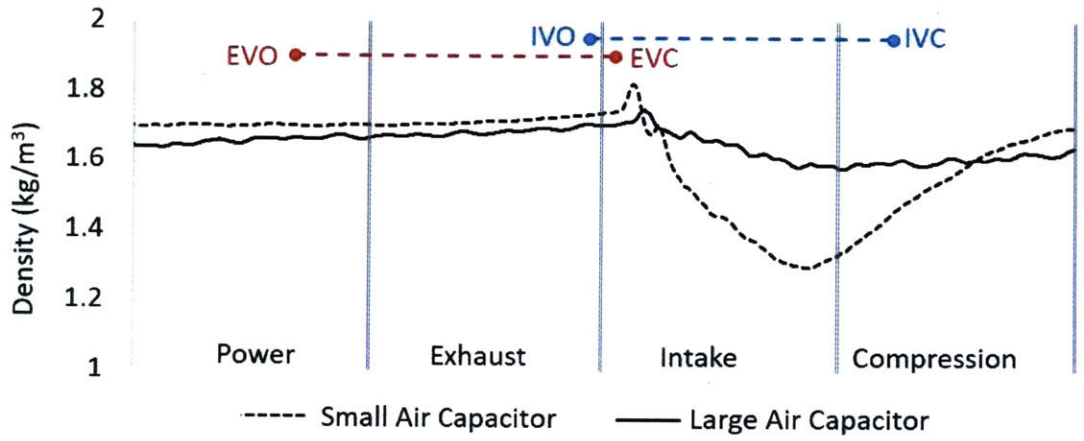

Figure 2-15: Comparison of the air density in the capacitor throughout the cycle for the large air capacitor (10 times engine volume) and the small air capacitor (2 times engine volume) for an engine running at 3500 rpm with an equivalence ratio of 2.

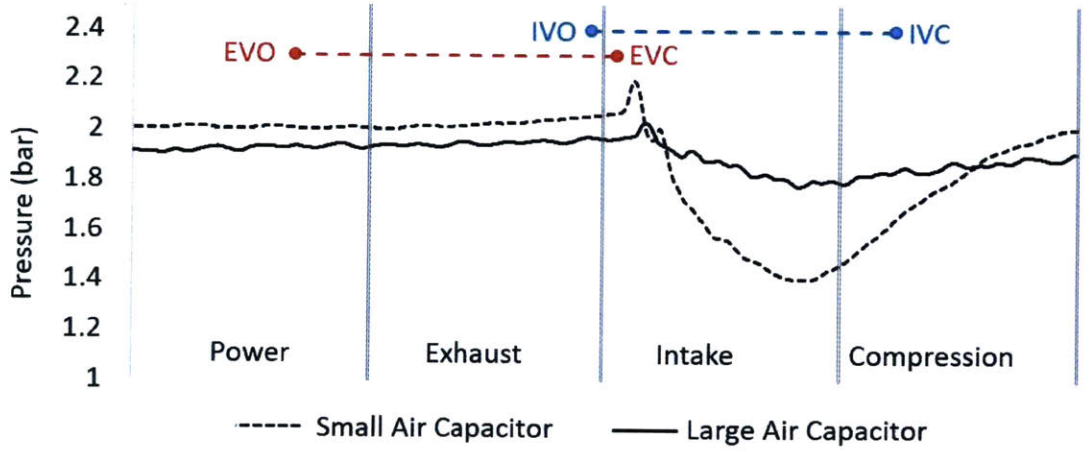

Figure 2-16: Comparison of the pressure in the capacitor thought the cycle for the large air capacitor (10 times engine volume) and the small air capacitor (2 times engine volume) for an engine running at 3500 rpm with an equivalence ratio of 2.

manifold size on engine performance. The benefit of having a larger air capacitor that can store a significant amount of air is clearly shown. There is also backflow into the intake manifold during the beginning of the intake stroke when the intake and exhaust valve are both open. This effect can be mitigated by adjusting the valve timings.

2.3.3 Heat Transfer Effects

One of the potential sources of heat transfer losses is the compression of the intake air. In order to model the effects of this loss the long tubes connecting the compressor, air capacitor, and engine were simulated as high heat transfer metal instead of rubber (ducts 1 & 2 in Figure 2-6).

The results of the model with heat transfer elements are shown in Figure 2-17. The first plot shows power output as a function of equivalence ratio. The model shows that when heat transfer elements are added, the power output of the engine increases by up to 80% over the naturally aspirated condition, which is a significant increase over the 30% power gain that was observed with no heat transfer. The increase in power gain is due to two factors. First, the intake air density is higher since it is cooler. Second, there is a reduction in heat transfer losses due to the cooler intake air.

The model also demonstrated that intercooling significantly decreases nitrous oxide emissions. This is due to the intake air being cooler, resulting in less nitrous oxide forming.

The effect of heat transfer on fuel economy is also shown in Figure 2-17. Adding heat transfer has a minimal effect on fuel economy at lower power and a notable effect on fuel economy at higher power. This is due to the fact that heat transfer has a minimal effect at low power when the turbocharger does not significantly compress the air and, as a result, does not increase the intake air temperature. At higher powers the effect of heat transfer is more noticeable due to the intake air being heated by the process of compression. However, the fuel consumption with heat transfer is still larger than the naturally aspirated fuel consumption.

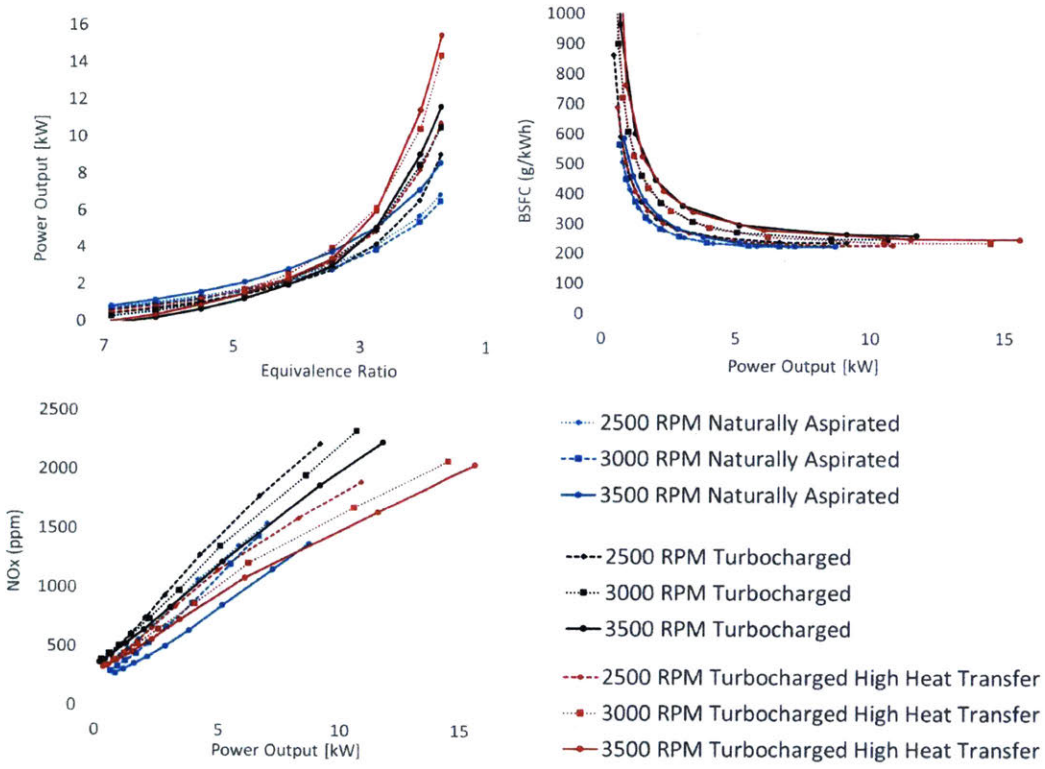

Figure 2-17: Model comparison of the naturally aspirated case to the standard turbocharged case (in the configuration that matches the experiment) and the high heat transfer turbocharged case. Top left: Power output as a function of equivalence ratio. Top right: Brake specific fuel consumption (BSFC) as a function of power output. Bottom Left: Nitrous oxide emissions as a function of power output.

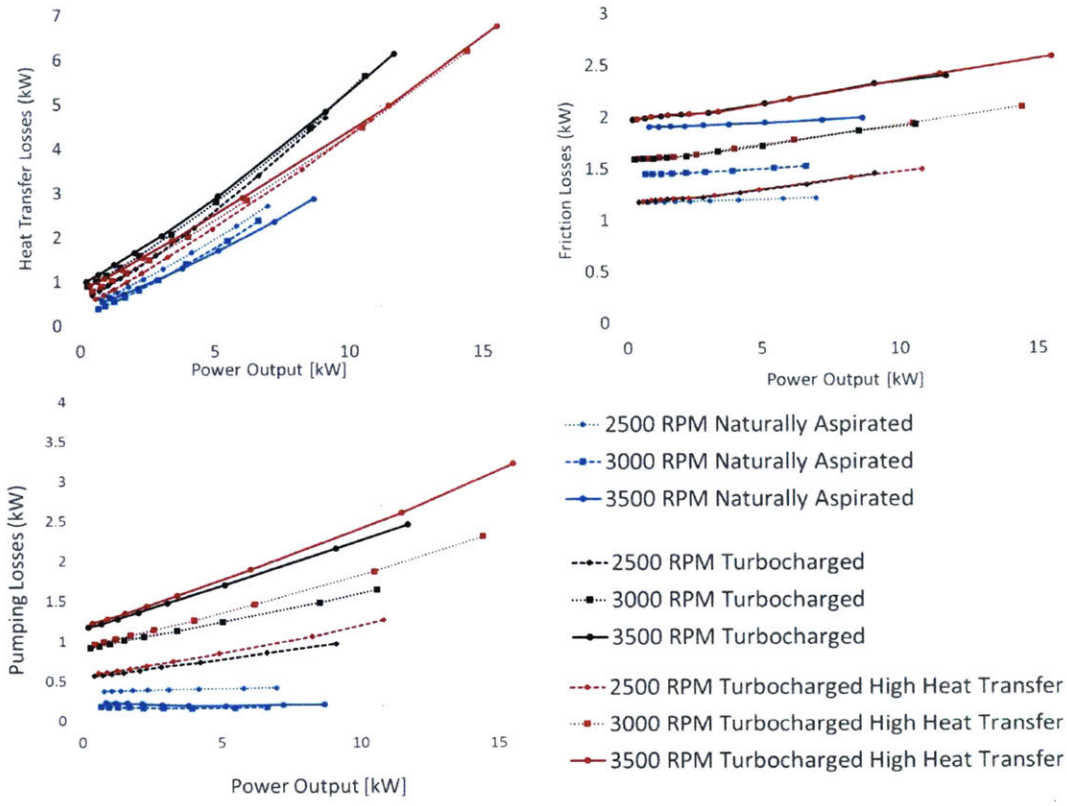

Figure 2-18: Model comparison of engine losses in the naturally aspirated case, the standard turbocharged case (in the configuration that matches the experiment), and the high heat transfer turbocharged case. Top left: Heat transfer losses. Top right: Friction losses. Bottom Left: Pumping losses.

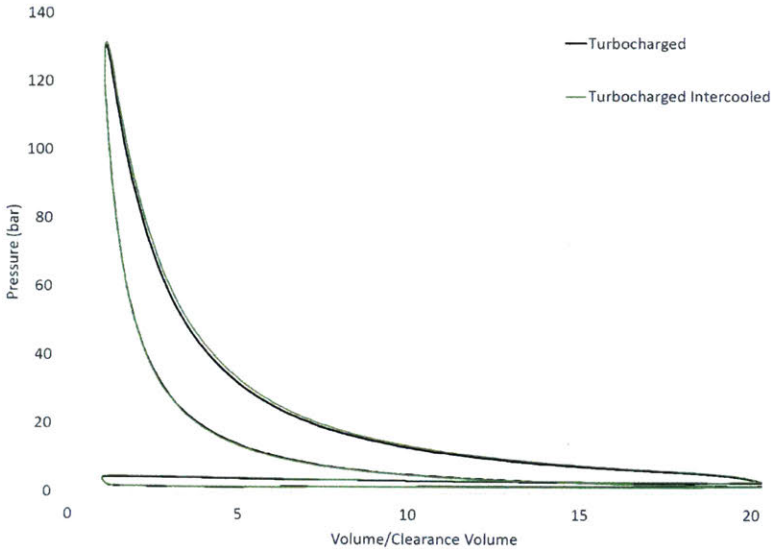

Figure 2-19: Comparison of Pressure Vs. Volume for the standard turbocharged case and the intercooled turbocharged case at 3500 RPM with an equivalence ratio of 2.

In order to analyze the effect of adding heat transfer on engine efficiency the modeled losses are plotted in Figure 2-18. The heat transfer losses were noticeably affected by cooling the intake manifold. At lower powers cooling had a minimal effect on heat transfer losses while at higher powers it had a significant effect. This is due to the increase in intake temperatures caused by the compressor being larger at higher powers.

Adding the heat transfer elements to the intake manifold had no effect on frictional losses and only a small effect on pumping losses due to the increase in the air mass flow rate. However, in the modeled case, the shape of both the heat transfer and other manifolds were the same. In the case of adding a real intercooler to the engine the flow channels will be smaller and the pumping losses would be expected to increase [40].

The effect of heat transfer on a thermodynamic level cn be observed through the pressure vs. volume (PV) and temperature vs. entropy curves (TS) which are plotted for the 3500 RPM case with an equivalence ratio of 2 (Figs. 2-19 & 2-20). The PV curve shows that the inter cooled case produces higher pressures during the power stroke and, as a result, produces more power per cycle than the naturally aspirated

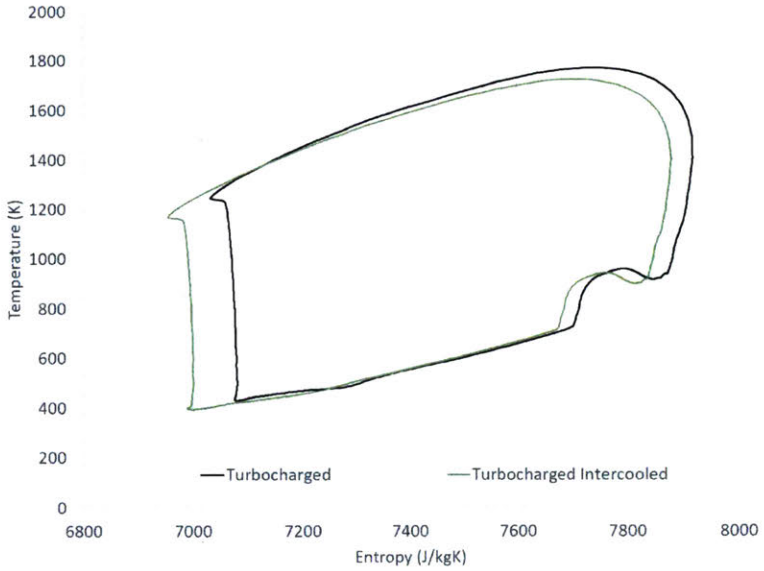

Figure 2-20: Comparison of Temperature vs. Entropy for the standard turbocharged case to the inter cooled turbocharged case at 3500 RPM with an equivalence ratio of 2.

case. Both case have a similar pumping loop which results in a similar amount of pumping losses. The TS curve shows that the inter cooled case operates over a larger temperature range at a lower temperature than the baseline turbocharger case and, as a result, is more efficient.

2.3.4 Injection Timing

An analysis on injection timing was done in order to determine the effects of injection timing on fuel economy and emissions and to determine if the optimal injection timing for the turbocharged case was different from the naturally aspirated case. To test the effects of injection timing on engine performance, a sweep of engine timings were modeled for an engine running at 3500 rpm with an air to fuel equivalence ratio of 2 (Fig 2-21).

The optimal injection timing to minimize fuel consumption was fourteen degrees before top dead center. The fuel-consumption-minimizing timing was earlier than the power-maximizing timing of 8 degrees before top dead center. However, both of these

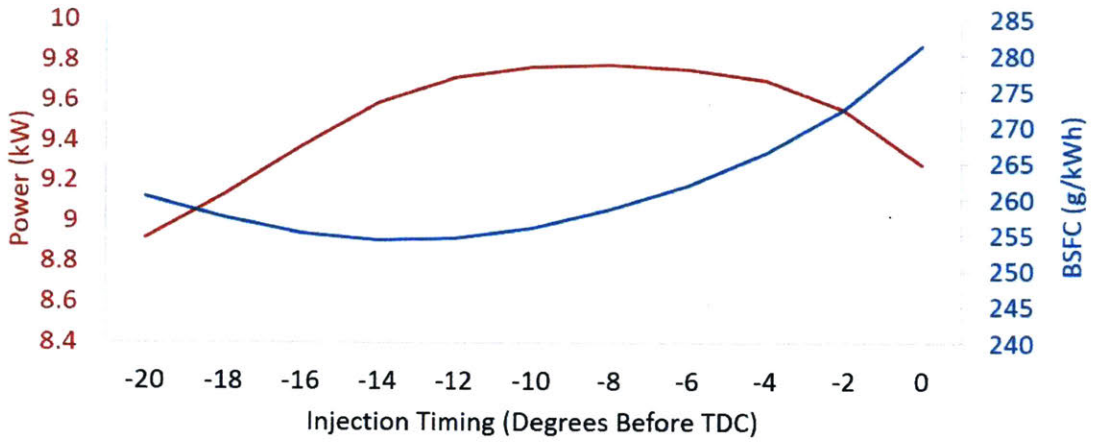

Figure 2-21: The effect of injection timing on an air capacitor turbocharged 3500 RPM engine with an air to fuel equivalence ratio of 2.

timings are earlier than the naturally aspirated injection timing of six degrees before top dead center.

Chapter 3

Experimental Setup

A test engine was designed and built with the goals of demonstrating the air capacitor method for turbocharging single cylinder engines and validating the model. The engine consisted of a single cylinder diesel engine modified to be fitted with a turbocharger, an interchangeable manifold system, and a series of sensors. An eddy current dynamometer was used to load the engine. This system could measure emissions, fuel economy, manifold temperatures, manifold pressures, and power output.

The experimental setup is diagrammed in Fig. 3-1 and pictured in Fig. 3-2. The setup consists of five subsystems: a controls system, an engine, a dynamometer, a data acquisition system, and a series of sensors. The setup was designed to run both steady-state and transient engine tests in order to determine the effect of turbocharging and manifold design on a single cylinder engine.

3.1 Goals of Experimental Setup

Four key performance characteristics of the engine were tested:

1. Power Output: This will determine how much added utility the engine user will get. Models and previous work have shown that power output can be improved by 40% to 60% through turbocharging [15].

2. Emissions: Diesel emissions can cause environmental damage and impact health

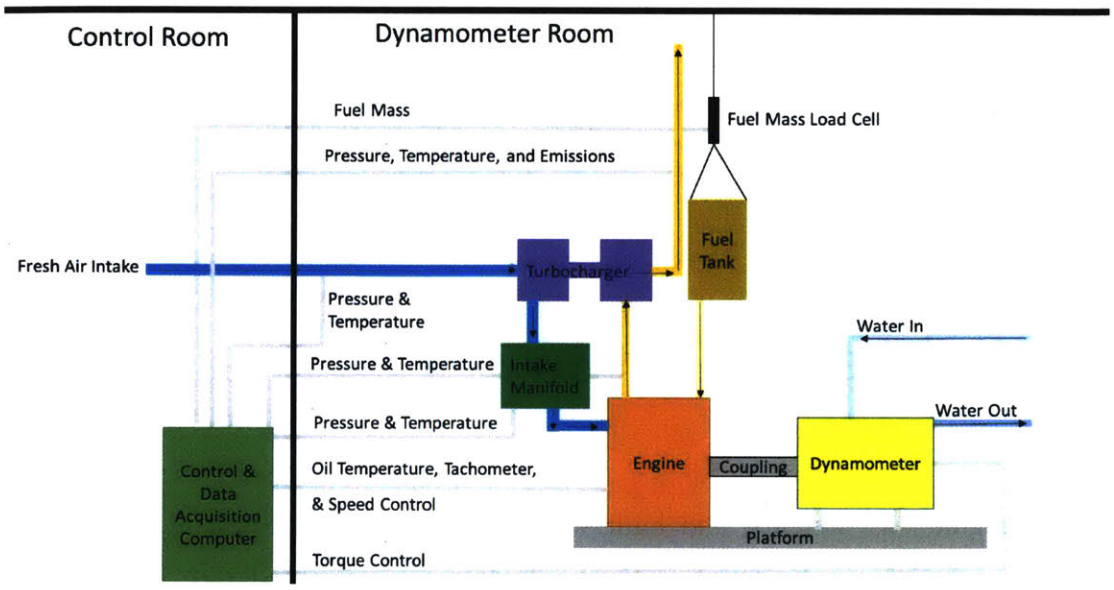

Figure 3-1: Block diagram that shows the layout of the experimental setup.

Figure 3-2: Photographs of the experimental setup with key parts identified. A: Full view of dynamometer room (Fig. 3-1). B: Focused view of the dynamometer and engine platform. C: Focused view of the controls system.

both chronically and acutely [71, 43]. Due to the volume of engines sold, incremental improvements in emissions can result in a significant improvement in air quality [22]. Regulatory bodies have already noted this and small engines which previously had no emissions regulations are now being regulated [39]. Turbocharging can be used to mitigate some of the performance losses caused by emissions after treatment [55]. Characterizing the turbochargers' tailpipe emissions is important in order to determine appropriate emissions after treatment strategies.

3. Fuel Economy: Turbocharging can affect fuel economy in many ways and, as a result, impact commercial viability of an engine. Turbocharging a smaller engine can improve fuel economy by having the engine produce the same power output as a larger engine, partially by allowing for fewer frictional losses. This is because a smaller engine has less frictional area between the piston and the cylinder. It can also improve fuel economy due to larger mass flow rates of air, which increase heat transfer in the engine, thus reducing cooling losses. However, turbocharging can also increase fuel consumption by increasing pumping losses [67, 34].

4. Transient Response: One of the effects of turbocharging is the added response time to speed and torque changes [53, 52, 17, 31]. Turbocharging by default has a lag time associated with the spooling of the turbine that is dependent on the engine speed and turbocharger size. Air capacitor based turbocharging of single cylinder engines will entail additional lag time due to the time it takes to fill the air capacitor. This will be a concern in certain applications such as single cylinder rickshaws and small vehicles, which are prevalent in developing nations such as India. Adequate transient performance is necessary for vehicles to navigate traffic.

In order to characterize and optimize the engine, the engine was initially tested under turbocharged conditions with multiple intake manifold sizes and under a naturally aspirated condition. Additional experiments were run in order to validate the

Table 3.1: Taylor DE20 Eddy Current Dynamometer specifications

Maximum Power	20 kW
Maximum Torque	80 Nm
Maximum speed	12,000 RPM
Inertia Value	0.0125 $m^2 \cdot kg$
Calibration Arm Length	0.4572 m
Calibration mass	9.07 kg

**Data From Manufacturer [63]*

computational model.

3.2 Dynamometer

The dynamometer selected was a Taylor DE 20 small engine dynamometer (Fig. 3-3). This dynamometer was selected for its small size, relatively low cost, and high accuracy. The dynamometer's accuracy is determined by the load cell used, the distance from the dynomometer's center to the load cell, and the calibration accuracy [63]. In order to get the most accurate reading possible the load cell used was one with the narrowest possible range while still being able to accommodate the maximum expected torque from the engine. In the model, the maximum torque from the engine was expected to be up to 60% larger than the rated torque due to turbocharging. Equations 3.1-3.2 show the calculation of how the load-cell was sized. It was found that a load cell with a range of at least 207 N was needed. The Sherborne Sensors U400 load cell with a 250 N range was selected because the brand was recommended by Taylor Dynamometer for reliability & accuracy and it was in the required range (Tab. 3.2).

$$LoadCellSize = \frac{MaximumTorque}{LeverArm} \tag{3.1}$$

$$LoadCellSize = \frac{1.6 * 22 \text{ Nm}}{0.17 \text{ m}} = 207 \text{ N} \tag{3.2}$$

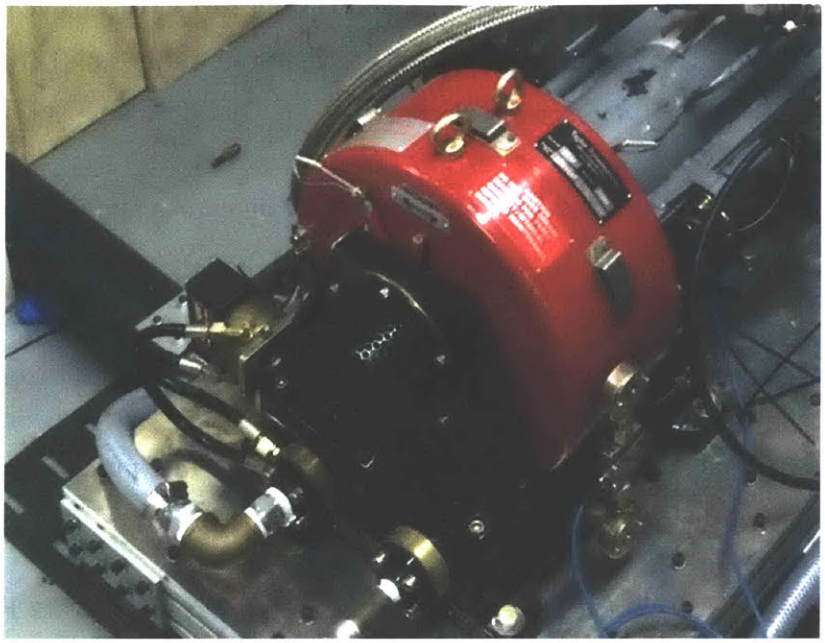

Figure 3-3: Photograph of the dynamometer installed and mounted to the engine pallet.

Table 3.2: Sherborne Sensors U400 Load Cell specifications

Length Mounted From Dynamometer Center	0.17 m
Load Cell Range	250 N
Excitation Voltage	10 VDC
Full Scale Output	2.7 $mV/Volt$
Combined Error	± 0.03 % $FullScale(max)$
Non-repeatability Âś	± 0.015 % $FullScale(max)$
Thermal Zero Shift	± 0.002 % $FullScale/C$
Thermal Sensitivity Shift	± 0.002 % $FullScale/C$

**Data From Manufacturer [57]*

3.3 Engine

The engine selected was the Kholer KD440, a direct injected diesel engine with a 0.44 liter displacement. The engine specifications are shown in Table 3.3. This particular engine was selected for the following reasons:

- It is readily available and is commonly used in numerous applications.
- It has a built-in mechanical governor that allows for simple speed control.
- Due to the way it is designed, it is simple to modify and add a turbocharger.

The fuel used in this experiment was standard diesel fuel purchased at a local Shell Station and the oil used was SAE 10W-30.

Table 3.3: Kholer KD440 Air Cooled Diesel Engine specifications (Data From Manufacturer [41])

Maximum Power	6.8 kW
Maximum Torque	22 Nm
Maximum speed	3,600* RPM
Displacement	441 cm ^{3}· kg
Bore	86 mm
Stroke	76 mm
Compression Ratio	20.3:1

**note that the engine has data for up to 3,600 RPM but is recommended for operation at a maximum of 3,000 RPM*

3.4 Turbocharger

Turbocharger selection was simplified by the lack of options. At the time the experiment was set up there was only one commercially available turbocharger that was small enough for this application, a third party version of the IHI RHB31 turbocharger made by Ecotrons (note that the IHI model was unavailable. This turbocharger (Fig 3-4) is designed for an engine between 150cc & 600cc [25]. An oil system was built for

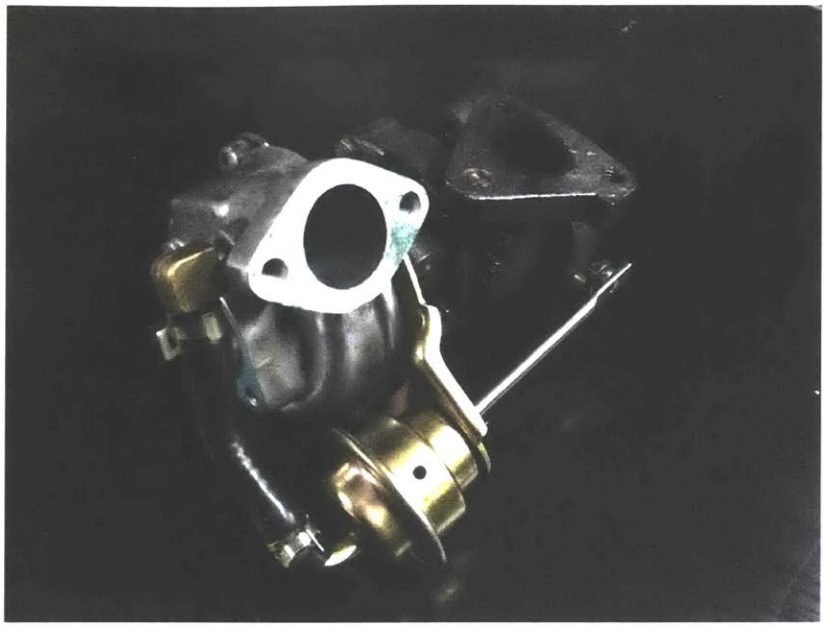

Figure 3-4: Photograph of the IHI turbocharger.

the turbocharger since the engine did not have a built-in oil pump. This oil system consisted of two gear pumps, an oil reservoir, an oil cooler, and an oil filter. The temperature of the reservoir was monitored using a k type thermocouple to ensure that the oil did not overheat.

The IHI turbocharger was able to increase the intake density of the air and demonstrate the effect of an air capacitor. However, it underperformed, only increasing air density by up to 0.3 Bar and the manufacturer did not provide any performance data making it difficult to model. To address these shortcomings a Garrett GT0632SZ was procured. The Garrett turbocharger was able to increase pressure by 0.7 Bar and came with data from the manufacturer allowing it to be well characterized.

3.5 Manifolds

For the initial set of experiments, five intake manifolds were created that connected the turbocharger's compressor outlet to the engine intake. These manifolds (Fig. 3-5) were designed with minimal flow losses to test how different intake manifold volumes affected the engine's overall performance. They were also designed to have

approximately the same length in order to control for the effect of manifold resonances on engine performance. To achieve this, the smaller two manifolds were high pressure hoses with 1.5 inch internal diameter. The larger three manifolds consisted of a volume made out of steel connected to the engine intake and compressor intake by two high pressure hoses with a one and a half inch internal diameter.

A custom exhaust manifold was created to connect the engine to the turbocharger's turbine inlet. The exhaust manifold was designed to be structural, as small as possible, and to minimize flow losses [69].

3.6 Sensors, Data Acquisition, & Controls

A sensor setup that allowed for the measurement of all of the parameters associated with the goals of the experiment was needed. The setup also needed to be able to vary the engine speed and the load induced by the dynamometer. The Dyne Pro 2 data acquisition and control (DAQ) system made by Taylor Dynamometer was selected since it was built to interface directly with the dynamometer. In addition, the system offered eight pressure channels, sixteen thermocouple channels, four load cell channels, four analog inputs, four digital outputs, a mechanical throttle controller, and a way to directly interface with an emissions sensor.

The system (Fig. 3-6) consisted of three main components: a computer control center, a sensor box, and a connections enclosure all controlled by the Dyne Pro 2 software. The computer control station is located outside the dynamometer room and allows the operator to control the system. The sensor box contains all of the pressure junctions, the temperature junctions, and the weather station. The connections enclosure contains the load cell inputs, the analog inputs, the mechanical throttle controller and the digital outputs. In addition to these there are auxiliary systems: the dynamometer load controller, the emissions data acquisition system, and the electrical junction box.

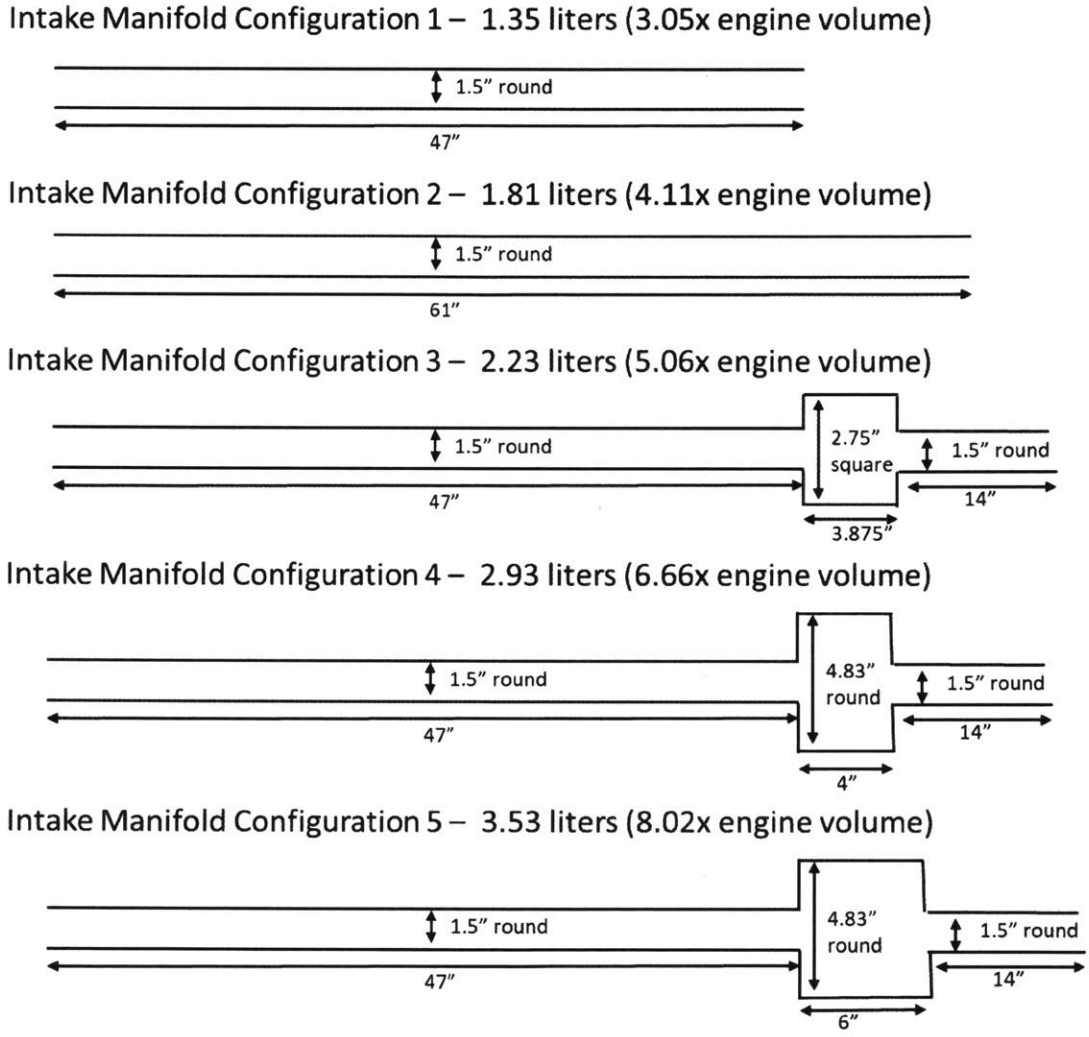

Figure 3-5: Diagram of the five intake manifold configurations tested initially. Figure is not to scale.

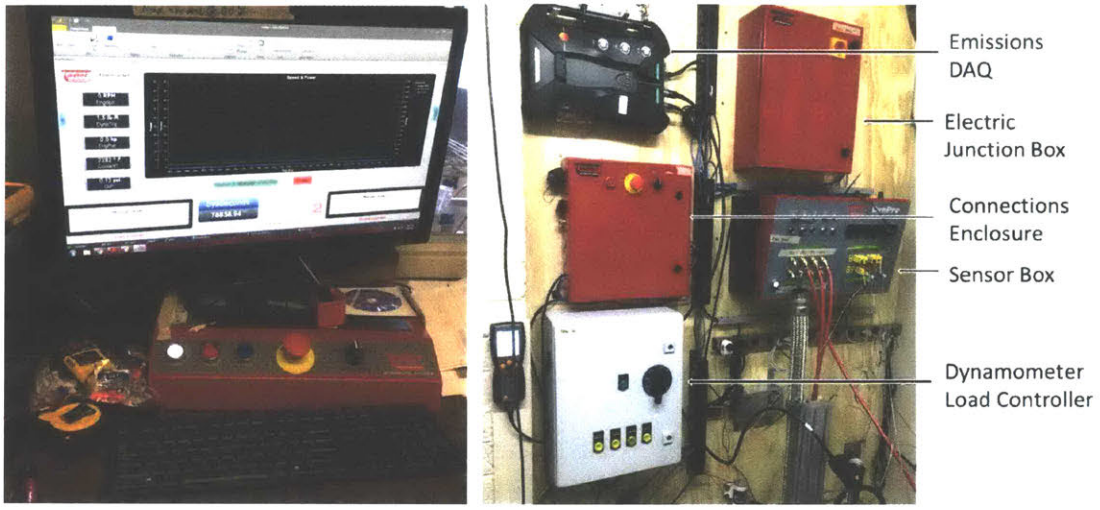

Figure 3-6: Photographs of the data acquisition and controls setup. Left: the operator control computer. Right: Labeled DAQ components.

3.6.1 Emissions

One of the key elements analyzed was steady state emissions characteristics (it was determined that transient emissions would be too expensive to test). The Testo 350 Portable Emissions Analyzer, was chosen to measure these characteristics due to its ease of integration with the engine and the data acquisition unit and its low cost relative to other emissions analyzers. The emissions analyzer sampled the exhaust gas through a port created in the exhaust manifold upstream of the turbocharger (Fig. 3-7). The analyzer's range, accuracy, and reaction time specifications for the gases analyzed in the experiment are listed below in Table 3.4.

3.6.2 Pressure

Pressure measurements were used to determine the effectiveness of the turbocharger and the manifolds. Pressure measurements were taken in the exhaust manifold both before and after the turbocharger, as well as in the intake manifold immediately after the compressor and just before the engine intake.

The sensors used to take the pressure measurements were built into the Taylor Dynamometer Sensor Box and connected to the experiment using pressure lines.

Table 3.4: Testo 350 Exhaust Gas Analyzer specifications [65] (mv stands for the measured value).

Gas	**Range**	**Accuracy**	**Reaction Time**
O_2	$0-25$ *vol %*	± 0.2 % *volume*	$20s$
CO_2	$0-50$ *vol %*	$\pm(0.3+0.01\cdot mv)$ % *volume*	$10s$
CO	$0-10000$ *ppm*	$\pm 5ppm$ (0 to 199 ppm) $\pm(5\cdot mv)$ % (100 to 2000 ppm) $\pm(10\cdot mv)$ % (2000 to 10000 ppm)	$40s$
NO_2	$0-500$ *ppm*	$\pm 5ppm$ (0 to 99 ppm) $\pm(5\cdot mv)$ % (100 to 500 ppm)	$30s$
NO	$0-4000$ *ppm*	$\pm 5ppm$ (0 to 99 ppm) $\pm(5\cdot mv)$ % (100 to 1999.9 ppm) $\pm(10\cdot mv)$ % (2000 to 4000 ppm)	$30s$

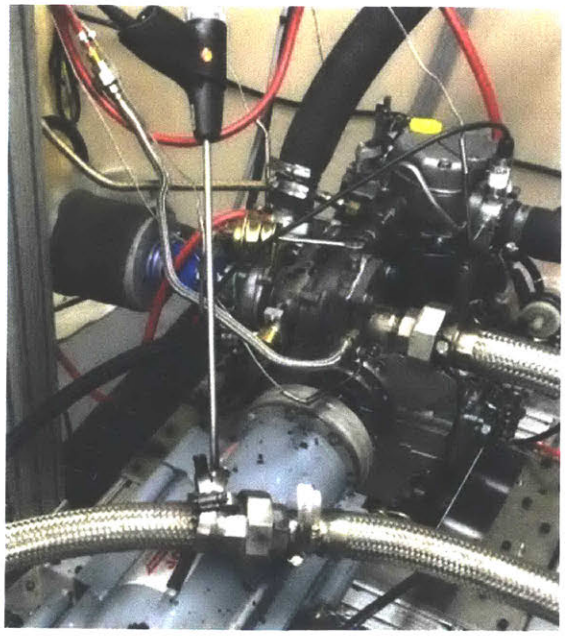

Figure 3-7: Photograph of the emissions probe sampling setup.

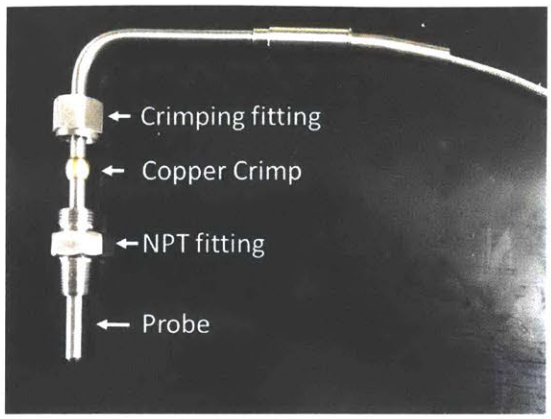

Figure 3-8: Photograph of the thermocouple probe with airtight fitting.

Each sensor was calibrated using a Fluke 718 pressure sensor calibrator to ensure the accuracy of the sensors and automatically compensate for the pressure drop in the pressure hoses.

3.6.3 Temperature

The temperature in the manifolds was measured using k type thermocouples. They have a range of 0 - 12000° C and are accurate to ±.75% of reading [20]. The thermocouples integrated directly with the Taylor Dynamometer Sensor Box, which has calibrated k type thermocouple inputs. Thermocouples were installed at the compressor inlet, compressor outlet, turbocharger inlet (same one as engine outlet), turbocharger outlet, and engine intake. The selected thermocouples were sealed using an NPT fitting with a copper crimp (Fig. 3-8). Additional thermocouples were also used to monitor ambient air temperature and the turbocharger oil temperature. The thermocouples would occasionally fail mid test, resulting in some tests with incomplete temperature data.

3.6.4 Fuel Mass

In order to measure fuel economy, the fuel mass was continuously measured using a load cell. The method works by calculating the mass of fuel used over time. This method was chosen due to its low cost relative to mass flow meters. While this

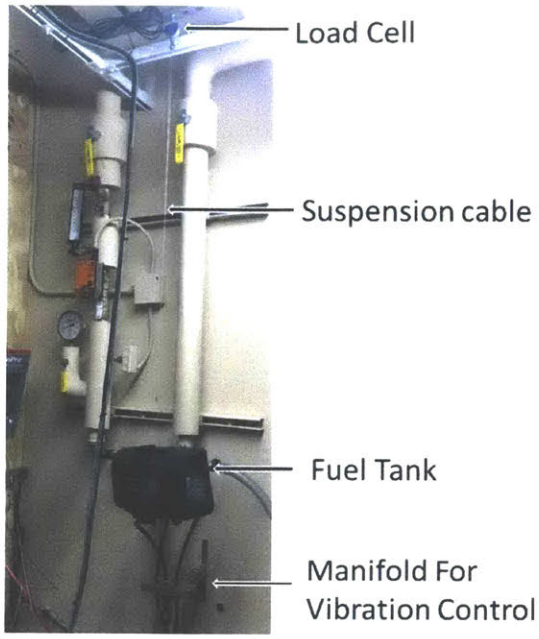

Figure 3-9: Photograph of the fuel measurement system.

method works well for steady state experiments, its effectiveness is limited in transient applications.

A wire suspended the fuel tank from a Omega S-Beam rugged load cell that had a twenty-five pound capacity (Fig. 3-9). The load cell specifications are shown in Table 3.5. In order to isolate the fuel tank from the engine vibrations, the fuel lines were run through a manifold mounted in the wall. The load cell was calibrated using 500 gram calibration weights.

Table 3.5: Omega load cell specifications (data from manufacturer [49])

Load Cell Range	25 lbs
Excitation Voltage	10 VDC
Full Scale Output	3.0 $mV/Volt \pm 0.25\%$
Linearity	$\pm 0.03\ \%FullScale(max)$
Non-repeatability Âś	$\pm 0.01\ \%FullScale(max)$
Creep (20 min)	$\pm 0.02\ \%FullScale/C$
Thermal Sensitivity Shift	$\pm 0.0027\ \%Reading/C$

Data from a test was analyzed to determine the frequency and duration of data

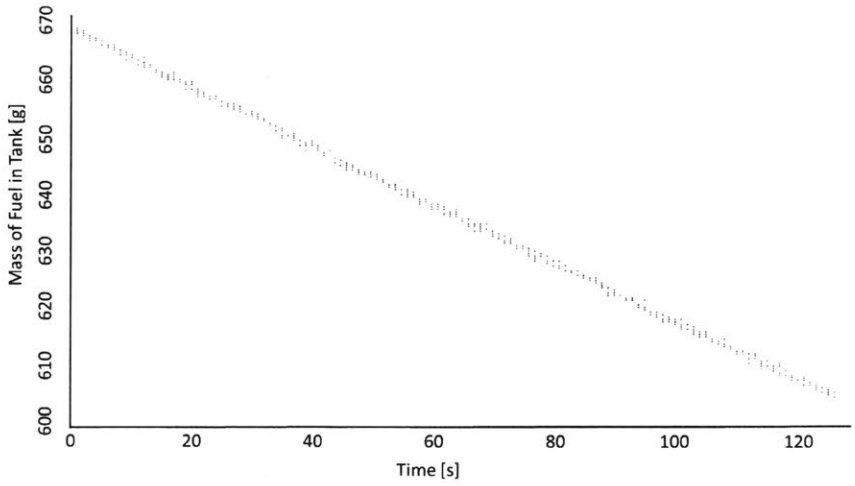

Figure 3-10: Sample data from the steady state fuel economy tests conducted at 3500 RPM & 6.8 kW. Individual points represent the load cell data collected at 4 Hz. The line is the best fit line generated by the Matlab linear regression function. The fuel consumption is 263.33 grams per kW hour with a 95% confidence interval of $\pm$ 0.55 grams per kW hour.

collection required to accurately measure fuel economy. The test was performed at low speed and low power in order to have the most conservative estimate on how long the tests would run, since the fuel flow rate is the slowest at low power and thus the error will be at its largest. It was found that a 120 second test at 4 Hz resulted in a 95% confidence interval that was less than one percent of the brake specific fuel economy value (Fig. 3-12).

3.7 Steady State Data Output and Analysis

For each steady state test (power sweep at a fixed speed and engine configuration) data were collected at 4 hz for at least 120 seconds at each load level and stored as a CSV file. A Matlab function would take the raw data and find the average value and a 95% confidence interval for each relevant parameter. The Matlab function was also used to calculate other engine characteristics and to output a CSV file for each test configuration that summarized the results for simpler analysis.

The summarized data file is approximately three orders of magnitude smaller than

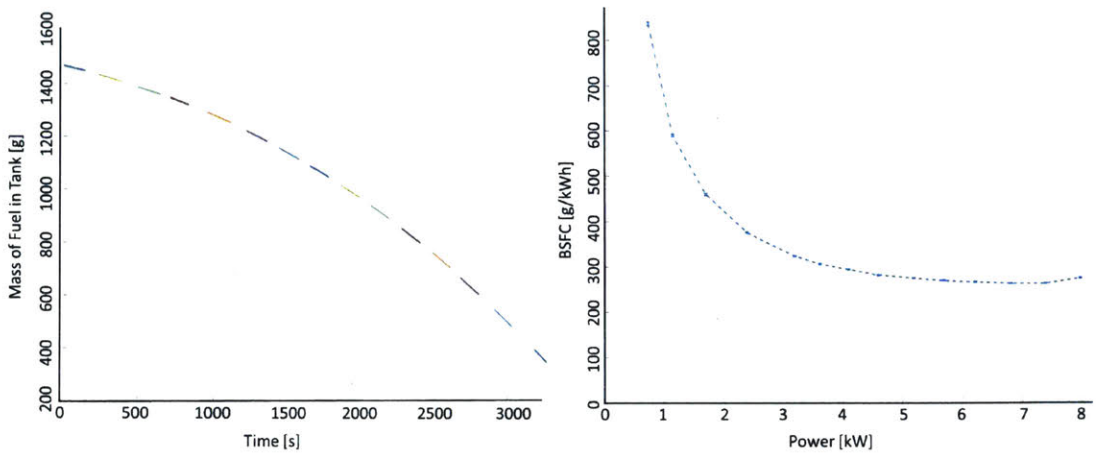

Figure 3-11: Sample data for a steady state test of the naturally aspirated engine configuration at 6.8 kW & 3500 RPM. Left: Raw data from the load cell showing the mass of fuel in the tank over time. Each line is a single load test. The load starts low and increases with each test. The gaps between lines represent the periods between tests where data are not collected. Right: Calculated brake specific fuel consumption using a linear regression (Fig. 3-10).

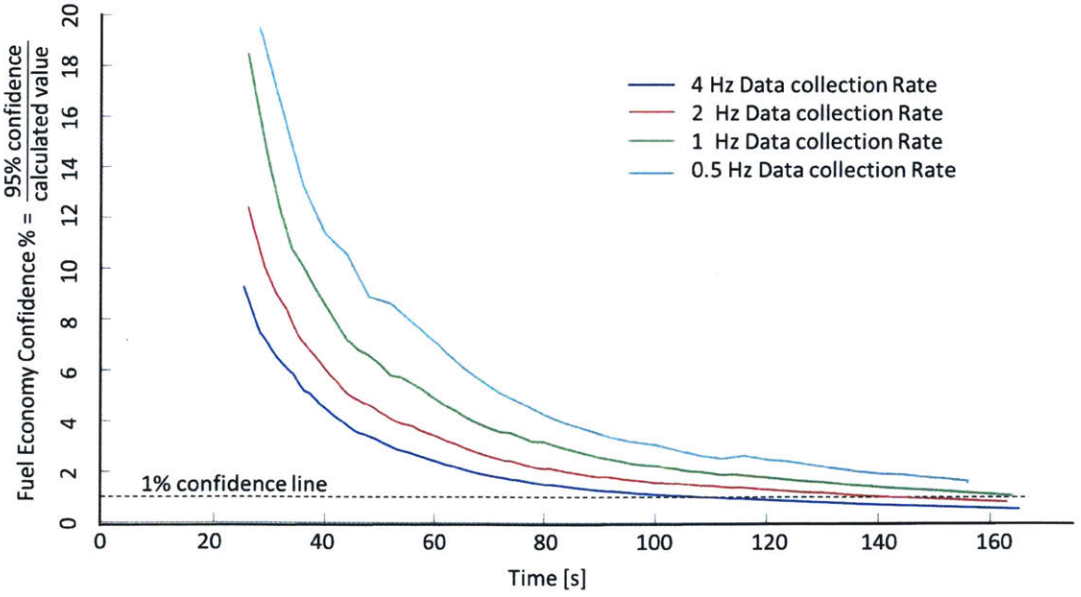

Figure 3-12: Plot of the error in the steady state fuel economy as a function of test duration and sampling frequency

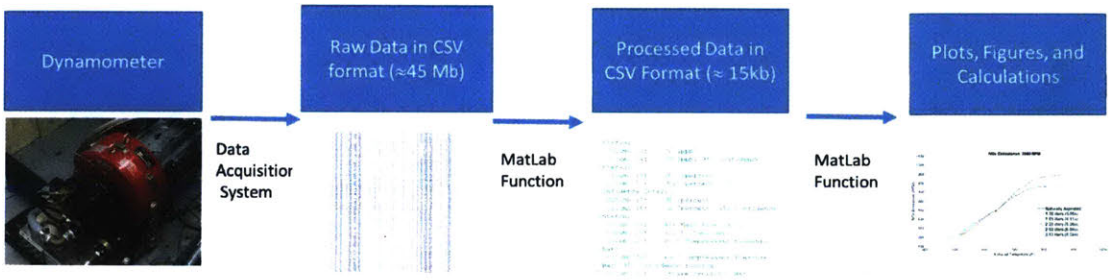

Figure 3-13: Flow for data processing.

the raw data file. The compression is due to reducing the over 500 data points taken at each power level to a single average value and a single confidence interval value. The compression is also furthered by the discard of unused channels that are stored in the raw data file such as empty analog input channels and timer channels. A separate Matlab function takes these summarized data files and plots them. This process is shown in Figure 3-13.

3.7.1 Statistical Analysis

The data collected for emissions, torque, pressure, and temperature were summarized by taking the mean of the data at each operating point. The standard deviation for each operating point was calculated using the standard deviation function in Matlab. The 95% confidence interval for each sensor at each operating point was calculated using a student's t-distribution test (Eqn. 3.3). The T_{value} is the inverse of the Student's t cdf for a 95% confidence interval calculated using the tinv function in Matlab.

$$95\%\ Confidence\ interval = mean \pm T_{value} * \frac{standard\ deviation}{\sqrt{number\ of\ samples}} \tag{3.3}$$

3.7.2 Calculating Air Flow

One of the key characteristics that needed to be measured was air mass flow rate, which was calculated for every steady state operating point. In order to avoid hav-

ing to obtain an expensive air mass flow meter, steady state air mass flow rate was calculated from emissions and fuel flow rate data (Eqn. 3.4-3.5). The concentration of NOx, CO, and other exhaust gas elements were small enough to be considered irrelevant.

The combustion of diesel fuel can be described by the simple stoichiometric equation [34]

$$(\frac{1.8n}{4} + n)O_2 + C_nH_{1.8n} \longrightarrow \frac{1.8n}{2}H_2O + nCO_2. \tag{3.4}$$

From this equation the molar balance of the combustion of diesel can be calculated.

$$per\ mol\ C_nH_{1.8n}\ Burned \longrightarrow (\frac{1.8n}{4} + n)\ mol\ O_2\ Consumed \tag{3.5}$$

The mass balance of the system can be used to determine the mass of oxygen that is consumed for every gram of fuel burned.

$$Molar\ Mass\ C_nH_{1.8n} = (13.8 * n)\frac{g}{mol} \tag{3.6}$$

$$Molar\ Mass\ O_2 = 32\frac{g}{mol} \tag{3.7}$$

$$1\ mol\ C_nH_{1.8n} * (13.8 * n)\frac{g}{mol}\ Burned \longrightarrow (\frac{1.8n}{4} + n)\ mol * 32\frac{g}{mol}\ O_2\ Consumed \tag{3.8}$$

$$13.8g\ C_nH_{1.8n}\ Burned \longrightarrow (\frac{1.8}{4} + 1) * 32g\ O_2\ Consumed \tag{3.9}$$

$$For\ Every\ g\ C_nH_{1.8n}\ Burned\ 3.36g\ O_2\ Consumed \tag{3.10}$$

$$\dot{m}_{O_2\ burned} = \dot{m}_{fuel} * 3.36 \tag{3.11}$$

By making an assumption that the mass fraction of oxygen burned is equal to the volume fraction of oxygen burned, it is possible to calculate the intake mass flow rate of oxygen as a function of the volume percent of oxygen in the exhaust stream, fuel mass flow rate, and the volume percent of oxygen in the intake stream. All of these are known values.

$$\frac{\%O_{2\ burned\ by\ volume}}{\%O_{2\ intake\ by\ volume}} \approx \frac{\dot{m}_{O_2\ burned}}{\dot{m}_{O_2\ intake}} \tag{3.12}$$

$$\dot{m}_{O_2\ intake} \approx \frac{\%O_{2\ intake\ by\ volume}}{\%O_{2\ burned\ by\ volume}} * \dot{m}_{O_2\ burned} \tag{3.13}$$

$$\dot{m}_{O_2\ intake} \approx \frac{\%O_{2\ intake\ by\ volume}}{\%O_{2\ intake\ by\ volume} - \%O_{2\ exhaust\ by\ volume}} * \dot{m}_{fuel} * 3.36 \tag{3.14}$$

The engine's intake stream is ambient air where oxygen makes up 20.95% of ambient air composition by volume and 23.2% by mass [37]. Combining this data with the fuel flow rate data makes it possible to calculate the mass flow rate of air.

$$\dot{m}_{air} = \frac{\dot{m}_{O_2\ intake}}{Mass\ Fraction\ Oxygen\ in\ Air} \tag{3.15}$$

$$\dot{m}_{air} = \frac{20.95}{20.95 - \%O_{2\ exhaust\ by\ volume}} * \dot{m}_{fuel} * \frac{3.36}{0.232} \tag{3.16}$$

This analysis allows for the calculation of air mass flow rate, air to fuel ratio, and the air to fuel equivalence ratio. These values are important for evaluating the performance of the engine and the effectiveness of the turbocharger air capacitor system.

3.7.3 Other Steady State Calculated Values

From the steady state experiment data other steady state parameters were calculated in order to better characterize the engine and understand the performance of the system. These parameters are shown below in Table 3.6.

Table 3.6: Equations for steady state values

Calculated Value	**Symbol**	**Units**	**Equation**
Air to Fuel Ratio	A/F	1	$\frac{\dot{m}_{air}}{\dot{m}_{fuel}}$
Break Mean Effective Pressure	BMEP	bar	$\frac{2*6.28*Torque}{Displacement}$
Pumping Work	$\dot{W}_{pumping}$	w	$\dot{Q} * (P_{exhaust} - P_{intake})$
Exhaust Mass Flow Rate	$\dot{m}_{exhaust}$	g/s	$\dot{m}_{air} + \dot{m}_{fuel}$
Exhaust Molar Mass*	$M_{exhaust}$	g/mol	$\frac{\%CO_2*44}{100} + \frac{\%N_2*28}{100} + \frac{\%O_2*32}{100} + \frac{\%Ar*44}{100}$
Exhaust Molar Flow Rate*	$\dot{n}_{exhaust}$	mol/s	$\frac{Exhaust\ Mass\ Flow\ Rate}{Exhaust\ Molar\ Mass*}$
Break Specific NO_2	$BSNO_2$	g/kWh	$\frac{\dot{n}_{exhaust}*PPMNO_2}{Power*3600*46*1000000}$
Break Specific NO	$BSNO$	g/kWh	$\frac{\dot{n}_{exhaust}*PPMNO}{Power*3600*30*1000000}$
Break Specific CO	$BSCO$	g/kWh	$\frac{\dot{n}_{exhaust}*PPMCO}{Power*3600*28*1000000}$
Break Specific NO_x	$BSNO_x$	g/kWh	$BSNO + BSNO_2$

*assumes that the primary components in the exhaust are oxygen, carbon dioxide, nitrogen, and argon.

Chapter 4

Steady State Experiment

4.1 Goals of Experiment

The experiment was initially run with the IHI turbocharger and the five sizes of air capacitor shown in Figure 3-5, in order to demonstrate the effect of air capacitor sizing on engine performance. Additional tests were then run with a Garrett turbocharger to show the effect of the turbocharger itself on the engine's performance and to validate the computational model. While the Garrett turbocharger outperformed the IHI turbocharger the results of the IHI turbocharger tests were used to demonstrate the effect of air capacitor volume on engine performance.

4.2 Experimental Procedure

An experimental procedure was designed to produce an accurate picture of the engines performance over a range of loads and at low, medium, and high speeds. An individual experiment consisted of testing an engine configuration at a specific speed over a range of loads. There were two procedures created; one setup procedure and one for the experiment itself.

4.2.1 Experimental Setup Procedure

Between experiments, the following procedure was preformed in order to safely operate the test setup and ensure that the subsequent experiment would not be affected by the previous one. Tests were spaced out to allow the engine and turbocharger oil to cool.

1. Ensure that the engine is completely shut off and that the engine fuel solenoid switch is set to closed.

2. Check the exhaust manifold thermocouple to ensure that the temperature of the engine is cool enough such that it is safe to handle.

3. Disconnect the engine from the battery and cover the battery leads.

4. If not already on, turn on the dynamometer water.

5. If the test is a turbocharged condition, turn on the turbocharger oil pumps.

6. Turn on the emissions probe. Ensure that the emissions sensor is at operational temperature, by waiting for at least 20 minutes.

7. Configure the engine manifold for the test.

8. Fill the fuel tank with at least 1.5 liters of fuel in increments of 250 ml. Make sure that the load cell is calibrated such that for every 250 milliliter added to the tank the load cell reading increases by 208 grams.

9. Turn on the ventilation system and ensure that it is working properly.

10. Reconnect the starter motor to the battery

11. Clear the memory on the data acquisition system (make sure to save the results of the previous test first)

12. Turn on engine fuel solenoid

4.2.2 Experimental Operating Procedure

The steady state experiments followed a careful procedure to ensure that the data collected were accurate. The experimental operating procedure is detailed below.

1. Check that all safety systems are on and that the load on the engine is set to zero.
2. Turn on the engine.
3. Set the engine speed to the test speed.
4. Wait for the engine exhaust temperature and emissions output to reach steady state (approximately 2 minutes).
5. Collect enough data to have an accurate measure of fuel consumption (400 to 800 data points at a collection rate of 4 Hz).
6. Increase the load on the engine by less than 1 Nm.
7. Wait for the engine exhaust temperature and emissions output to reach steady state (approximately 2 minutes).
8. Collect enough data to have an accurate measure of fuel consumption (400 to 800 data points at a collection rate of 4 Hz).
9. Repeat steps 6-8 until the engine starts to stall.
10. Reduce engine load to zero and engine speed to 2000 RPM.
11. Turn off engine by turning off the fuel flow solenoid.
12. Save the data output to a CSV file.

4.3 Manifold Volume Experiments

The first set of experiments run were the manifold volume tests. These experiments analyzed the effect of the air capacitor volume on the performance of a turbocharged

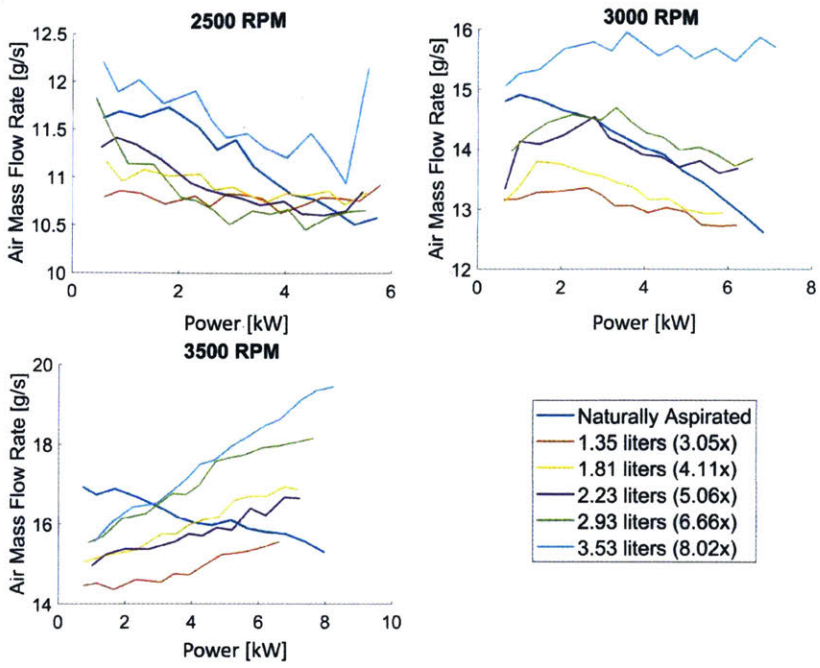

Figure 4-1: Air mass flow rate through the engine for the five turbocharged cases (RHB 31 turbocharger) and the naturally aspirated case, for all three speeds.

single cylinder engine. They were run with the IHI turbocharger in order to gauge the effect of manifold volume on power density, air mass flow, fuel economy, emissions, manifold pressures, and manifold temperatures.

4.3.1 Air Mass Flow

Figure 4-1 shows the air mass flow rate through the engine as a function of engine power output for the five turbocharged cases and the naturally aspirated case. It was observed that at lower speed the turbocharger had a minimal effect on air mass flow rate. At 2500 RPM the turbocharged case had a lower air mass flow rate relative to the naturally aspirated case for all but the largest capacitor size. At 3000 RPM the turbocharger noticeably increased the air mass flow rate for the larger air capacitors at higher powers. At 3500 RPM the turbocharger outperformed the naturally aspirated case by up to 30% at the highest power.

It is observed that the air mass flow rate dependence on power is determined by

engine speed. For the Naturally aspirated case the air mass flow rate decreases as power increases. This is most likely due to scavenging inefficiency and the intake air temperature increasing. For the turbocharged case at the lowest speed (2500 RPM) the air mass flow rate decreases with power, while at higher speed (3500 RPM) it increases with power. The decreased performance of the turbocharged engine at low power and speed is due to low exhaust enthalpy, that causes the turbocharger to act like a flow constrictor; the turbocharger is not spooling to the level required to provide adequate pressure and, as a result, is limiting the air flow. At higher power and speed, the turbocharger increases the air mass flow rate relative to the naturally aspirated case. The air mass flow rate increased with capacitor size, as expected, when the exhaust enthalpy is sufficient to spool the turbocharger. The increase in air mass flow rate with increasing power for the high speed turbocharged conditions demonstrates the turbocharger's efficacy.

Compared to the naturally aspirated case, turbocharging with the largest air capacitor was able to increase the air flow by approximately 30%. This corresponds to a 30% increase in air density in the engine, which should result in a 30% increase in power density [67]. However, a significantly lower power density increase was observed due to inefficiencies in the system and an inability to inject enough fuel in the high speed turbocharged case.

4.3.2 Power Density

To demonstrate the increase in power density, an air to fuel equivalence ratio (lambda) engine map was created. The equivalence ratio (λ) was calculated using equation 4.1. Figure 4-2 compares the air to fuel equivalence ratios of the largest capacitor turbocharged case to the naturally aspirated case. This plot shows that, as expected, the naturally aspirated case outperforms the turbocharged case at low power and at low speed where the enthalpy in the exhaust gas is lower. At higher speed and load, the turbocharger outperforms the naturally aspirated engine. However, the turbocharger only increases the power output of the engine by approximately 10% for the lowest equivalence ratio (2) at the maximum speed (3500 RPM). At this

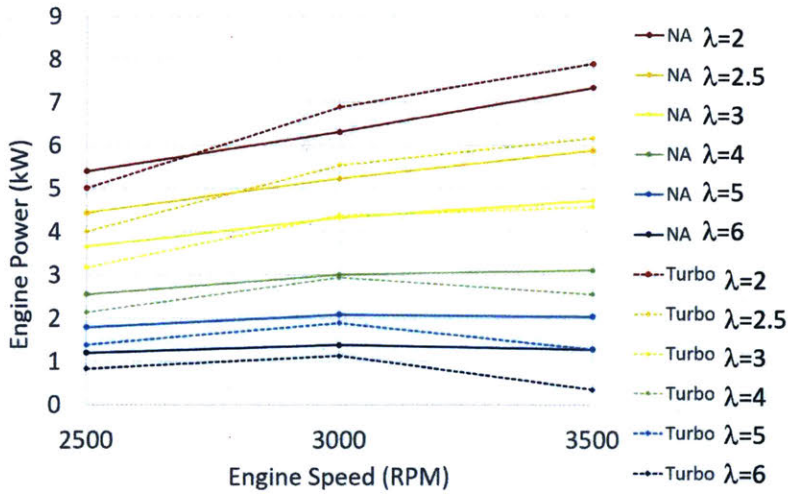

Figure 4-2: Plot of the equivalence ratio of the engine for different speeds and powers. The solid lines show the map for the naturally aspirated (NA) case and the dotted lines show the map for the turbocharged case with the largest capacitor size (RHB 31 turbocharger).

operating point the intake air mass flow is increased by 30% so a similar increase in equivalence ratio is expected. This implies there are inefficiencies in the system most likely due to added pumping losses, heat transfer losses, and frictional losses. These additional losses were observed in the computational model described in chapter 2 and are consistent with the experimental inefficiencies.

$$AF = \frac{\dot{m}_{air}}{\dot{m}_{fuel}} \tag{4.1}$$

$$\lambda = \frac{AF}{AF_{Stoichiometric}} = \frac{AF}{14.5} \tag{4.2}$$

Figure 4-3 shows the equivalence ratio as a function of power output for the five capacitor sizes and the naturally aspirated case at low (2500 RPM), mid (3000 RPM) and high (3500 RPM) speed. As expected, the larger the capacitor size creates the better the engine performance. The performance benefit of the larger capacitor size

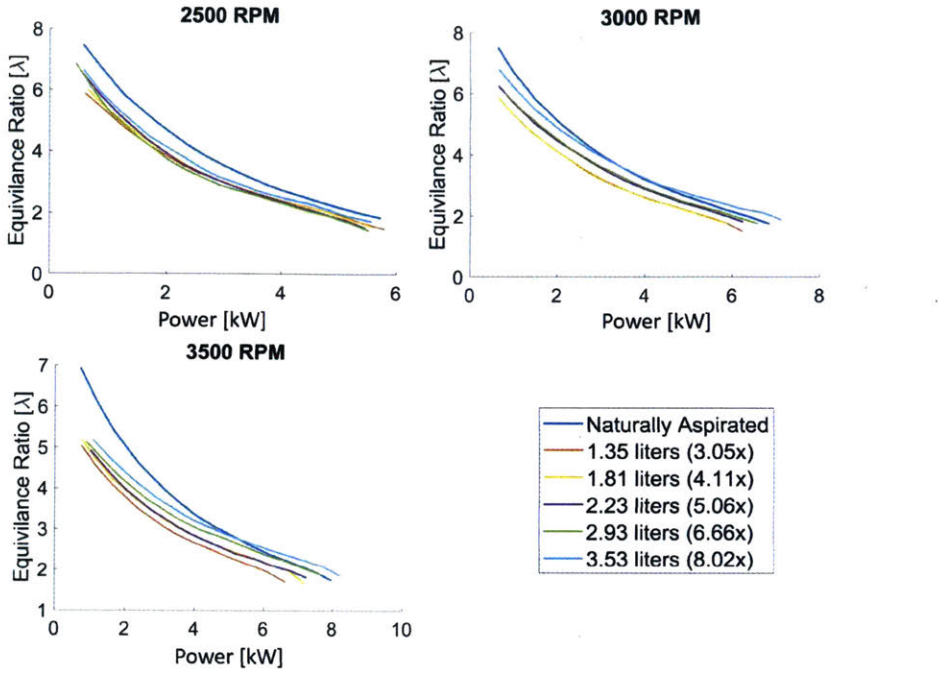

Figure 4-3: Equivalence ratio as a function of power output for the RHB31 turbocharger in the five manifold cases and the naturally aspirated case at low, medium, and high speed operation.

also increases at higher engine speed. It is also observed that only the largest capacitor sizes outperform the naturally aspirated engine. It is noted that the largest capacitor hits its maximum power output at a notably lower air to fuel ratio than the naturally aspirated case. This is due to the engine reaching its maximum rate of fuel injection with its default fuel injection configuration.

4.3.3 Fuel Economy

In order to further study the experimental inefficiency, the brake specific fuel consumption (BSFC) is plotted in Figure 4-4. This plot also shows that the turbocharged engine is operating at a lower efficiency than the naturally aspirated one, thus matching the equivalence ratio results. However, this result is unexpected. Two possible sources of this inefficiency are pumping losses and premature combustion due to an excessive effective compression ratio. Note that, as the air capacitor size increases the BSFC decreases. This demonstrates that increasing the volume of the air capacitor

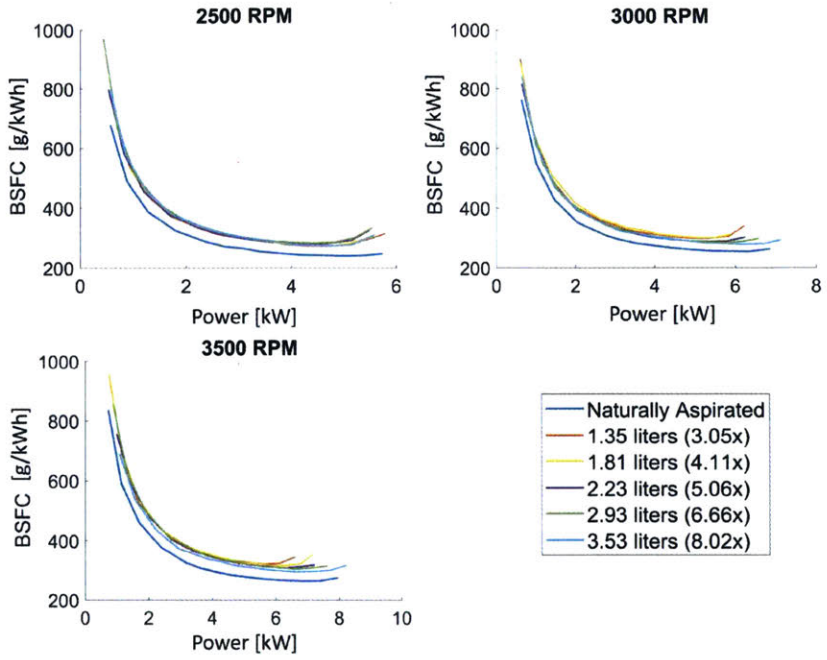

Figure 4-4: Break Specific Fuel Consumption vs. Power for all three speeds (RHB 31 turbocharger).

can increase efficiency.

Pumping losses can be calculated from the engine volume, the exhaust pressure, and the intake pressure (Eqn. 4.3). The pumping losses for the five turbocharged engine configurations were found to start high and decrease as the engine power increases while that of the naturally aspirated case started low and increased with increasing engine power (Fig. 4-5). To see the effect of pumping losses on the system, the BSFC was adjusted to include pumping work (Eqn. 4.4). This adjustment accounted for the difference in efficiency at lower power levels but did not explain the efficiency losses at higher power (Fig. 4-6).

$$PumpingLosses \approx Q * \Delta P \approx \frac{RPM * V_{eng}}{2 * 60} * \Delta P \tag{4.3}$$

$$AdjustedBSFC \approx \frac{FuelFlow}{(ShaftPower + PumpingLosses)} \tag{4.4}$$

The efficiency losses at higher power are most likely due to heat transfer losses,

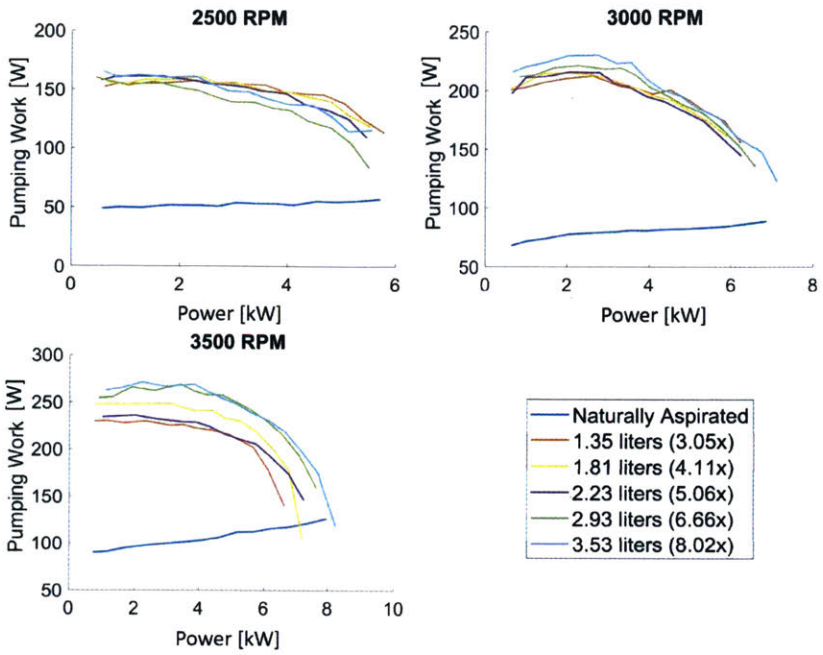

Figure 4-5: Pumping work vs. Power for all three speeds (RHB 31 turbocharger).

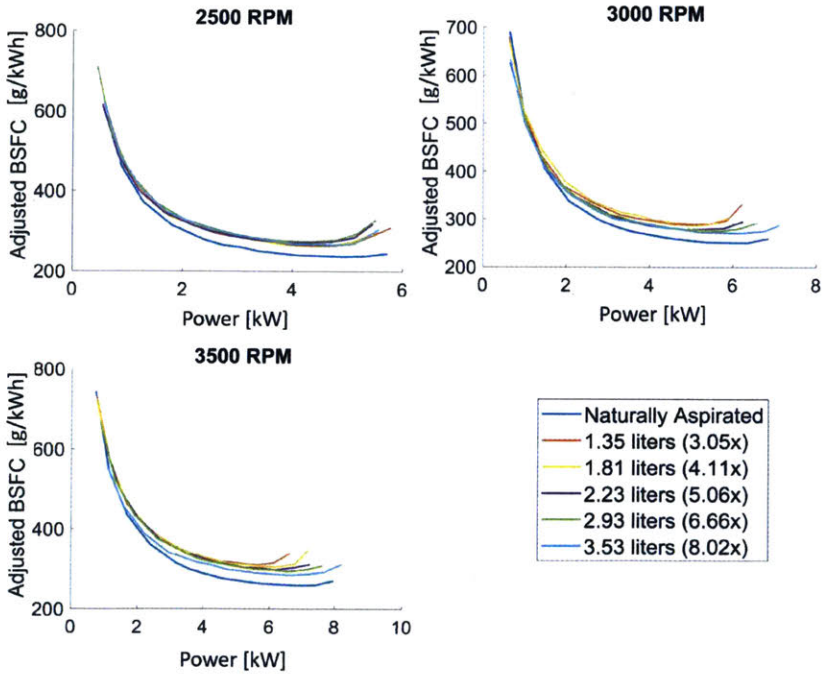

Figure 4-6: Brake Specific Fuel Consumption adjusted for pumping loss vs. Power for all three speeds (RHB 31 turbocharger).

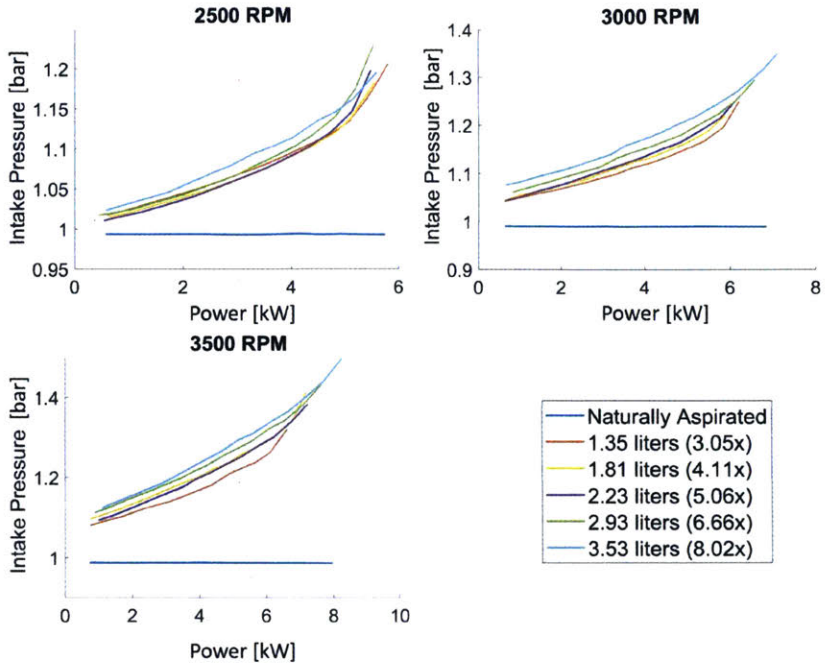

Figure 4-7: Plots of the engine intake air pressure as a function of power output for the five turbocharged cases and the naturally aspirated case at 2500, 3000, & 3500 RPM (RHB 31 turbocharger).

pumping losses, and frictional losses. This hypothesis is supported by the computational model results described in Chapter 2. As capacitor size increases, the combination of an increase in efficiency with higher pumping losses implies that a larger capacitor size reduces heat transfer losses and/or increases overall thermal efficiency due to the cycle operating over a wider temperature difference.

4.3.4 Pressures

Figure 4-7 shows the pressure in the intake manifold (measured at approximately 10 cm before the intake valve) as a function of power output for the five capacitor cases and the naturally aspirated case at 3500 RPM. As expected, the intake pressure increases with power output, engine speed, and air capacitor size. The intake air pressure in the naturally aspirated case is just under 1 bar due to the pressure drop across the air filter.

The exhaust pressure was measured before the turbocharger, approximately 10 cm

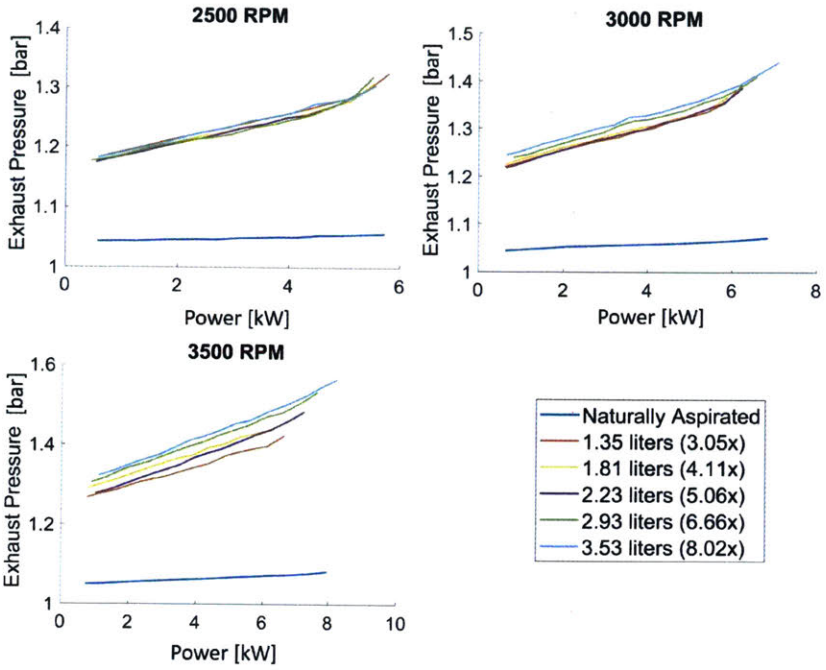

Figure 4-8: Plots of the engine exhaust air pressure as a function of power output for the five turbocharged cases and the naturally aspirated case at 2500, 3000, & 3500 RPM (RHB 31 turbocharger).

after the exhaust valve (Fig. 4-8). At lower speed it was found that the capacitor had no noticeable effect on exhaust pressure. However, at higher speed and power when the turbocharger was producing higher intake pressures exhaust pressure increased with capacitor size.

4.3.5 Temperature

Manifold temperatures provide insight into the engine's performance. The intake temperature was measured about 10 cm before the intake valve. It was found that the measurement has significant fluctuations due to the sensor being too close to the engine and thus resulting in the engine's temperature influencing the reading. However, the measurement was sufficiently accurate to show that turbocharging noticeably increased the intake air temperature relative to the naturally aspirated engine. This increase in temperature results in a decrease in intake density relative to an inter cooled engine, an increase in NOx emissions, and a decrease in efficiency.

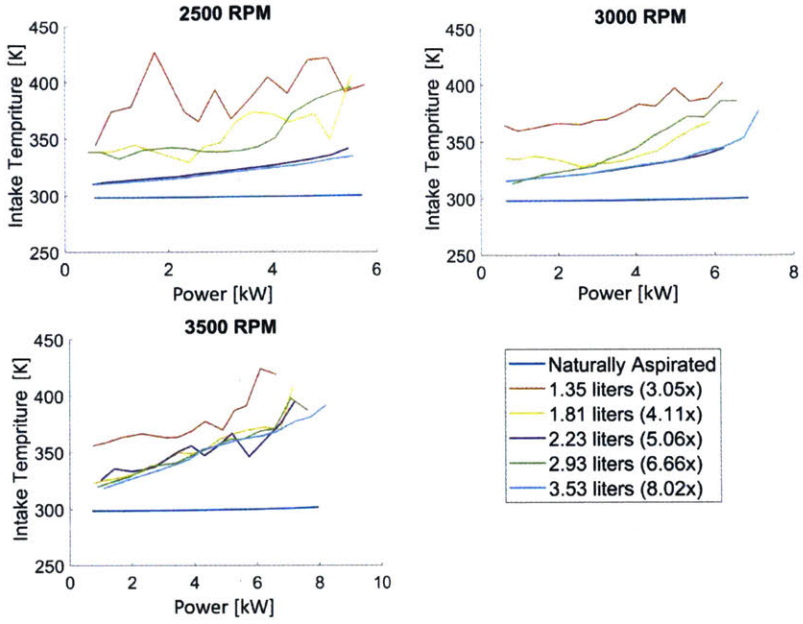

Figure 4-9: Plots of the engine intake temperature as a function of power output for the five turbocharged cases and the naturally aspirated case at 2500, 3000, & 3500 RPM (RHB 31 turbocharger).

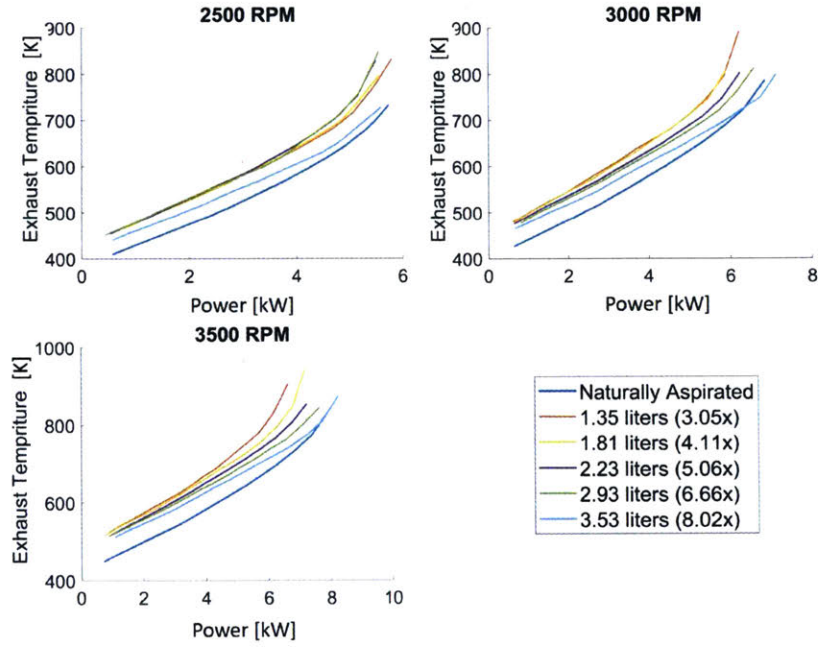

Figure 4-10: Plots of the engine exhaust temperature as a function of power output for the five turbocharged cases and the naturally aspirated case at 2500, 3000, & 3500 RPM (RHB 31 turbocharger).

The exhaust temperature was measured before the turbocharger at about 10 cm after the exhaust valve. It was found that turbocharging increased exhaust temperature, which is expected due to the higher exhaust pressures. It was also observed that increasing capacitor size resulted in lower exhaust temperatures. The effect of manifold size on exhaust temperature is due to the higher mass flow rate resulting in more air flow into the engine which cools the engine.

4.3.6 Emissions

Both nitrous oxide and carbon monoxide emissions from the engine were measured in order to determine the effects of turbocharging and air capacitor sizing on emissions. An understanding of emissions is key to understanding how to size and specify appropriate exhaust after treatment systems for an engine.

Nitrous oxide emissions are a function of temperature and the amount of oxygen available. Figure 4-12 shows how the NOx concentration increases with capacitor size for a given temperature. This is due to air mass flow rates increasing with capacitor size, resulting in more oxygen available in the engine for the reaction with the nitrogen.

Figure 4-11 shows the brake specific nitrous oxide production which demonstrates that the available oxygen NOx increase is magnified by the higher air mass flow rate. With no emissions control systems, this is to be expected since the engine is running in a leaner state where the air mass flow rate is higher [60, 47].

The collected data also provide insights into how incorporating air capacitor turbocharging with emissions strategies can improve engine performance. Larger air capacitor volume resulted in lower exhaust temperatures (Fig. 4-10). This can be used with an active exhaust gas recirculation (EGR) system to reduce the amount of oxygen in the engine during lower power states. A potential solution to reduce NOx emissions is to use an EGR system combined with a diesel particulate filter (compensating for the increased particulate emissions due to the EGR system) to minimize NOx emissions .

Figure 4-13 shows carbon monoxide emissions as a function of power output. The

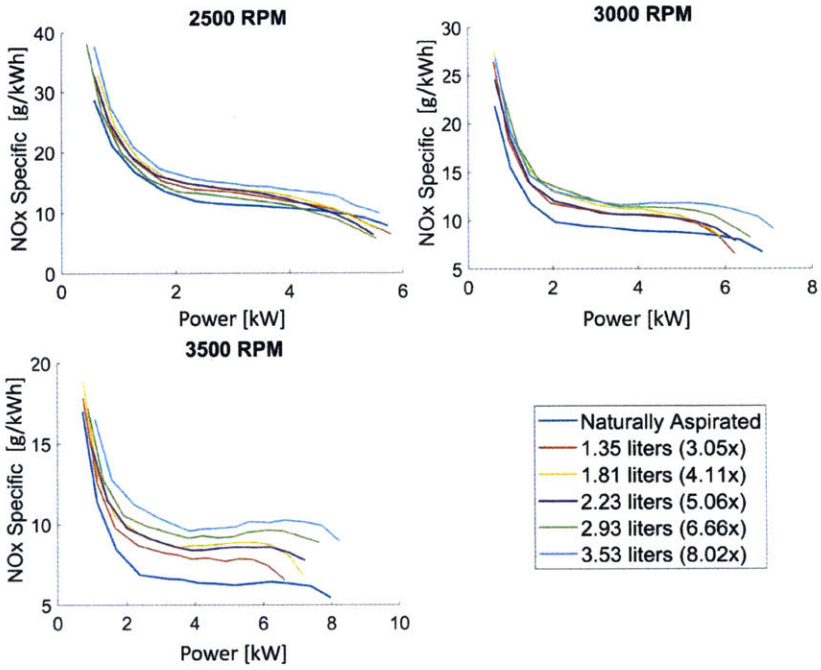

Figure 4-11: Plots of brake specific NOx output as a function of power output for the five turbocharged cases and the naturally aspirated case at 2500, 3000, & 3500 RPM (RHB 31 turbocharger).

combustion process is more likely to favor carbon monoxide at certain temperatures and when less oxygen is available. At lower power carbon monoxide output was reduced in the turbocharged case due to the increase in oxygen and the higher temperature. At higher power the lack of oxygen becomes the dominant factor in carbon monoxide formation [47]. As a result the smaller capacitor sizes, which are at a lower equivalence ratio and have a lower air mass flow rate, produce significantly more carbon monoxide. This implies that using a large air capacitor can be used as a strategy to control carbon monoxide emissions.

4.4 Model Validation with Garrett Turbocharger

The engine was then fitted with a Garrett turbocharger. This was done to show the effect of the turbocharger and to show that the computational model was accurate since an operating MAP was available for the Garrett turbocharger.

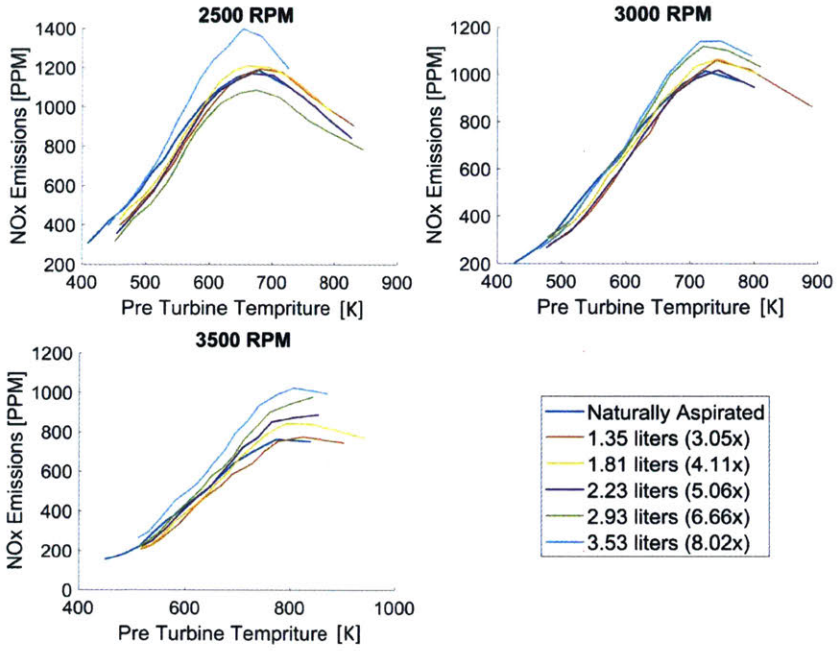

Figure 4-12: Plots of nitrous oxide emissions as a function of exhaust temperature for the five turbocharged cases and the naturally aspirated case at 2500, 3000, & 3500 RPM (RHB 31 turbocharger).

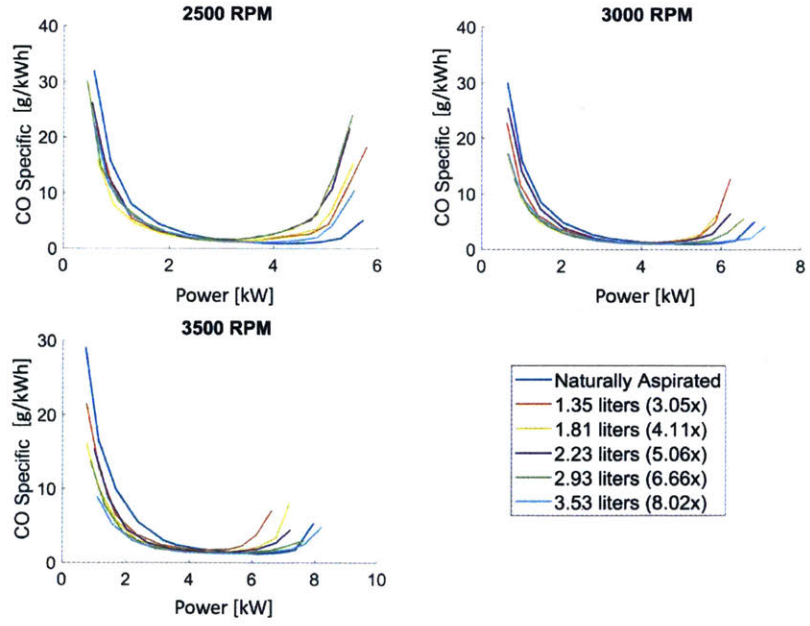

Figure 4-13: Plots of CO specific emissions as a function of power output for the five turbocharged cases and the naturally aspirated case at 2500, 3000, & 3500 RPM (RHB 31 turbocharger).

The computational model, used to evaluate fuel consumption, power output, and emissions, had to be validated in order to demonstrate its applicability in optimizing the engine. The validation was done by comparing the experimental results to the model results for the three cases that were modeled in the Ricardo Wave software: naturally aspirated, turbocharged with a low heat transfer air capacitor, and turbocharged with a high heat transfer air capacitor.

Three metrics were used to evaluate how closely the model fit the experiment. An R squared value described how well the model predicted the trend, as shown in Eqn. 4.5, where x is the value predicted by the model, y is the value measured from the experiment, and n is the number of samples. A mean percent error was used to determine how closely the model predicted engine performance (Eqn. 4.6) [54]. To compensate for large fluctuations observed in the percent error at the extremes, a mean value error was used as a second metric to determine how closely the model predicted the experiment (Eqn. 4.7).

$$R^2 = \frac{\sum (x - \bar{x})(y - \bar{y})}{\sqrt{\sum (x - \bar{x})^2 \sum (y - \bar{y})^2}} \tag{4.5}$$

$$MeanError\% = \frac{\sum abs(\frac{x}{y} - 1)}{n} \tag{4.6}$$

$$MeanErrorValue = \frac{\sum abs(x - y)}{n} \tag{4.7}$$

Figure 4-14 shows the comparison of the model's predictions to the measured values for power output. The model is shown to be able predict the power output of the engine with no tuning. The turbocharged model had a mean error of approximately 0.6 kW and the naturally aspirated model had a mean error of approximately 0.2 kW. As expected, it was found that the turbocharger was able to increase power output notably (14% relative to naturally aspirated at an equivalence ratio of 1.6, the minimum equivalence ratio achieved). The Garrett turbocharger also produces noticeably more power at lower equivalence ratios then the IHI turbocharger (6% relative to the IHI turbocharger at an equivalence ratio of 1.9 , the minimum equiva-

lence ratio achieved). It was also observed that when the inter-cooler was added the power output increased notably as predicted by the model (21 % relative to naturally aspirated at an equivalence ratio of 2, the minimum equivalence ratio achieved). One shortcoming of this experiment was that the fuel injector had a limited maximum flow rate. As a result, we were unable to run the turbocharged engine at any power beyond 8.6 kw (significantly below the maximum power predicted by the model) and at the low end of equivalence ratios that were achieved in the naturally aspirated engine case.

Figure 4-15 shows the comparison of the model's predicted fuel consumption to the experiment's measured fuel consumption. The power error is based on the maximum observed load cell drift (0.4 Nm). The model predicts fuel consumption accurately at low to mid power levels and under-predicts fuel consumption at high power for all cases. This is due to the model not capturing the effects of incomplete combustion that occur at low air to fuel equivalence ratios. It is also observed that the model is able to predict the magnitude in fuel consumption changes between the three experimental cases. The model predicts fuel economy trends and values with a maximum mean error of 7.1%, accurate enough to be used in the optimization scheme.

Figure 4-16 shows the comparison of the model's predicted air mass flow to the experiment's measured air mass flow. The baseline Garrett turbocharger improves flow rate by 16% relative to the baseline IHI case and the intercooled Garrett case improves flow rate by 23% relative to the IHI case. It was found that the model accurately predicts naturally aspirated air mass flow and under-predicts the turbocharged air mass flow rate by 10%. This discrepancy is most likely due to the turbocharger map having an error. Since the map was provided by the manufacturer, it was determined that this error was more acceptable than attempting to modify the Garrett turbocharger map in the model to match the experiment.

Figure 4-17 shows the comparison of the model's predicted manifold pressures to the experiment's measured manifold pressures. The pressures indicated how accurately the model predicted the turbocharger's characteristics. The model accurately predicted exhaust pressure but under predict intake pressure by approximately 6%.

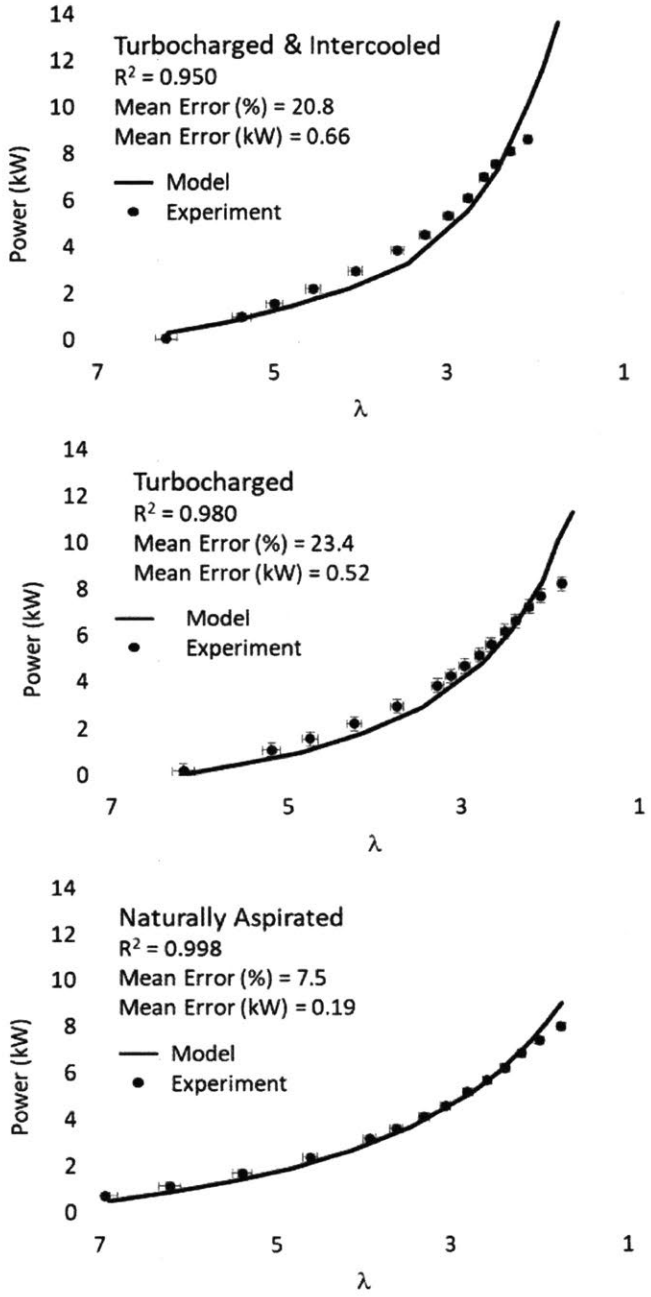

Figure 4-14: Plots comparing the model predictions to experimental results for air to fuel equivalence ratio vs. power output for a power sweeps at 3500 RPM (Garrett GTO632SZ turbocharger).

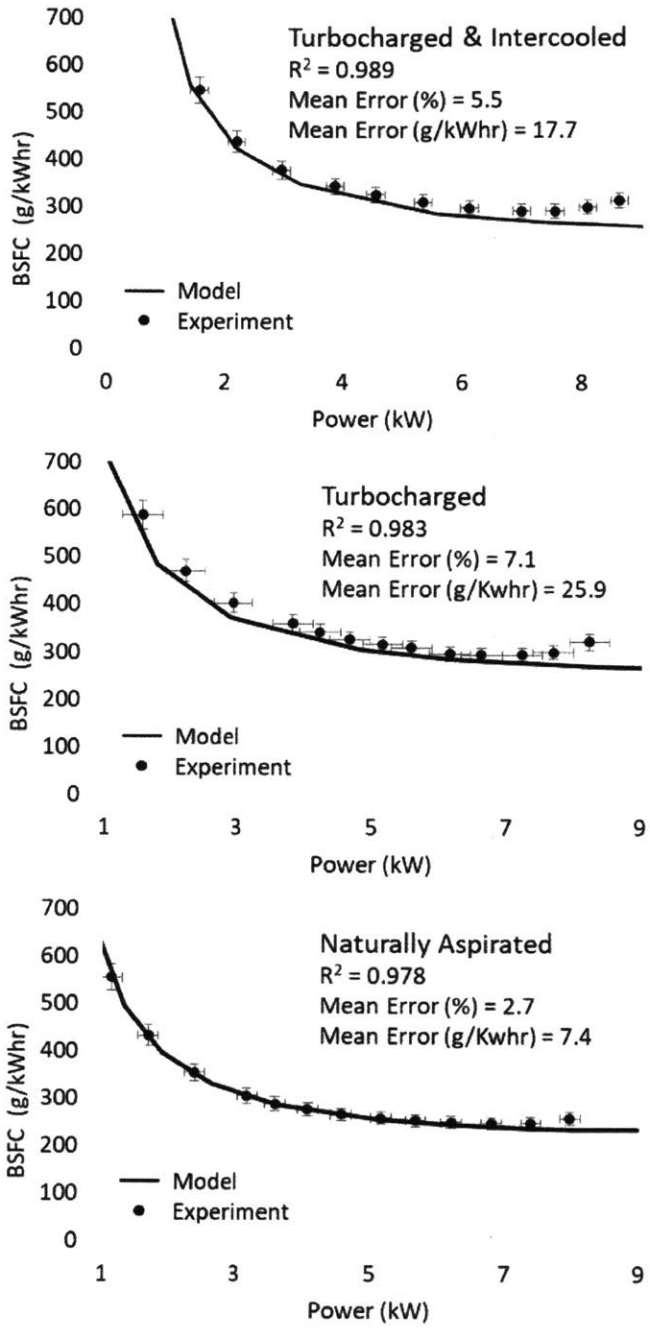

Figure 4-15: Plots comparing the the model predictions to experimental results for power vs. fuel consumption ratio for a power sweeps at 3500 RPM (Garrett GTO632SZ turbocharger).

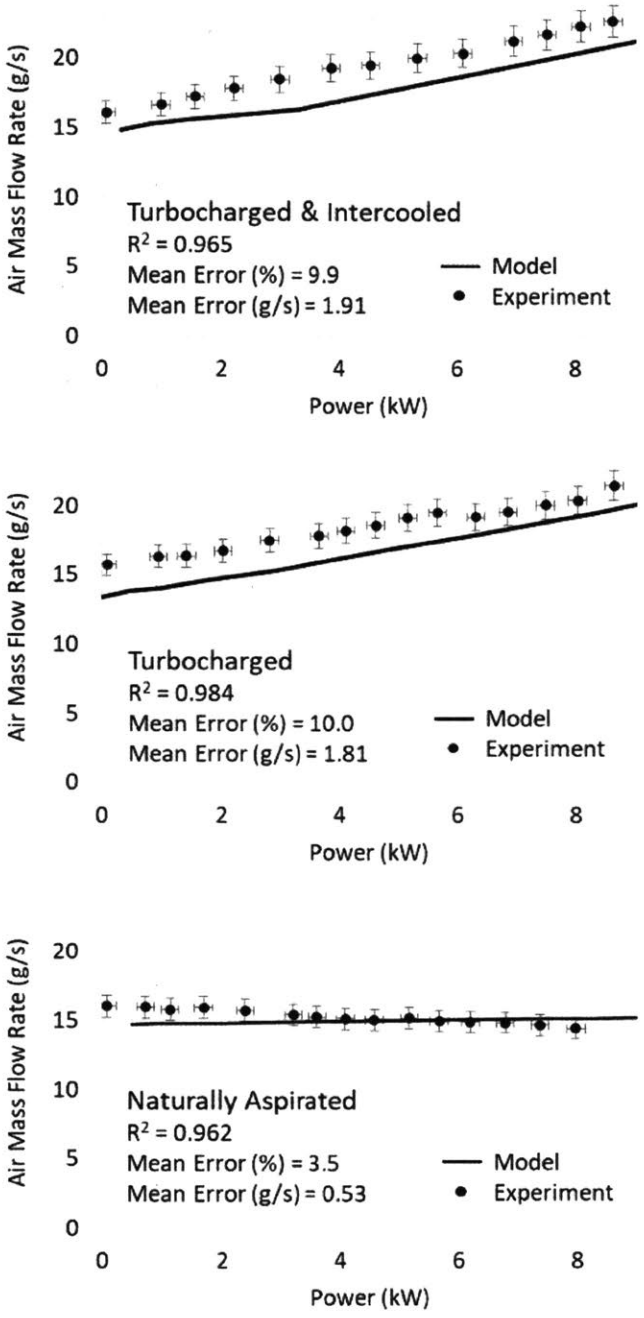

Figure 4-16: Plots comparing the model predictions to the experimental results for power output vs. air mass flow rate for a power sweeps at 3500 RPM (Garrett GTO632SZ turbocharger).

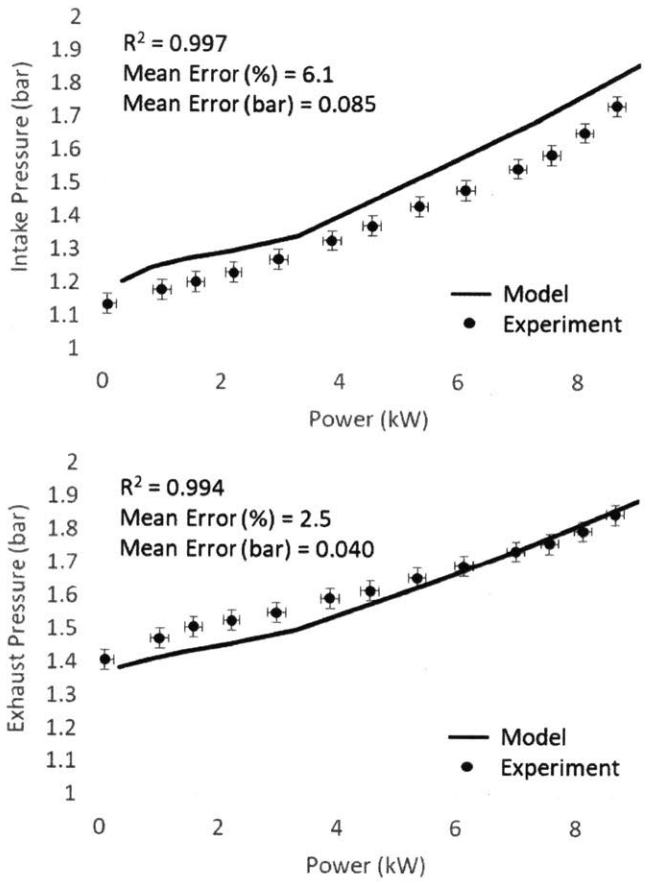

Figure 4-17: Plots comparing the model prediction to experimental results for power output vs. pressure for the turbocharged inter-cooled case during power sweeps at 3500 RPM (Garrett GTO632SZ turbocharger).

In this case, the error was also most likely due to the turbocharger map having an error, but this error was more acceptable than attempting to create a new turbocharger map. The Garrett turbocharger had intake pressures about 50% larger than the IHI turbocharger, indicating that it performed significantly better than the IHI turbocharger.

The model was found to have significant error when predicting nitrous oxide emissions. Literature suggests that predicting engine emissions in a one-dimensional CFD can have high error and that the model may be able to be improved by calibrating it using experimental data [60]. In order to address the high mean NOx error, the scalers in the emissions model were calibrated using a simulated annealing algorithm

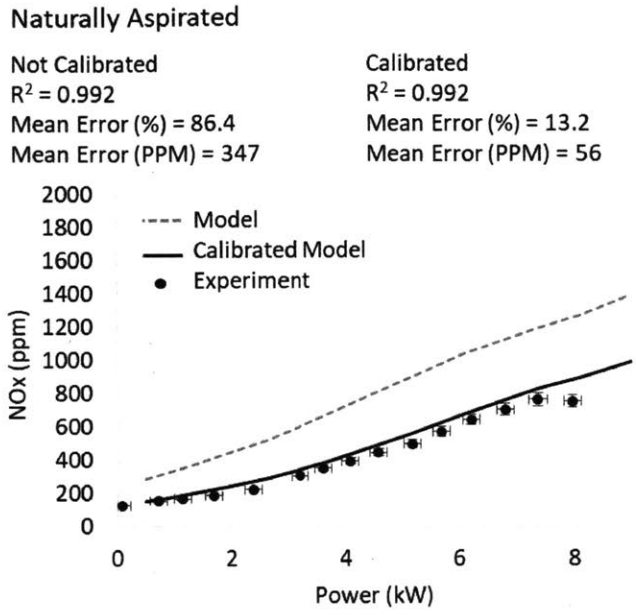

Figure 4-18: Plots comparing the power output vs. nitrous oxide emissions for experiment, original model and calibrated model results for the naturally aspirated case during power sweeps at 3500 RPM (Garrett GTO632SZ turbocharger).

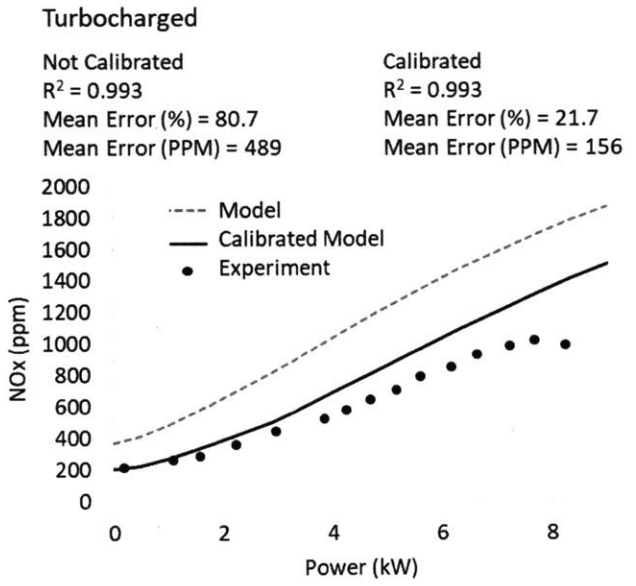

Figure 4-19: Plots comparing the power output vs. nitrous oxide emissions for experiment, original model and calibrated model results for the turbocharged case during power sweeps at 3500 RPM (Garrett GTO632SZ turbocharger).

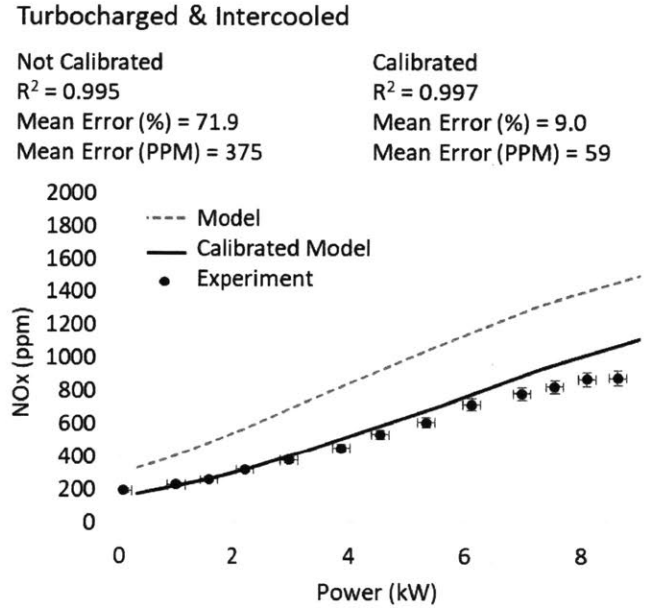

Figure 4-20: Plots comparing the power output vs. nitrous oxide emissions for experiment, original model and calibrated model results for the turbocharged and intercooled case during power sweeps at 3500 RPM (Garrett GTO632SZ turbocharger).

Table 4.1: NOx calibration parameters

Variable	Initial Value	Lower Bounds	Upper Bounds	Calibrated Value
NOx	1	0.5	2	1.08
NOx Pre	1.5	0.5	2	1.76

to harmonize the model's predictions to the data from the experiment for the naturally aspirated condition. The calibration was built into MatLab and operated the Ricardo Wave model. The bounds for the calibration scalers were defined using the recommended values given by the software (0.5-2.0). The results of the calibration are shown in Table 4.1. For the turbocharged cases, the calibrated NOx model had a notably smaller mean error than that of the uncalibrated case while maintaining the same high R squared value as in the uncalibrated case.

Figures 4-18, 4-19, & 4-20 show the comparisons between the calibrated and uncalibrated model's predicted nitrous oxide emissions and the experiment's measured nitrous oxide emissions. The Ricardo Wave model determines nitrous oxide emissions using an exponential model with two scalers. The uncalibrated nitrous oxide emissions with the model's default values were found to correlate to the data with R squared values of greater than 0.99 but with mean errors of between 70-90%. This implies that the NOx model can be used to accurately predict emissions trends but cannot be used to predict the amount of emissions produced.

4.5 Conclusion

The goals of the steady state engine tests were to analyze the effect of air capacitor turbocharging on key factors that affect the commercial viability of the engine such as emissions, fuel economy, and power density, as well as to validate the computational model.

Initially, a set of experiments were run to determine how turbocharging and air capacitor sizing affect key performance parameters in a single cylinder engine. This initial experiment confirmed that the turbocharger and air capacitor system could be used to increase the intake air density and air mass flow through the system, and that air capacitor size was affected the intake air mass flow. The turbocharged engine was able to increase power density; however, it fell short of its modeled potential due to inefficiencies in the system. Turbocharging introduced an inefficiency that resulted in an increase in fuel consumption. The turbocharger had an effect on emissions,

increasing NOx emissions while reducing CO emissions. In the future EGR can be used to mitigate some of these effects.

The experiment was then run with a Garrett turbocharger to demonstrate that the model can predict engine performance and the effect of turbocharger selection on engine performance. The Garrett turbocharger was shown to outperform the IHI turbocharger, providing significantly more intake pressure and increasing air mass flow rate by a large margin (up to 28% higher absolute pressure and 18% higher air mass flow rate). Additionally, it was determined that the model was able to predict engine performance to a level of accuracy where it could be used with confidence. The model was found to accurately predict fuel economy and power output without calibration and accurately predict NOx emissions with calibration. Another key observation was that the inter-cooled engine significantly outperformed the engine that was only turbocharged. Therefore, the model can be used to optimize the single cylinder turbocharged engine and the optimization will assume that an inter cooler will be used as an air capacitor.

Chapter 5

Transient Response

The drawback of the air capacitor turbocharging method is that there is an added response time to speed and torque variations [66]. By default, turbocharging has a lag time associated with the spooling of the turbine that is dependent on the engine speed and the turbocharger size [67, 52, 53]. It is expected that air-capacitor based turbocharging of single cylinder engines will entail additional lag time due to the time taken to fill the air capacitor to the new steady state[16]. This additional delay will affect the performance in transient applications, for instance single cylinder rickshaws and small vehicles, that are ubiquitous in developing nations such as India. Adequate transient performance is necessary for vehicles to navigate traffic.

We expect that capacitor size will affect transient response characteristics, with fill time increasing with capacitor size [16]. However, it is not known how these transient response times compare to those of the engine. In order to analyze the transient response times, a simple analytical model was created, and an empirical experiment was performed to test the response characteristics of a turbocharged single cylinder engine with an air capacitor. The response time of the baseline condition, the naturally aspirated engine, was also measured experimentally. This response time will change based on the inertia of the application where it is used. Two experiments were run for each size capacitor and for the naturally aspirated engine. The first experiment was designed to measure the response to speed transients. The second experiment was designed to measure the response to torque transients. Both experiment were

run with the IHI 31 turbocharger.

5.1 Using an Analytical Model to Approximate Characteristic Transient Response Time

Turbocharging will have two effects on the transient response time of the engine. The first effect is a function of the inertia of the turbocharger which introduces a time delay for the turbocharger to accommodate changes in speed [23]. The second effect is the additional time needed to pump up the capacitor to accommodate changes in pressure. The goal of this analytical model is to derive the characteristic response time for the system.

Calculating the time it takes for a turbocharger to reach its new steady state speed relies on a significant number of factors and cannot be calculated simply nor precisely [23, 67, 35]. However, a characteristic value for the time it takes for the turbocharger to reach its new operating speed can be approximated using a series of calculations from literature.

The approximate time it takes for the turbocharger to reach 90% of its final speed during a transient operation can be calculated using the inertia of the turbocharger, the speed change, the mechanical efficiency of the turbocharger, the turbine power, and the compressor power (Eqn. 5.1) [48].

$$t_{spool} = \frac{I * \Delta\Omega^2}{\eta_{mech} * P_{turbine} - P_{compressor}} \tag{5.1}$$

The compressor and turbine power can be estimated from their pressures and the change in enthalpy across these components (Eqn. 5.2-5.3). Note that the compressor efficiency is not needed since the energy calculation using enthalpy change across the compressor takes into account inefficiency [42, 28].

$$P_{turbine} = \eta_{turbine}\dot{m}\Delta h = \eta_t \dot{m} C_p \Delta T \tag{5.2}$$

$$P_{compressor} = \dot{m}\Delta h = \dot{m} C_p \Delta T \tag{5.3}$$

The temperature drop can be calculated using the isotropic relationship for an ideal gas (Eqn. 5.4).

$$T_{final} \approx T_{initial} * (\frac{P_2}{P_1})^{(\gamma-1)/\gamma} = T_{initial} * (\frac{P_2}{P_1})^{0.286} \tag{5.4}$$

Equations 5.1-5.4 can be combined in order to determine the characteristic response time of the system based on manifold pressures, turbocharger efficiencies, manifold temperatures, turbocharger inertia, and the turbocharger speed change (Eqn. 5.5). Due to mass conservation, the mass flow in the exhaust can be approximated as being the same as the intake mass flow rate.

$$t_{spool} \approx \frac{I * \Delta\Omega^2}{\dot{m} C_p (\eta_{mech}\eta_t T_{ex} * (1 - (\frac{P_{amb}}{P_{ex}})^{0.286}) - (T_{amb} * ((\frac{P_{cap}}{P_{amb}})^{0.286}) - 1))} \tag{5.5}$$

For each of these variables, a value, or a range of expected values, can be found from either the experiment or from literature (Table 5.1). Data from the experiment is used to approximate mass flow-rate, pressures, and temperatures, while literature data is used to estimate the other variables.

Based on these values, the expected turbocharger spool time for a 3000 RPM engine can be estimated to be approximately 2.46 seconds.

The time needed to pump up the capacitor can be approximated using a mass flow model of the system (Fig. 5-1) [17]. The steady state mass flow of the system can be evaluated from the experimental data. In this case, the data used were from the IHI turbocharger experiments that were presented in Chapter 4. The mass flow can be described as a function of engine speed for a constant torque system, (Eqns.

Table 5.1: Characteristic value ranges used to approximate spool time of the turbocharger. [29, 5]

Variable	Estimated Value
Inertia	$2.4 * 10^{-6}$ kg m^2**
Turbocharger Speed	10^4 rad/s**
$\dot{m}$ (3500 RPM)	18 g/s*
$\dot{m}$ (3000 RPM)	15 g/s*
$\dot{m}$ (2500 RPM)	12 g/s*
P_{amb}	1 bar
P_{ex}	1.5 bar*
P_{cap}	1.5 bar*
T_{amb}	300 K
T_{ex}	800 K*
C_p	1005 (kJ/kgK)
η_t	0.55**
η_{mech}	0.85***

**Based on values obtained from the Kholer engine steady state tests with the IHI 31 turbocharger*
***Based on data from similarly sized turbochargers [29]*
****Values From literature which show the high speed efficiency of the turbocharger to be between 80-98% based on turbocharger speed. A conservative estimate of 85% was used. [27]*

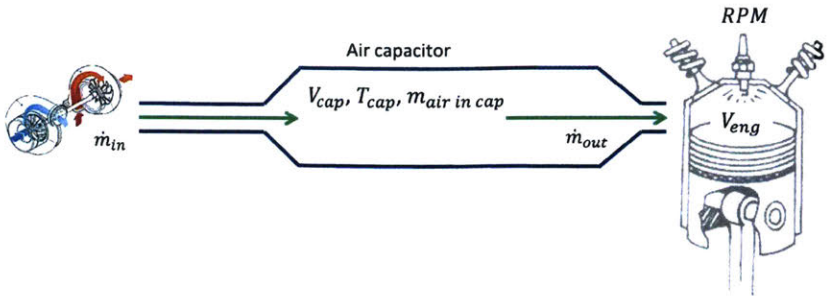

Figure 5-1: Diagram of the transient mass flow model.

5.6-5.7) or as a function of torque for a constant speed system (Eqns. 5.8-5.9).

$$\dot{m}_{\tau=0} \approx 0.0031 * RPM + 3.4553[g/s] \tag{5.6}$$

$$\dot{m}_{\tau=10} \approx 0.0058 * RPM - 3.192[g/s] \tag{5.7}$$

$$\tau_{RPM=3000} \approx 13.55 + 0.056 * \tau[g/s] \tag{5.8}$$

$$\tau_{RPM=3500} \approx 14.188 + 0.513 * \tau[g/s] \tag{5.9}$$

The mass flow rate of air out of the capacitor can be estimated using the assumption that the pressure inside the air capacitor and the pressure inside the engine equalize during the intake stroke (Eqn. 5.10).

$$\dot{m}_{out} \approx \frac{V_{eng}}{V_{cap} + V_{eng}} * m_{air\ in\ cap} \tag{5.10}$$

The mass of air in the capacitor can be estimated from the mass flow-rate of air through the engine (Eqn. 5.11).

$$m_{air\ in\ cap} \approx \frac{V_{cap} + V_{eng}}{V_{eng}} * \dot{m} \tag{5.11}$$

From this model a characteristic time to pump up the capacitor can be found. The characteristic time is defined as the amount of time it takes to fill the capacitor to 90%

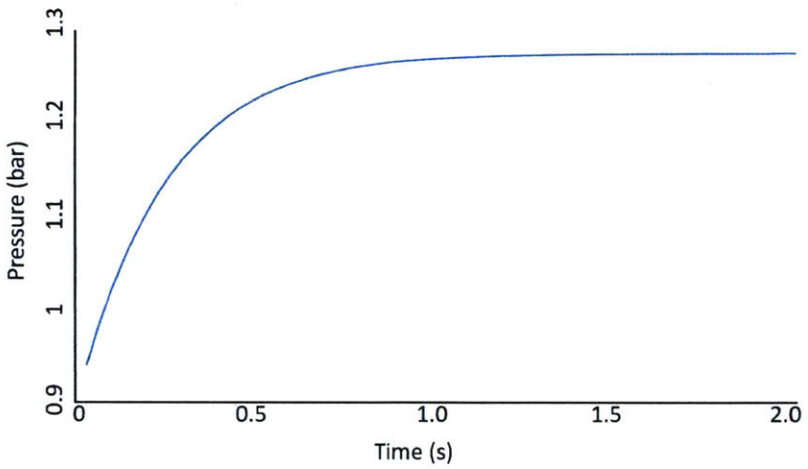

Figure 5-2: Plot of the pressure increase in the air capacitor as a function of time for the pump-up model.

of the way from its initial pressure to its final pressure. The characteristic fill time calculation assumes that the mass flow rate into the air capacitor is the steady state mass flow rate at its final engine running condition. This system is solved iteratively in MatLab with the mass of air inside the capacitor being recalculated every engine cycle. For a 3000 RPM engine, with an air capacitor volume equal to 7 times the engine volume and going from 0 Nm to 13.5 Nm of torque, the characteristic time to fill the capacitor is predicted to be 0.833 seconds (Fig. 5-2).

The total characteristic response time for the air capacitor of the turbocharger will be a combination of spool time and capacitor pressurization time. To approximate how these two effects combine, it is assumed that during the spool-up phase the mass flow rate is linearly dependent on the turbocharger speed and that the turbocharger speed also increases linearly. Once the turbocharger is fully spooled, the mass flow-rate into the capacitor is approximated to be the maximum mass flow-rate. This system is solved iteratively in MatLab with the mass of air inside the capacitor being recalculated every engine cycle (Eqns. 5.12 - 5.13).

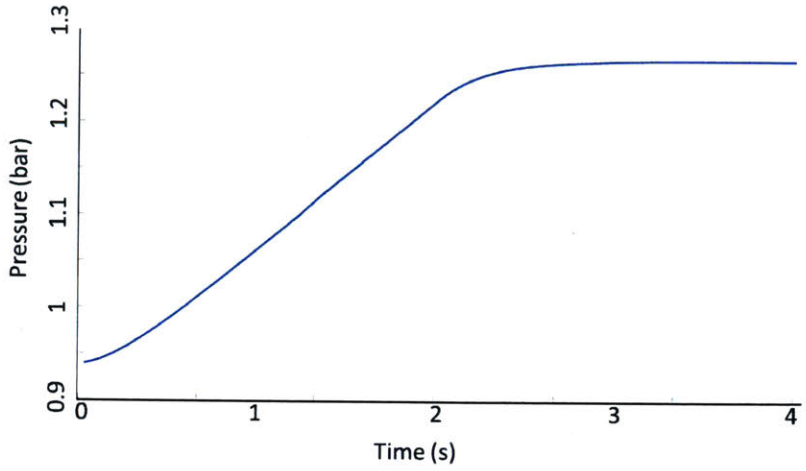

Figure 5-3: Plot of pressure increase in the 7 times volume air capacitor as a function of time for the combined turbocharger transient model at 3000 RPM with a load varying from 0 Nm to 13.5 Nm.

$$m_{in} = \begin{cases} (\dot{m}_{initial} + (\dot{m}_{final} - \dot{m}_{initial}) * t/t_{spool}) * \frac{120}{RPM} & if\ t < t_{spool} \\ \dot{m}_{final} * \frac{120}{RPM} & else \end{cases} \tag{5.12}$$

$$m_{airincap}(c) = m_{airincap}(c-1) - m_{out} + m_{in} \tag{5.13}$$

The combined characteristic turbocharger response time was found to be 2.56 seconds (Fig. 5-3). It is observed that the initial pressure response is slow due to the spooling of the turbocharger. Once the turbocharger is spooled the pressure inside the air capacitor increases relatively quickly until it approaches its final value at which point the pressure increases slowly. This response profile matches predictions from literature [28].

In order to see how capacitor size affects the characteristic response time, the characteristic response times for different capacitor sizes are compared for identical pressure conditions (starting at 1 bar and going to 1.5 bar) (Fig. 5-4). Capacitor size

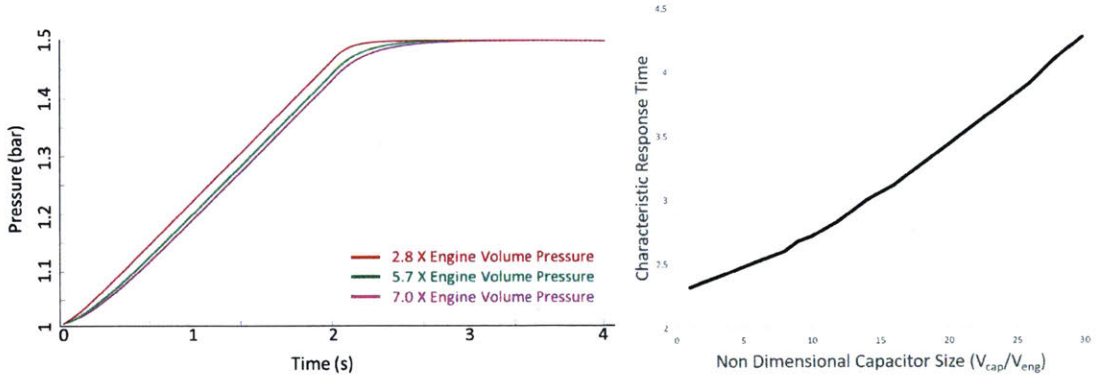

Figure 5-4: Left: Model Prediction of pressure response profile for different capacitors being pressurized from 1 bar to 1.5 bar. Right: Characteristic air capacitor pressurization time as a function of capacitor size for a capacitor being filled from 1 bar to 1.5 bar

has a significant effect on characteristic response time. For small capacitors (less than 8 times engine volume), the spool time lag dominates the response while the fill time lag dominates for larger capacitors. The change in which response time dominates is indicated by the change in slope of the response time vs capacitor size curve shown in Fig. 5-4.

The goal of this calculation was to find the characteristic response time of the turbocharger. This is not a calculation of the exact pressure response time of the air capacitor since the calculation assumes the engine response time is instantaneous. The relevance of the response time is in how it compares to the response time of the naturally aspirated engine. If the engine's response time is significantly greater then the turbocharger calculated response time, then the effect of turbocharger lag will be small. If the effect of the turbocharger is on the same order of magnitude or larger then the engine's characteristic response time then the effect of turbocharger lag will be notable.

5.2 Speed Response Experiment

The first experiment was a transient speed response test. In this test, the engine governor was quickly repositioned using a linear electric actuator to quickly increase

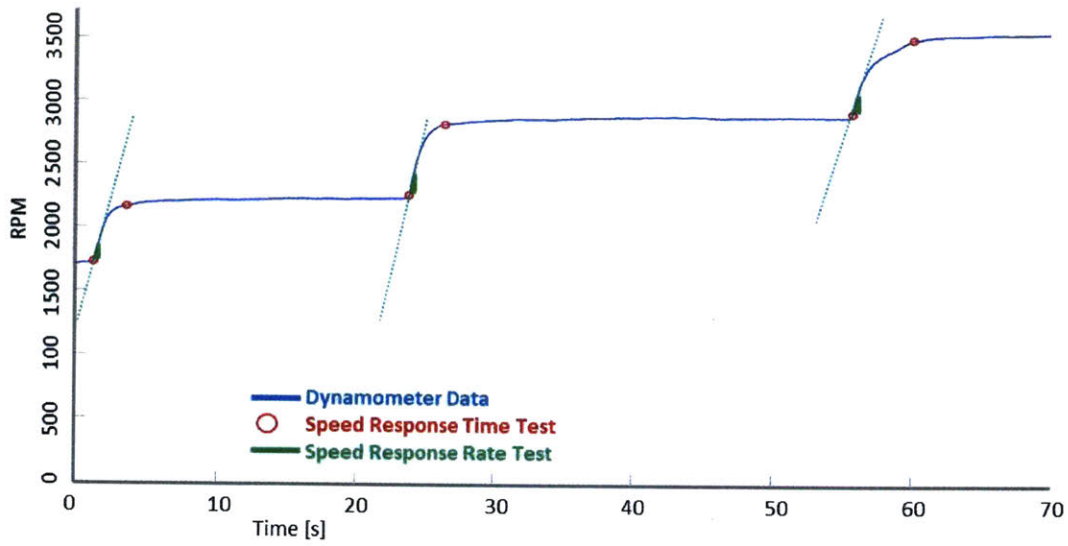

Figure 5-5: Plot of sample speed response from a set of three naturally aspirated tests. The blue line is the dynamometer speed data. The red circles represent the end points (initial and final time) for the speed response time test. The green lines represent the speed response rate.

speed. Two different measures of speed response were obtained from this test. The first measure of speed response is the speed response time, which is the amount of time it takes to reach a new steady state speed. For this test, the time it takes to go from the initial speed (measured from when speed is 1% larger than the speed half a second before the throttle movement) to the final speed (measured when the speed is 90% of the final steady state speed, defined as the speed one second after this point) was measured [31]. The second measure of speed response is the response rate, which is the slope of the initial response to the new throttle position. The slope is measured using the initial 0.2 seconds of response time. This gives a value with units of RPM per second. Figure 5-5 illustrates how this test was run.

The speed response analysis was run for two cases: no load on the engine and 60% of rated load on the engine. The speed test was run enough times to generate a 95% confidence interval for each capacitor load combination. The pressure response to speed changes matches the same trend that is predicted in the analytical model (Fig. 5-6). There is an initial delay and slow response due to the turbocharger spooling.

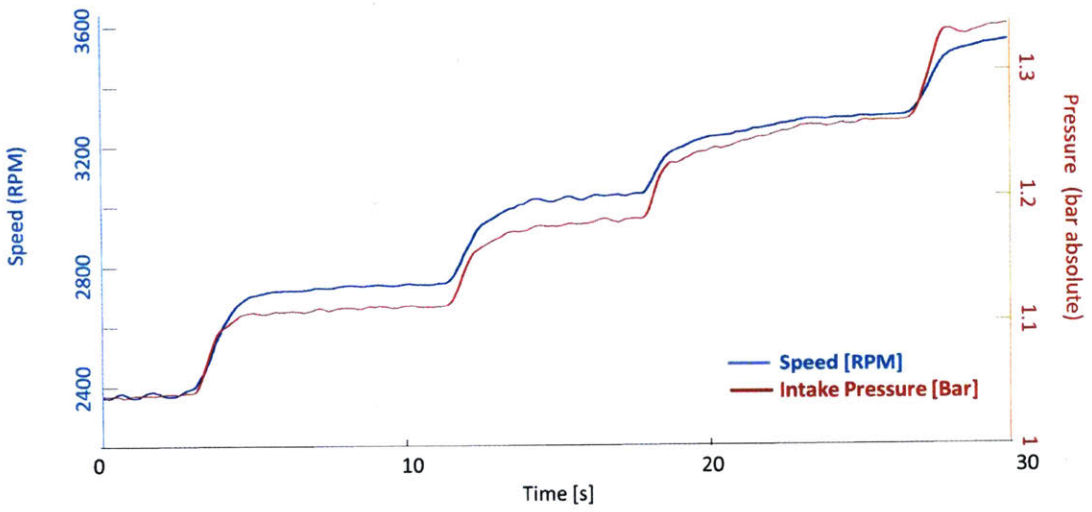

Figure 5-6: Speed response for the large capacitor loaded case shown next to the engine's intake pressure. The intake pressure quickly responds to speed changes in a single cylinder turbocharged engine with an air capacitor

Then, the pressure inside the air capacitor increases quickly as it is filled and then tapers off as it approaches its steady state pressure.

To test the speed response rate, the test was run using different initial and final speeds that were then normalized. In order to normalize the data, the response time was adjusted by the initial speed (Eqn. 5.14). Adjustment based on initial engine speed was chosen since the response rate will be dependent on the number of cycles the engine has to respond to an impulse.

$$non - dimensionalised\ response\ rate = \frac{\sqrt{Response\ Rate * 60} * 60}{Initial\ Speed} \tag{5.14}$$

Figure 5-7 shows the normalized speed response rate for the speed response tests. The results of these tests show that the dimensionless response rate was greater in the naturally aspirated case than for the turbocharged case by about 25% to 30% for both the loaded and unloaded conditions. This response rate delay is due to the

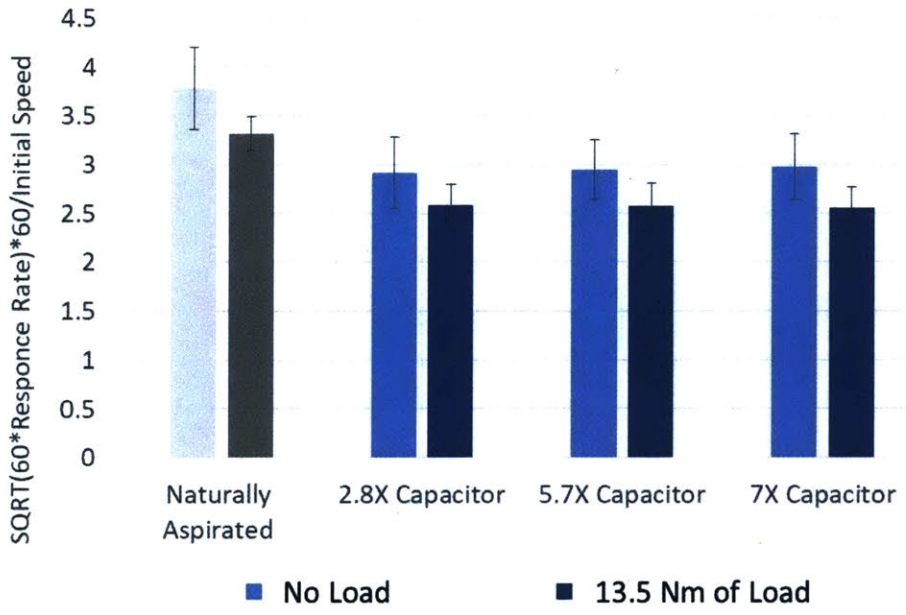

Figure 5-7: Adjusted speed response rate for the loaded and unloaded speed response tests. The error bars represent the 95% confidence interval.

back pressure caused by the turbocharger since it is happening both at low and high loads. The experiment also shows that the response rate is slower in the loaded case for both the naturally aspirated and turbocharged engine.

Figure 5-8 shows the speed response times from the speed response tests. These tests show that the response rate and time are not affected by capacitor size. This can be attributed to the capacitors all being sized in the regime where turbocharger spool time dominates capacitor fill time. This result combined with the initial response rate result imply that the engine's speed change is mostly a factor of the engine's response time and not the turbochargers response. The engine's governor is able to overcome the initially slower response rate in the turbocharged cases and match the response time of the naturally aspirated engine.

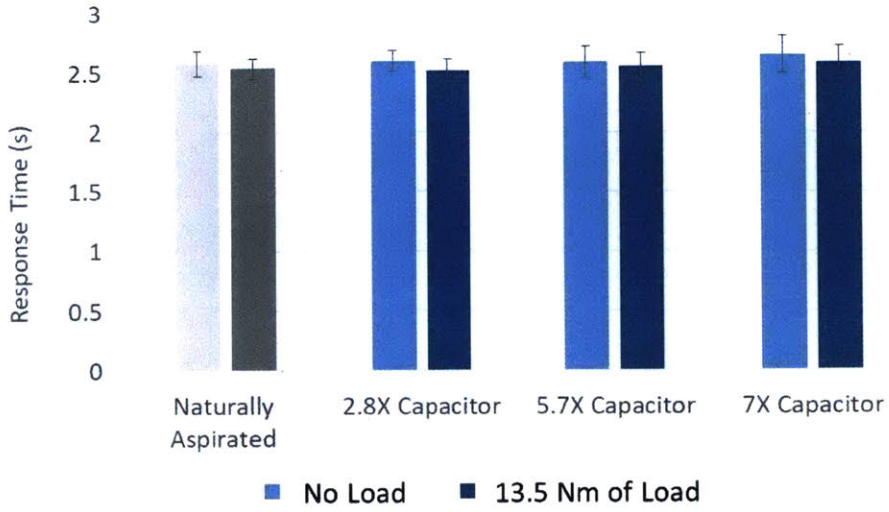

Figure 5-8: Speed response time for the loaded and unloaded speed response tests. The error bars represent the 95% confidence interval.

5.3 Torque Response Experiment

The second experiment was the load response test. In this test the load on the dynamometer was increased and the time it took for the engine to react and reach a new steady state air capacitor pressure was measured. The torque profile was mainly a function of the dynamometer's ability to apply a load. As a result, the pressure response profile was analyzed in order to obtain an empirical estimate of torque response and to verify that the response profile is similar to the response profile that the analytical model predicts.

The pressure response to a torque impulse is shown in Fig. 5-9. This plot shows that the torque response for all three turbocharged cases with different capacitor sizes is approximately the same. As expected, the intake pressure increases with capacitor size. The shape of the pressure response profile matches the shape of the predicted analytical pressure response profile. There is an initial delay and slow response which is due to the turbocharger spooling. Subsequently the pressure inside the air capacitor increases rapidly, as it is filled, and then tapers off as it approaches its steady state pressure.

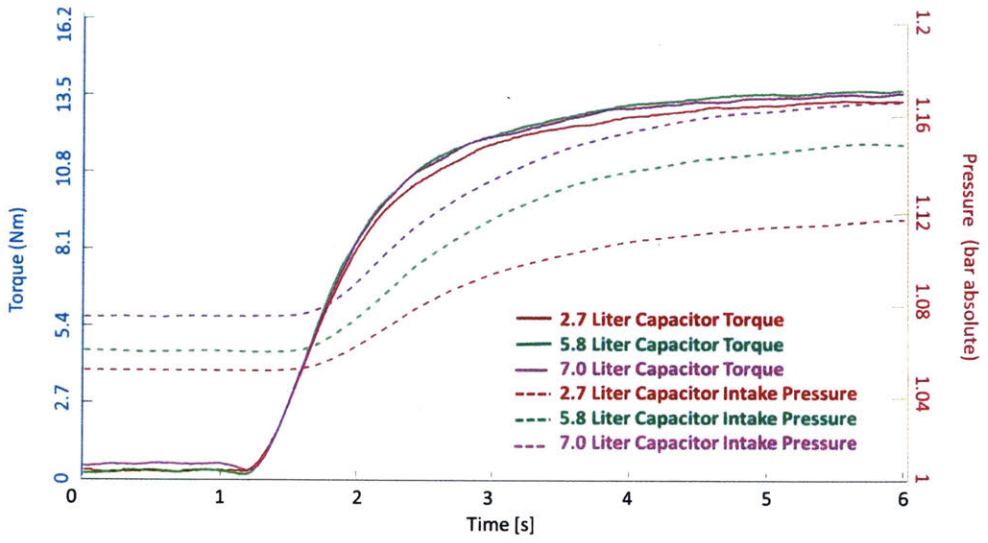

Figure 5-9: Experimental results for the average normalized torque and pressure response to a torque input signal at 3000 RPM. Each line represents the average response from multiple tests for each engine configuration.

5.4 Conclusion

It was initially hypothesized that capacitor size would affect the transient response characteristics of a single-cylinder, four-stroke engine. An analytical model was used to predict characteristic turbocharger spool time, characteristic capacitor fill time, and the transient response profile of the pressure in the air capacitor. This model predicted an initial delay and slow response due to the turbocharger spooling. Afterwards, the pressure inside the air capacitor increases quickly as the turbocharger reaches its final speed. Finally, the rate of pressure increase inside the air capacitor tapers off as it approaches its new steady state. This model also predicts how capacitor size affects characteristic response time.

An experiment was designed and run to determine how capacitor sizing affects transient engine response characteristics. Transient speed and torque response characteristics were measured. The transient speed response tests found that the turbocharger reduced the initial rate of response to speed changes but had little effect on response time for both the loaded and unloaded case. In this case, the response

times are dominated by the engine's response time and not that of the turbocharger. The transient torque response test found that the time to pressurize the capacitor and the pressure inside the capacitor are affected by capacitor size. These tests also showed that the pressure response profile matched the shape of the pressure response profile predicted by the analytical model.

Future tests are proposed where different turbochargers are tested and pressures in the capacitor are measured at high frequency in order to analyze the pressure throughout each cycle. Additionally, future tests are proposed to analyze a wider range of engine running conditions, with larger and smaller capacitor sizes and different torque transients, that could affect the engine transient response differently.

Chapter 6

Computational Model Multi-Variable Optimization

Being able to optimize the engine's performance is key to commercial viability. In order to optimize engine geometry, engine timings, and manifold geometry for specific applications, the Ricardo Wave model was combined with a simulated annealing optimization methodology using Simulink and Matlab (Fig. 6-1).

Different engine applications required different optimization scoring functions and different variable engine parameters. The simulated annealing scheme was then run until a suitable minimum was found that also maintained a practical engine geometry and timings. This minimum was then refined using a linear optimizer. Finally, the

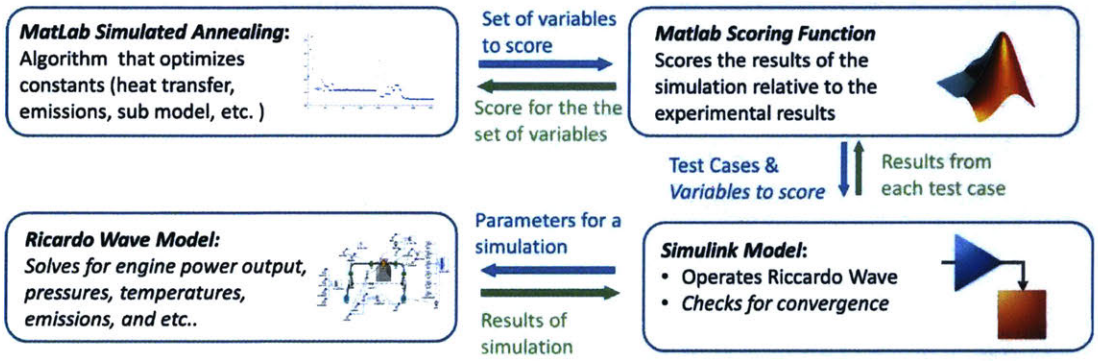

Figure 6-1: Flow chart of the optimization method combining the computational model of Ricardo Wave and Matlab simulated annealing.

optimization's sensitivity to each of the variables was calculated.

For these studies, up to 14 variables that could be optimized were identified. Initial values and reasonable bounds were set for each identified variable (Table 6.1). The intake manifold was modeled as an intercooler with 14 rectangular channels whose dimensions could be varied. The exhaust manifold was modeled as a tube with a variable diameter and length. The bore and stroke of the cylinder could be changed. The valve lift and connecting rod lengths change proportionally with the stroke. The diameter of the valves changed proportionally with the bore, such that decreases in engine size resulted in decreases in frictional losses and increases in the pressure drop across the valves.

There were five studies performed using the model. Each of these studies were designed to analyze different engine configurations for insights into how to design engines for different potential applications.

1. An initial sensitivity analysis to determine how the different engine parameters affected power, fuel economy, and emissions.

2. An optimization used to determine the engine geometries and timings of an air capacitor turbocharged engine system designed for a specific power output.

3. An optimization used to determine the manifold geometries and timings of a retrofitted air capacitor turbocharged engine system designed to minimize fuel consumption.

4. An optimization used to determine the manifold geometries and timings of a retrofitted air capacitor turbocharged engine system designed to maximize power output.

5. An optimization used to determine the engine geometries and timings of an air capacitor turbocharged engine system designed for a specific power output at high elevation.

Table 6.1: Adjusted variables in the engine optimization experiments.

Variable	Initial Value	Lower Bound	Upper Bound
IVO[1]	10	0	20
IVC[2]	42	30	50
EVO[3]	58	45	65
EVC[4]	10	0	20
Injection Start[3]	6	15	3
Injection Duration	20	7	25
Channel Width (mm)	60	30	120
Channel Hight (mm)	6	4	12
Channel Length (mm)	230	150	500
Exhaust Diameter (mm)	40	30	50
Exhaust Length (mm)	40	20	60
Bore (mm)	86	60	105
Stroke (mm)	76	55	100
Compression Ratio	20.3	15	22

1. *Degrees before bottom dead center*
2. *Degrees after top dead center*
3. *Degrees before top dead center*
4. *Degrees after bottom dead center*

6.1 Sensitivity Analysis

Sensitivity analyses were performed to determine how the different engine parameters affected power, fuel economy, and emissions. The sensitivity analysis was performed for an engine running at 3500 RPM and an air to fuel equivalence ratio of 2 (close to maximum power). Results for the optimized turbocharger and intercooled engines are shown in Table 6.2. The sensitivity for dimensional variables is reported as percent change in the output value per percent change for the given input (Eqn 6.1). The sensitivity for timing variables is reported as the percent change in the output value per change in degree of the given input (Eqn 6.2).

$$Sensitivity = |\frac{Value(Var/1.01)}{2 * Value(Var)}| + |\frac{Value(Var/0.99)}{2 * Value(Var)}| \tag{6.1}$$

$$Sensitivity = |\frac{Value(Var+1)}{2 * Value(Var)}| + |\frac{Value(Var-1)}{2 * Value(Var)}| \tag{6.2}$$

The two most influential parameters for the turbocharged and intercooled engines were engine geometry and fuel injection timing. Engine geometry had the largest effect on power output and a notable effect on fuel economy and NOx emissions. The injection timing had the largest effect on fuel economy and emissions while also having a notable effect on power output.

Both intake valve timing and compression ratio had comparatively little influence on fuel economy but a noticeable influence on power and NOx emissions. Meanwhile, the exhaust valve timings had little effect on the engines overall performance relative to other parameters.

The intake manifold geometry was found to have a minimal effect on fuel economy but a noticeable effect on power output and NOx emissions. The intake manifold's influence on power is due to the air capacitor effect, while its influence on emissions is most likely due to the cooling effect of the inter cooler changing with engine geometry.

Table 6.2: The sensitivity of engine performance metrics to different variables

Variable	Power	Fuel	NOx
IVO (%/°)	0.324	0.065	0.413
IVC (%/°)	0.260	0.02	0.361
EVO (%/°)	0.048	0.042	0.066
EVC (%/°)	0.023	0.014	0.058
Injection Start(%/°)	0.274	0.799	3.576
Injection Duration (%/°)	0.009	0.016	0.05
Channel Width (%/%)	0.129	0.024	0.047
Channel Hight (%/%)	0.087	0.024	0.195
Channel Length (%/%)	0.195	0.034	0.050
Exhaust Diameter (%/%)	0.033	0.057	0.198
Exhaust Length (%/%)	0.001	0.018	0.204
Bore (%/%)	2.181	0.628	2.800
Stroke (%/%)	0.995	0.377	1.470
Compression Ratio (%/%)	0.027	0.069	0.413

The exhaust manifold dimensions were found to have minimal influence relative to other parameters on fuel economy and power output but have some influence on NOx emissions.

6.2 Optimization Results

Different engine use scenarios were determined based on possible common use cases. The goals of these optimizations were to show that a turbocharged engine with an air capacitor will have better performance than a naturally aspirated engine and demonstrate how these engines should be designed. For each scenario an objective function was created and a simulated annealing algorithm was used to optimize the engine to minimize the objective function.

6.2.1 Designing a 6.8 kW Engine to Minimize Fuel Consumption

The first optimization example is to design a 6.8 kW (9 hp) engine with maximum fuel efficiency. This power level was chosen since it is the rated power of the Kholer engine used in the experiment and it is a common size for agricultural single cylinder engines. The degrees of freedom in this case would be the engine geometry, engine timings, and manifold geometry.

Equation 6.3 describes the objective function for this optimization. The air to fuel ratio needed to achieve 6.8 kW was calculated for each iteration, and then the fuel consumption for that ratio was calculated. If the air to fuel ratio was below 25 (the minimum steady state air to fuel ratio achieved on the Dynamometer) the simulation was determined to be nonviable and the objective function changed to give such simulations high scores to guide the simulation back to a viable engine configuration.

Table 6.3: The optimized values and the sensitivity of engine performance metrics to different variables for the full engine optimization.

Variable	Optimized Value	Fuel Sensitivity	Power Sensitivity
IVO	5.5[1]	0.01 (%/°)	0.02 (%/°)
IVC	24.6[2]	0.02 (%/°)	0.11 (%/°)
EVO	66[3]	0.03 (%/°)	0.03 (%/°)
EVC	19.5[4]	0.01 (%/°)	0.06 (%/°)
Injection Start	13[3]	0.11 (%/°)	0.60 (%/°)
Injection Duration	14	0.10 (%/°)	0.20 (%/°)
Channel Width	151.5 mm	0.01 (%/%)	0.07 (%/%)
Channel Hight	5.1 mm	0.02 (%/%)	0.08 (%/%)
Channel Length	296 mm	0.01 (%/%)	0.13 (%/%)
Exhaust Diameter	36.5 mm	0.03 (%/%)	0.03 (%/%)
Exhaust Length	20.5 mm	0.03 (%/%)	0.05 (%/%)
Bore	76.8 mm	0.32 (%/%)	2.58 (%/%)
Stroke	62 mm	0.20 (%/%)	1.30 (%/%)
Comp Ratio	22.2	0.07 (%/%)	0.20 (%/%)

1. *Degrees before bottom dead center*
2. *Degrees after top dead center*
3. *Degrees before top dead center*
4. *Degrees after bottom dead center*

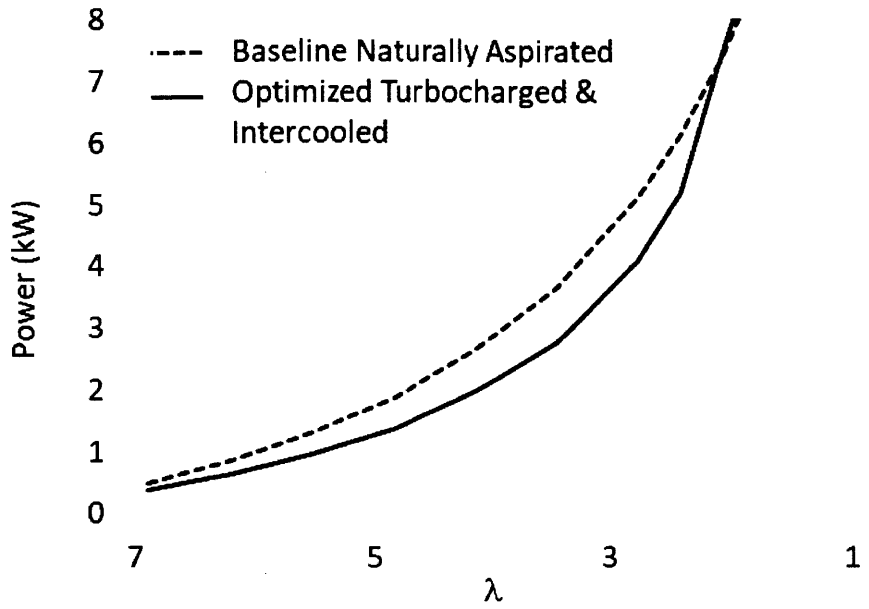

Figure 6-2: Power Output as a function of air to fuel equivalence ratio for the fully optimized engine compared to the baseline naturally aspirated engine.

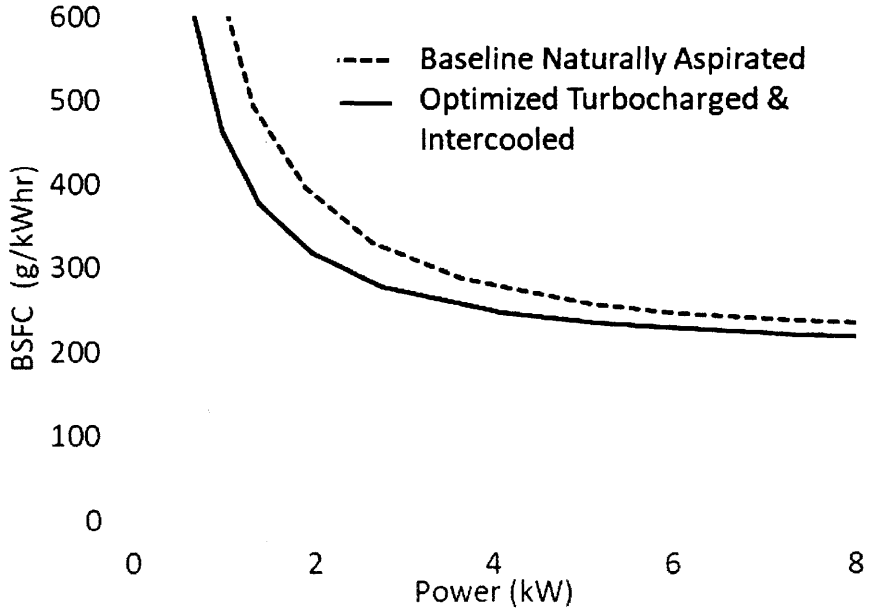

Figure 6-3: Fuel economy as a function of power output for the fully optimized engine compared to the baseline naturally aspirated engine.

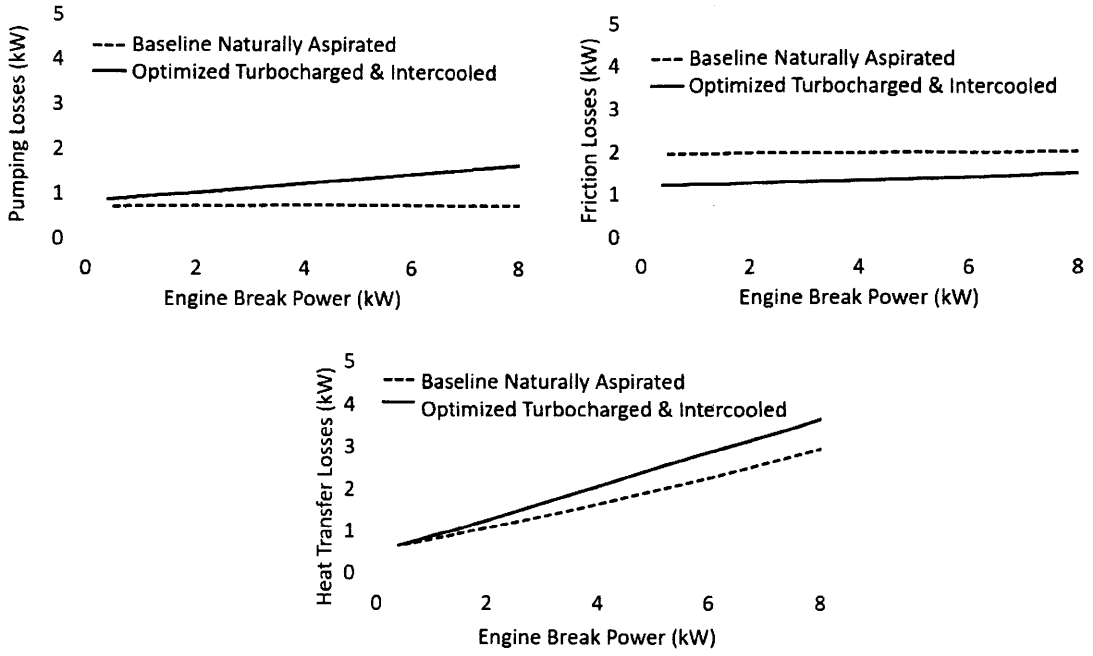

Figure 6-4: Engine losses as a function of power output for the fully optimized engine compared to the baseline naturally aspirated engine.

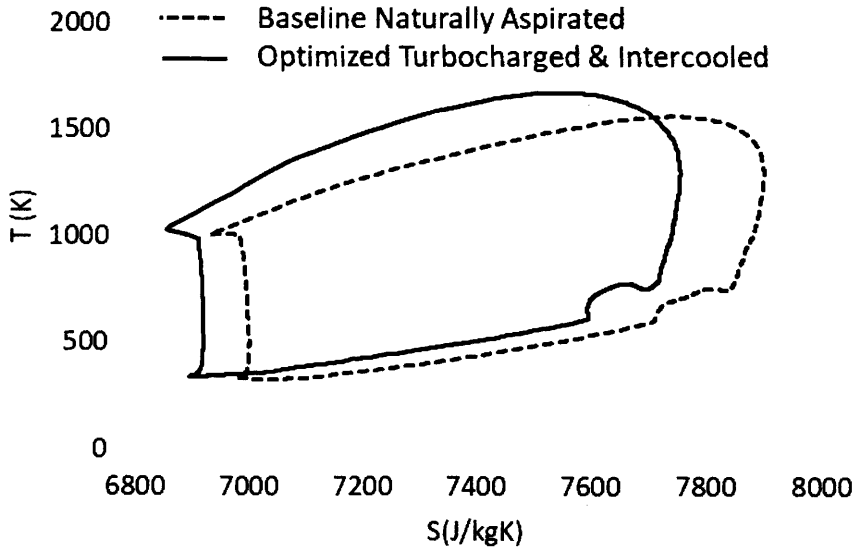

Figure 6-5: Entropy vs. temperature for the fully optimized engine's cycle compared to the baseline naturally aspirated engine's cycle.

$$Score = \begin{cases} 20 - \frac{af}{2} & \text{if air to fuel ratio} < 25 \\ \frac{BSFC - BSFC_{baseline}}{BSFC_{baseline}} & \text{if air to fuel ratio} > 25 \end{cases} \tag{6.3}$$

The results of this optimization and the sensitivity of the engine's performance to each variable are shown in Table 6.3. The engine's geometry and injection timing had the largest effect on improving the engine's overall performance. The manifold dimensions had little effect on fuel economy or power output. This implies that as long as there is a large intake manifold with significant heat transfer and a small exhaust manifold with minimal heat transfer, optimal performance will be achieved. The valve timings and compression ratio also had a minimal effect on the engine's overall performance.

Figure 6-2 shows how the fully optimized engine's power, as a function of air to fuel equivalence ratio, compares to the naturally aspirated case. The fully optimized engine produced less power at higher air to fuel equivalence ratios than the naturally aspirated engine. However, at low air to fuel equivalence ratios, the effect of the turbocharger is maximized and the fully optimized engine produces a larger power output than the naturally aspirated engine.

The fully optimized engine had a notable fuel economy advantage over the naturally aspirated engine (Fig. 6-3). The gains in efficiency result primarily from a reduction in frictional losses (Fig. 6-4) and from the engine operating over a larger temperature range (Fig. 6-5). However, it was found that the engine had an increase in pumping losses, due to increased back pressure from the turbocharger, and an increase in heat transfer losses, due to the higher operating temperature of the engine.

6.2.2 Retrofitting an Engine to Minimize Fuel Consumption

Another example of the application of the air capacitor method is retrofitting an existing engine to minimize fuel consumption while increasing power. In this case,

Table 6.4: The optimized values and the sensitivity of engine performance metrics to different variables fuel consumption minimized retrofitted engine.

Variable	Optimized Value	Fuel Sensitivity	Power Sensitivity
IVO	9[1]	0.01 (%/°)	0.13 (%/°)
IVC	33.5[2]	0.01 (%/°)	0.14 (%/°)
EVO	63.9[3]	0.01 (%/°)	0.08 (%/°)
EVC	14.2[4]	0.01 (%/°)	0.08 (%/°)
Injection Start	12.6[3]	0.12 (%/°)	0.61 (%/°)
Injection Duration	11	0.05 (%/°)	0.14 (%/°)
Channel Width	71.7 mm	0.01 (%/%)	0.12 (%/%)
Channel Hight	4.5 mm	0.04 (%/%)	0.14 (%/%)
Channel Length	290 mm	0.03 (%/%)	0.27 (%/%)
Exhaust Diameter	50 mm	0.05 (%/%)	0.06 (%/%)
Exhaust Length	25 mm	0.02 (%/%)	0.08 (%/%)
Comp Ratio	21	0.01 (%/%)	0.10 (%/%)

1. *Degrees before bottom dead center*
2. *Degrees after top dead center*
3. *Degrees before top dead center*
4. *Degrees after bottom dead center*

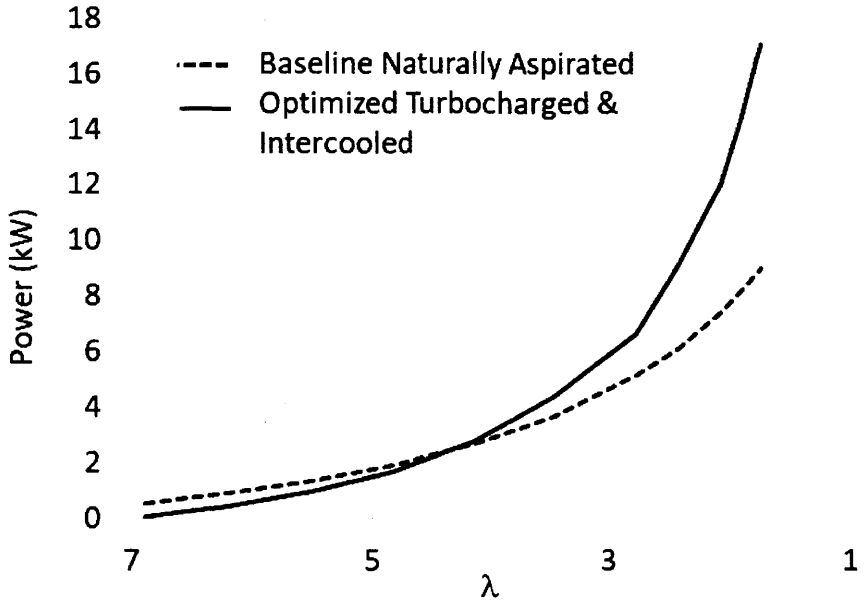

Figure 6-6: Power output as a function of air to fuel equivalence ratio for the fuel consumption optimized retrofitted engine compared to the baseline naturally aspirated engine.

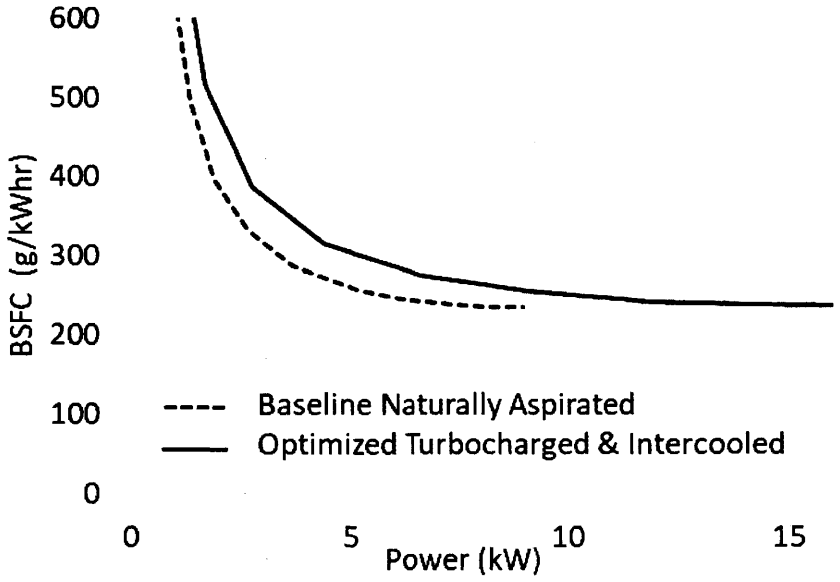

Figure 6-7: Fuel economy as a function of power output for the fuel consumption optimized retrofitted engine compared to the baseline naturally aspirated engine.

the bore and the stroke are kept constant while the other 12 variables are being optimized. The engine geometry is based on the Kholer KD440.

Equation 6.4 shows the objective function for this optimization. For each iteration, the operation of the engine was simulated with an air to fuel equivalence ratio of 2. If the power output was below the target power output (9 kW), the simulation was determined to be nonviable and the objective function was changed to guide the simulation back to a viable engine configuration. The results of this optimization and the sensitivity of the engine's performance to each variable are shown in Table 6.4. Once again, injection timing had the largest effect on improving the engine's overall performance, while the manifold dimensions had little effect on fuel economy or power output. The valve timings and compression ratio were also found to have a minimal effect on the engine's overall performance.

$$Score = \begin{cases} 20 - Power & \text{if Power} < 9 \\ \frac{BSFC - BSFC_{baseline}}{BSFC_{baseline}} & \text{if Power} > 9 \end{cases} \tag{6.4}$$

Figure 6-6 plots power as a function of the air to fuel equivalence ratio for the optimized engine and the naturally aspirated engine. At higher air to fuel equivalence ratios the fully optimized engine produced approximately equal power to that of the naturally aspirated engine. However, at low air to fuel equivalence ratios the effect of the turbocharger is maximized and the fully optimized engine produced a larger power output than the naturally aspirated engine.

While the fuel consumption increased at lower powers, the optimized engine had a fuel economy performance advantage over the naturally aspirated engine at higher powers (Fig. 6-7). This is due to the engine having additional frictional, pumping, and heat transfer losses at lower powers. At higher powers these additional losses become relatively small due to the increase in power output of the engine. This optimization shows that it is possible to retrofit an existing engine with a turbocharger to produce significantly more power without sacrificing fuel economy at higher power levels. In

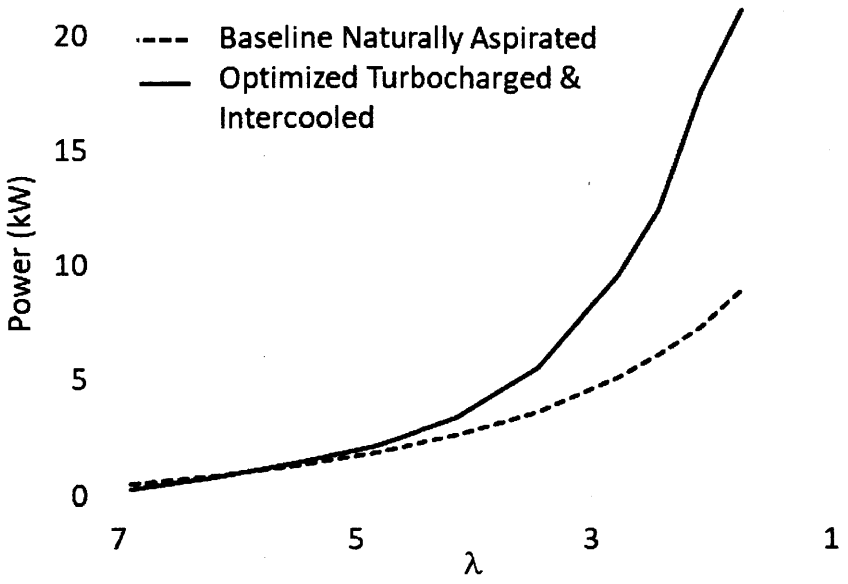

Figure 6-8: Power output as a function of air to fuel equivalence ratio for the power maximized retrofitted engine compared to the baseline naturally aspirated engine.

this scenario the tradeoff is per unit fuel consumption at lower power levels.

6.2.3 Retrofitting a Kohler Engine to Maximize Power

The next case study was the retrofit of an existing engine with the single goal of maximizing power output. In this case, the bore and the stroke remained constant and the engine was optimized for the other 12 variables. The baseline engine and the optimized engine's baseline geometry are based on the Kholer KD440.

In this scenario, the objective function was based on the power output (Eqn. 6.5). The air to fuel equivalence ratio was set to 2. The results of this optimization and the sensitivity of the engine's performance to each variable are shown in Table 6.5. Injection timing had the largest effect on improving the engine's overall performance, and the manifold dimensions had little effect on fuel economy or power output. The valve timings and compression ratio also had little effect on the engine's overall performance.

Table 6.5: The optimized values and the sensitivity of engine performance metrics to different variables for the power maximized retrofit engine.

Variable	Optimized Value	Fuel Sensitivity	Power Sensitivity
IVO	5.8[1]	0.02 (%/°)	0.15 (%/°)
IVC	26.4[2]	0.01 (%/°)	0.02 (%/°)
EVO	52.6[3]	0.04 (%/°)	0.08 (%/°)
EVC	6.1[4]	0.02 (%/°)	0.08 (%/°)
Injection Start	12[3]	0.18 (%/°)	0.12 (%/°)
Injection Duration	19.7	0.13 (%/°)	0.13 (%/°)
Channel Width	200 mm	0.01 (%/%)	0.14 (%/%)
Channel Hight	4.0 mm	0.02 (%/%)	0.06 (%/%)
Channel Length	498 mm	0.01 (%/%)	0.12 (%/%)
Exhaust Diameter	33.3 mm	0.01 (%/%)	0.05 (%/%)
Exhaust Length	35.7 mm	0.01 (%/%)	0.07 (%/%)
Comp Ratio	19.7	0.03 (%/%)	0.05 (%/%)

1. *Degrees before bottom dead center*
2. *Degrees after top dead center*
3. *Degrees before top dead center*
4. *Degrees after bottom dead center*

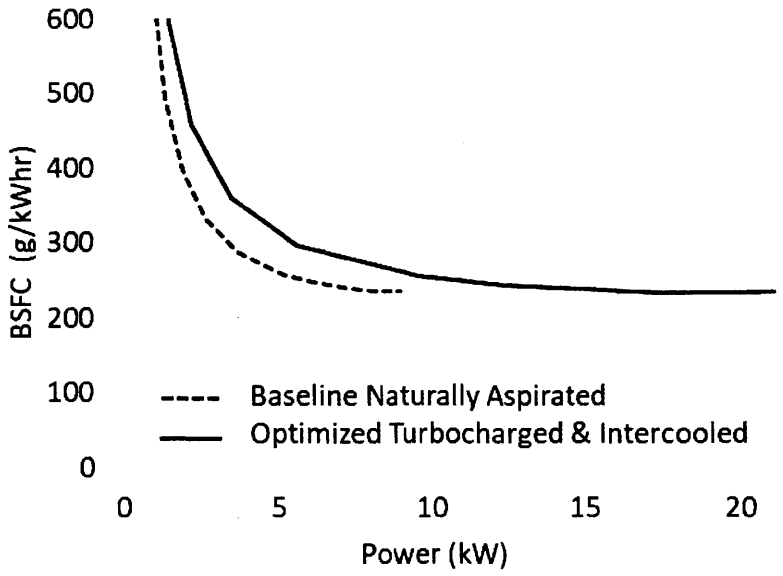

Figure 6-9: Fuel economy as a function of power output for the power maximized retrofitted engine compared to the baseline naturally aspirated engine.

$$Score = \frac{Power - Power_{baseline}}{Power_{baseline}} \tag{6.5}$$

Figure 6-9 shows how the optimized engine's power as a function of air to fuel equivalence ratio compares to that of the naturally aspirated engine. The fully optimized engine produced approximately equal power as the naturally aspirated engine at higher air to fuel equivalence ratios. However, at low air to fuel equivalence ratios the effect of the turbocharger was maximized and the optimized engine produced more than double the power output of the naturally aspirated engine.

While the fuel consumption increased at lower powers, the optimized engine was able to match the fuel economy of the naturally aspirated engine at higher powers (Fig. 6-9). This is due to the engine having additional frictional, pumping, and heat transfer losses at lower powers. At higher powers, these additional losses become relatively small due to the increase in power output of the engine.

It is worth noting that in this scenario the turbocharger is operating at significantly

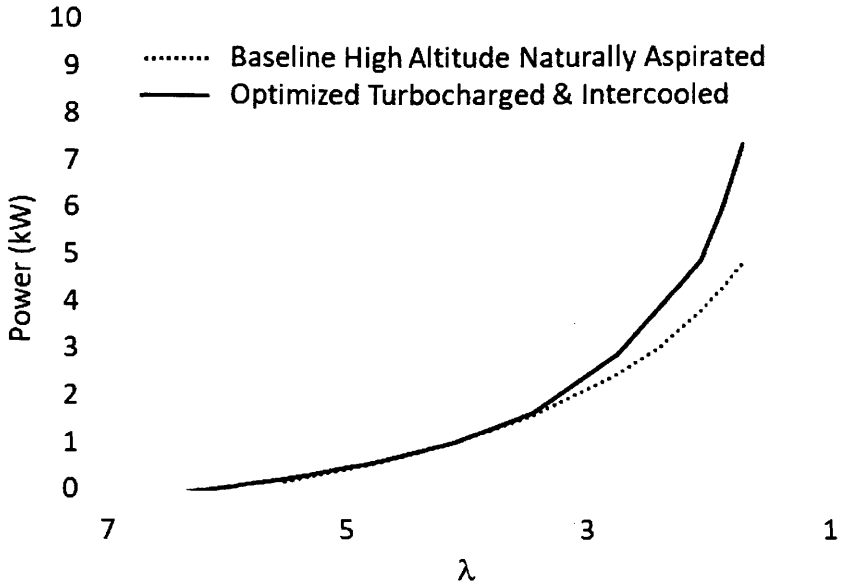

Figure 6-10: Power output as a function of air to fuel equivalence ratio for the high altitude optimized engine compared to the baseline naturally aspirated engine at high altitude.

higher pressures than the waste gate pressure set in the experiment. The peak cylinder pressure is also large enough to indicate that the engine implementation might not be practical. This scenario shows that the power maximizing optimized engine also results in comparable fuel consumption to the naturally aspirated engine at maximum power levels.

6.2.4 Designing an Engine for High Altitude Applications

In the final optimization, a fully turbocharged engine was designed for high altitude operation. Operating conditions for this simulation were derived from those of farms in Bolivia at altitudes of 4000 m where the air density is 39% lower than that at sea level [1, 5].

In this scenario, fuel consumption was minimized while maintaining a power rating of 6.8 kW (Eqn. 6.6). The air to fuel equivalence ratio was set to 1.725, the lowest equivalence ratio that the naturally aspirated engine was able to run at. when the power output was below the target power output of 6.8 kW the simulation was de-

Table 6.6: The optimized values and the sensitivity of engine performance metrics to different variables for the high altitude optimized engine.

Variable	Optimized Value	Fuel Sensitivity	Power Sensitivity
IVO	16.6[1]	0.13 (%/°)	0.59 (%/°)
IVC	41.1[2]	0.07 (%/°)	0.45 (%/°)
EVO	56.6[3]	0.03 (%/°)	0.09 (%/°)
EVC	4.2[4]	0.01 (%/°)	0.02 (%/°)
Injection Start	13[3]	0.11 (%/°)	0.90 (%/°)
Injection Duration	22	0.03 (%/°)	0.12 (%/°)
Channel Width	96.1 mm	0.05 (%/%)	0.20 (%/%)
Channel Hight	5.1 mm	0.04 (%/%)	0.13 (%/%)
Channel Length	310 mm	0.05 (%/%)	0.28 (%/%)
Exhaust Diameter	30.7 mm	0.05 (%/%)	0.13 (%/%)
Exhaust Length	40.7 mm	0.02 (%/%)	0.07 (%/%)
Bore	85.1 mm	0.13 (%/%)	3.68 (%/%)
Stroke	61.4 mm	0.02 (%/%)	1.92 (%/%)
Comp Ratio	22.1	0.04 (%/%)	0.10 (%/%)

1. *Degrees before bottom dead center*
2. *Degrees after top dead center*
3. *Degrees before top dead center*
4. *Degrees after bottom dead center*

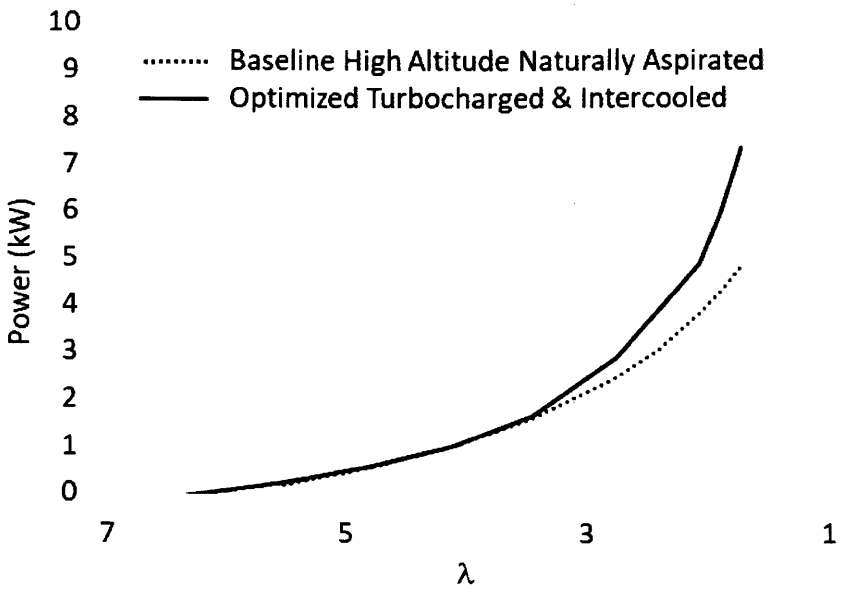

Figure 6-11: Fuel economy as a function of power output for the high altitude optimized engine compared to the baseline naturally aspirated engine at high altitude.

termined to be nonviable and the objective function changed to guide the simulation back to a viable engine configuration.

$$Score = \begin{cases} 20 - Power & \text{if Power} < 6.8 \\ \frac{BSFC - BSFC_{baseline}}{BSFC_{baseline}} & \text{if Power} > 6.8 \end{cases} \tag{6.6}$$

The results of this optimization and the sensitivity of the engine's performance to each variable are shown in Table 6.6. Once again, injection timing and engine geometry had a large effect on improving the engines overall performance, while the manifold dimensions had little effect on fuel economy or power output. However, it was found that the valve timing could affect engine performance significantly. This is due to the importance of air flow maximizing the engine's performance at higher altitudes.

Figure 6-10 shows how the optimized engine's power as a function of air to fuel equivalence ratio compares to that of the naturally aspirated case. The optimized en-

gine produced approximately equal power as the naturally aspirated engine at higher air to fuel equivalence ratios. However, at low air to fuel equivalence ratios, the effect of the turbocharger was maximized and the fully optimized engine produced significantly more power than the naturally aspirated engine at high altitude and almost as much power as the naturally aspirated engine at sea level.

The optimized engine had a significant fuel economy performance advantage over the naturally aspirated engine at low power (Fig. 6-11). The gains in efficiency resulted primarily from a reduction in frictional losses and the engine operating over a wider temperature range. However, it was found that the engine had an increase in pumping losses due to the back pressure caused by the turbocharger and an increase in heat transfer losses due to the higher operating temperature of the engine. At higher powers the high altitude fully optimized engine had approximately equivalent fuel economy performance to the baseline naturally aspirated engine operated at low altitude.

6.3 Conclusion

The Ricardo Wave model was integrated with MatLab and Simulink in order to implement a simulated annealing optimization scheme and a sensitivity analysis to explore different engine configurations. Four different applications were presented, and the engine's optimal timings, geometry, and manifold dimensions were analyzed in each case. The optimization provided a practical turbocharged engine design that outperformed the naturally aspirated engine for each of the four applications.

The analysis showed that the engine geometry and injection timing had the largest impact on engine performance. It was found that, while it is important to have a large intake manifold with good cooling properties, small changes in the intake manifold's geometry had minimal effect on performance. The compression ratio and valve timings were found to have a small effect on the engines performance. Small gains can be achieved by optimizing the valve timings to maximize air flow through the engine.

The next step in the optimization study is to work with an engine manufacturer to design, build, and test a turbocharged engine for one of their applications using the described optimization technique. To design an engine for industry, the costs of the turbocharger, manifolds, engine, and emissions after treatment systems need to be incorporated into the model. Accurate costs will be obtained from the engine manufacturer.

Another suggested future research subject is to expand the optimization to study the design of an engine around multiple operating points (a series of torque and speed settings) and creating a fuel injection timing map. In this scenario the engine geometry, manifold geometry and valve timings will be optimized for a set of potential operating points. Then, for each operating point, the optimal injection timing will be determined, with the timing controlled by electronic fuel injection. The potential drawback of multi point optimization is the computational time required. Currently, one single point optimization takes approximately a week to run on the current hardware. A multi-point optimization should be performed on a substantially more powerful system.

Chapter 7

Conclusions

The goal of this research was to understand the impact and the implementation of the air capacitor turbocharging technique for single cylinder engines on the key parameters that affect their commercial viability, including emissions, fuel economy, transient response, and power density. To accomplish this goal, a computational model was created that describes the system and predicts the impact of manifold volume, heat transfer, and other factors on the engine performance. An experiment was then constructed that quantifies the effects of turbocharging and air capacitor sizing on the key performance parameters in a turbocharged single cylinder engine. This experiment validated the computational model and was also used to evaluate the effect of turbocharging on the engine's transient performance. Finally, the validated model was used to optimize the engine for different potential applications.

This manifold sizing experiment confirmed that the turbocharger and air capacitor system increased the intake air density and the air mass flow through the system. The model validation experiments showed that the baseline model accurately predicts power output, fuel economy, and emissions. The transient analysis combined with the experimental results generate a method for calculating the characteristic transient time as well as quantify the effect of capacitor size on the transient response to both torque and speed changes.

After being validated, the model was integrated with MatLab and Simulink in order to implement a simulated annealing optimization scheme and a sensitivity anal-

ysis. Four different examples of commercial applications were presented with the engine's timing, geometry, and manifold dimensions analyzed for each case. From this analysis, the air capacitor size was found to have an impact on intake air mass flow, fuel consumption, emissions, and power output. The optimized model quantified the dependence of the performance of the turbocharged single cylinder engine on valve timings, injection timings, compression ratio, and the heat transfer properties of the air capacitor. The optimization provided a practical engine design with enhanced power and reduced fuel consumption for each of the four cases.

7.1 Contribution

In this thesis the concept of using an air capacitor to turbocharge a single cylinder engine was explored and the following contributions were made:

- Demonstrated the feasibility of turbocharging a single cylinder engine using an air capacitor to overcome the timing mismatch between the intake and the exhaust.
- Created a model that predicts the performance of a single cylinder turbocharged engine with an air capacitor and experimentally validated the model.
- Demonstrated the effect of manifold sizing, manifold cooling, and turbocharger selection on engine performance factors including: NOx emissions, air mass flow rate, power density, and fuel economy.
- Characterized the transient response of the air capacitor pressurization and the turbocharger. Experimentally demonstrated how the transient response of the turbocharger compares to the transient response of the engine.
- Found optimal engine configurations for four different cases using the computational model and optimization scheme. Used the model to find the sensitivity to different variables. Demonstrated a practical design with enhanced power and improved fuel efficiency for each case.

7.2 Future Work

Future work is proposed with the goal of making the air capacitor technology commercially viable. In order to achieve commercial viability, the following tasks should be undertaken in conjunction with a corporate partner, with the goal of transferring this technology to them.

- Work with a new single cylinder engine, provided by the commercial partner, with the goal of constructing a turbocharged version for small vehicles. This engine should have a computer controlled EGR system and electronic injection timing. The new engine should be fitted with an optimized manifold that will allow for the testing and the optimization of the injection timing, as well as incorporation of the EGR into the system to ensure emissions control.

- The engine optimization strategy described in Chapter 6 should be run with the new engine in order to determine the optimal manifold sizing and injection profiles for different speeds. This will be done on a more powerful computer due to the higher computational requirements for multi point engine optimization.

- Incorporate emissions, emissions after treatment, and cost (engine, emissions after treatment, and inter cooler costs) into the optimization.

- In order to investigate the small vehicle use case, the transients should be further explored on the new engine. This should include transient and speed response tests at higher load conditions. Injection timings to optimize transients should also be explored.

- To better understand manifold pressures and the potential back-flows during the intake valve opening, their fluctuations through an opening cycle should be accurately measured by installing high frequency pressure sensors at the intake and exhaust manifolds of the proposed experiment.

7.3 Single Cylinder Engine Turbocharging Guidelines

From this research the following design guidelines on how to turbocharge a single cylinder engine using an air capacitor were empirically, analytically, and experimentally derived:

- The key to the success of air capacitor turbocharging is to use a large capacitor (at least 8 times engine volume) with good heat transfer. For larger volumes the capacitor size does not significantly impact the turbocharger's performance; meaning a stock intercooler can be used to avoid the cost of designing and manufacturing a custom intercooler/air capacitor.
- Tuning the injection timing is essential to maximizing power output and minimizing fuel consumption.
- For transient applications, when oversizing the capacitor is impractical, a mass flow analysis can be used to determine the characteristic response time of the capacitor.
- Valve timing to optimize air flow into the engine will improve the performance.
- Turbocharging allows for an increase in power density resulting in the ability for an engine to be downsized, thus minimizing frictional losses and increasing overall efficiency.
- Turbocharger selection is crucial to optimizing the performance of the system. However, it could prove difficult to find commercial turbochargers small enough for this application.

Bibliography

[1] New agriculturist: Country profile - bolivia. www.new-ag.info/en/country/profile.php?a=3155, 2013.

[2] Turbocharging and its impact on fuel consumption. http://www.nrcan.gc.ca/energy/efficiency/transportation/cars-light-trucks/buying/16747, 2016.

[3] Cia world factbook. https://www.cia.gov/library/publications/the-world-factbook/, 2018.

[4] Nation master agricultural statistics. http://www.nationmaster.com/country-info/stats/Agriculture, 2018.

[5] Resources, tools and basic information for engineering and design of technical applications. https://www.engineeringtoolbox.com/, 2018.

[6] Turbo facts, history. http://www.turbos.bwauto.com/products/turbochargerHistory.aspx, 2018.

[7] What are superchargers? working, types, advantages, limitations. http://mechstuff.com/how-superchargers-work-types-advantages-limitations/, 2018.

[8] What is a turbocharger and how does it work? https://www.eagleridgegm.com/what-is-a-turbocharger-and-how-does-it-work/, 2018.

[9] World bank indicator. https://data.worldbank.org/indicator/SL.AGR.EMPL.ZS, 2018.

[10] Akhil Alha and Bijoyata Yonzon. Recent developments in farm labour availability in india and reasons behind its short supply. *Agricultural Economics Research Review*, (Vol. 24 (Conference Number) 2011 pp 381-390), 2011.

[11] Bharadwaj Aravand and Juttu Simhachalam. (personal communication august 20th 2013) conversion with partners at mahindra and mahindra corporation.

[12] L.G. Navale2 Atul A. Patil1 and V.S. Patil3. Experimental investigation and analysis of single cylinder four stroke c.i. engine exhaust system. *International Journal of Energy and Power (IJEP)*, (Volume 3 Issue 1), 2014.

[13] Peeyush Bachlaus and Amit Kumar. (personal communication january 20th 2015) conversion with partners at usha.

[14] M Buchman and A Winter. Method for turbocharging single cylinder four stroke engine. (DETC2014-35044), August.

[15] M Buchman and A Winter. Validating a method for turbocharging single cylinder four stroke engines.

[16] Michael Buchman and Amos Winter. Investigating the effect of intake manifold size on the transient response of single cylinder turbocharged engines. (2017-24-0170).

[17] C.N. Michos C.D. Rakopoulos and E.G. Giakoumis. Study of the transient behavior of turbocharged diesel engines including compressor surging using a linearized quasi-steady analysis. (2005-01-0225).

[18] Simon K. Chen and Patrick F. Flynn. Development of a single cylinder compression ignition research engine. (650733), 1965.

[19] Steven Chu and Arun Majumdar. Opportunities and challenges for a sustainable energy future. *Nature*, 488(11475):294–303, August 2012.

[20] REOTEMP Instrument Corporation. Type k thermocouple.

[21] Usha corporation.

[22] USHA corporation. Stationary diesel engines. Presentation on Stationary Diesel Engines by USHA for marketing purposes, 2014.

[23] DSc(Eng) G.D. Closs D.E. Winterbone, R.S. Benson and A.G. Mortimer. A comparison between experimental and turbocharged diesel engine analytical transient test results for a turbocharged diesel engine. (Vol 190, Issue 1, pp. 267 - 276).

[24] Chris Middlemass Dominique Petitjean, Luciano Bernardini and S. M. Shahed. Advanced gasoline engine turbocharging technology for fuel economy improvements. *SAE Technical Paper 2004-01-0988*, 2004.

[25] EcoEfi. *Turbo Charger Technical Spec*, 2016 (accessed January 18, 2018).

[26] The Economist. The little engine that could, why turbocharged four-cylinder engines now rule the road. (Jan 12th 2015).

[27] Experiments and Modeling of Automotive Turbochargers Under Unsteady Conditions. Luis miguel garcÃŋa-cuevas gonzÃąlez, 2014.

[28] J. Fredriksson and B. Egardt. Estimating exhaust manifold pressure in a turbocharged diesel engine. *Proceedings of the 2002 International Conference on Control Applications*, (Volume 2), 2002.

[29] Garrett. Turbocharger products. http://www.turbobygarrett.com/turbobygarrett/, 2015 (accessed 2015-02-09).

[30] J. Ghojel. Review of the development and applications of the wiebe function: a tribute to the contribution of ivan wiebe to engine research. *International Journal of Engine Research*, (Vol 11, Issue 4, pp. 297 - 312), 2010.

[31] Evangelos Giakoumis. Review of some methods for improving transient response in automotive diesel engines through various turbocharging configurations. (10.3389/fmech.2016.00004).

[32] Sanjeev Goyle. Mechanization trends in india. Presented to Mahindra and Mahindra, 2013.

[33] I Hakeem H Chen and R F Martinez-Botas. Modelling of a turbocharger turbine under pulsating inlet conditions. *Proceedings of the Institution of Mechanical Engineers, Part A: Journal of Power and Energy*, 210(5):397.

[34] John Heywood. *Internal Combustion Engine Fundementals*. McGraw-Hill, New York, Ny, 1988.

[35] H. Hiereth and P. Prenninger. *Charging the internal Combustion Engine*. Springer Vienna, Vienna, 2003.

[36] What Cetane Value Does in Diesel Engines. Bell performance. https://www.bellperformance.com/blog/bid/102350/What-Cetane-Value-Does-in-Diesel-Engines, accessed June 10, 2018.

[37] Universal Industrial Gasses Inc. Air: Its composition and properties the source of industrial gas products nitrogen, oxygen, argon.

[38] Fluent Incorporated. Fluent incorporated, thermal nox formation.

[39] The International Counsel on Clean Transport. *India Bharat Stage VI Emission Standards: India BS VI Policy Update*, April 2016.

[40] H.Climent J.Galindo, J.R.Serrano and O.Varnier. Impact of two-stage turbocharging architectures on pumping losses of automotive engines based on an analytical model. *Energy Conversion and Management*, (Volume 51, Issue 10, Pages 1958-1969), 2010.

[41] Kohler. *KD440 Workshop Manual*, 2012 (accessed January 12, 2018).

[42] Pierre Lermusiaux. 2.006 equation sheet. University Lecture Supplement, 2012.

[43] Alan C. Lloyd and Thomas A. Cackette. Diesel engines: Environmental impact and control. *Journal of the Air and Waste Management Association*, (51:6, 809-847, DOI: 10.1080/10473289.2001.10464315), 2001.

[44] Andrei Makartchouk. *Diesel Engine Engineering: Thermodynamics, Dynamics, Design, and Control.* Marcel Dekker, Inc., New York, Ny, 2002.

[45] C.R. Mehta. Agriculture mechanization strategies in india. Presented to Central Institute of Agricultural Engineering, Bhopal Indian Council of Agricultural Research, New Delhi, India, 2013.

[46] Arunachalam Narayanan. Downspeeding the diesel engine âĂŞ a performance analysis. (Master's Thesis 2011:50).

[47] Henry K. Newhall. Kinetics of engine-generated nitrogen oxides and carbon monoxide. *Symposium (International) on Combustion*, (Volume 12, Issue 1, Pages 603-613), 1969.

[48] Hung Nguyen-Schafer. *Rotordynamics of Automotive Turbochargers: Linear and Nonlinear Rotordynamics âĂŞ Bearing Design âĂŞ Rotor Balancing.* Springer., New York, Ny, 2015.

[49] Omega. *high-accuracy S-Beam Load Cells Rugged for Industrial Applications*, (accessed January 12, 2018).

[50] Sharad Pawar. Farm mechanization in india. Presented to the Indian Parlement by the Indian Dept. of Agriculture and Cooperation Mechanization and Technology Division, 2013.

[51] Neelkanth V Marathe Narendra Pawar Hirak Jyoti Gayen Dadarao Narwade Bhaskar Melage Prasanna G Bhat, Sukrut Thipse and S V A Achari. Upgradation of two cylinder na diesel genset engine into tcic configuration for achieving stricter emission norms for 19 kw to 75 kw power categories. *SAE Technical Paper*, 215.

[52] Giakoumis E. Hountalas D. Rakopoulos, C. and D. Rakopoulos. The effect of various dynamic, thermodynamic and design parameters on the performance of a turbocharged diesel engine operating under transient load conditions. *SAE Technical Paper 2004-01-0926*, 2004.

[53] Thomas Resch and Borislav Klarin. Analysis of engine dynamics under transient run-up conditions. (2004-01-1454).

[54] robert nau. Linear regression models. https://people.duke.edu/ rnau/compare.htm, accessed June 10, 2018.

[55] C P Garner S Cong and G P McTaggart-Cowan. The effects of exhaust back pressure on conventional and low-temperature diesel combustion. *Proceedings of the Institution of Mechanical Engineers, Part D: Journal of Automobile Engineering*, (Vol 225, Issue 2, pp. 222 - 235), 2011.

[56] R. F. Martinez-Botas S. Szymko and K. R. Pullen. Experimental evaluation of turbocharger turbine performance under pulsating flow conditions. *ASME Turbo Expo 2005: Power for Land, Sea, and Air*, (Volume 6: Turbo Expo 2005, Parts A and B), 2005.

[57] Sherborne Sensors. *U4000 Series Universal Tension/Compression Load Cell*, 2008 (accessed January 12, 2018).

[58] Bang Shift. The worlds most pissed off one cylinder engine is turbocharged and packs a screw blower! http://bangshift.com/bangshiftxl/the-worlds-most-pissed-off-one-cylinder-engine-is-turbocharged-and-packs-a-screw-blower/, 2015 (accessed 2015-05-01).

[59] Gajendra Singh. Relationship between mechanization and agricultural productivity in various parts of india. *Indian Journal of Agricultural Economics*, (AMA 32 (2): 68-76), 2001.

[60] J. Sodre. Modelling nox emissions from spark-ignition engines. *Proceedings of the Institution of Mechanical Engineers, Part D: Journal of Automobile Engineering*, (Vol 214, Issue 8, pp. 929 - 934), 2000.

[61] APT Turbocharger Systems. Turbochargers vs superchargers âĂŞ advantages and disadvantages.

[62] K. V. Tanin, D. D. Wickman, D. T. Montgomery, S. Das, and R. D. Reitz. The influence of boost pressure on emissions and fuel consumption of a heavy-duty single-cylinder d.i. diesel engine. *n-cylinder diesel particulate and NOx control 1999*, 1999.

[63] Taylor Dynamometer. *DE20 Eddy Current Dynamometer*, 2016 (accessed January 12, 2018).

[64] Honeywell Turbo Technologies. Small wastegate turbos. http://turbo.honeywell.com/our-technologies/small-wastegate-turbo/, accessed June 10, 2018.

[65] Testo. *Testo 350 Combustion and Emission Analyzer*, (accessed January 18, 2018).

[66] N. Watson. Transient performance simulation and analysis of turbocharged diesel engines. (810338).

[67] N. Watson and M. Janota. *Turbocharging the Internal Combustion Engine*. Jhon Wiley and Sons, New York, NY, 1982.

[68] A.G. Winter. Turbocharged single cylinder internal combustion engine using an air capacitor. Google Patents, jan 2015. US Patent App. 14/320,717.

[69] D. Winterbone and R. Pearson. *Design Techniques for Engine Manifolds*. Professional Engineering Pub. Limited, United Kingdom, 1999.

[70] G. Woschni. A universally applicable equation for the instantaneous heat transfer coefficient in the internal combustion engine. *SAE Technical Paper*, (670931), 1967.

[71] Nicholas C. Surawski Linda Morawska Kwun M. Fong Felicia Goh Zoran D. Ristovski, Branka Miljevic and Ian A. Yang. Respiratory health effects of diesel particulate matter. *Respirology*, (Volume17, Issue2), 2011.